Ministry of Education and Science of Ukraine

Sumy National Agrarian University

Qualifying scientific

work on the rights of the manuscript

Zhang Zhengchuan

UDC621.03.004:621.09.048

DISSERTATION

Technological support of friction unit at commissioning stage by forming the running-in coatings

133 « Industrial machinery engineering »

13 -Mechanical engineering

Applies for the degree of the doctor of philosophy

The dissertation contains the results of own research. The use of other authors' ideas, results and texts link to the source_____**Zhang Zhengchuan**

Scientific supervisor: Ievgen Konoplianchenko, PhD, Associate Professor, Candidate of Technical Sciences

Sumy – 2023

ANNOTATION

Zhang Zhengchuan Technological support of friction unit at commissioning stage by forming the running-in coatings. - The qualifying scientific work based on the manuscript.

The dissertation on competition of a scientific degree of the doctor of philosophy in the field of knowledge 13 - Mechanical engineering on a specialty 133 - Industrial machinery engineering. - Sumy National Agrarian University, Sumy, 2023.

The dissertation is devoted to the solution of the actual scientific and technical problem in the field of branch mechanical engineering: development of innovative, energy efficient and environmentally friendly technology to improve the working condition of the friction surface to promote running-in conditions, deformation under high specific load provides automatic adjustment and compensation of bronze bearing shells for manufacturing errors. Solving this problem will increase the reliability of the rotary machines, increase the life of their working bodies, and reduce energy consumption, which is very important for modern Ukraine.

Object of research - Technological process of formation of functional coatings on the surface of elements of machines with bronze bushes for sliding bearings of rotating mechanisms.

Subject of research - The running-in coatings on the surface of tin bronze bushes that was formed by electro-spark deposition (ESD) applying the antifriction material of silver, copper, Babbitt B83 or graphene oxide (GO).

The purpose of the study is ensuring the reliability and durability of the rotating mechanisms friction units by improving the tribosurfaces quality at commissioning stage the special running-in coating formation.

To achieve this goal, it is necessary to solve the following **tasks:**

1. To analyze the manufacturing technology and features of the friction units operation;

2. To analyze structural and technological methods of increasing the reliability and durability of friction units;

3. Develop a system of directional selection of technological parameters for forming running-in coatings on various contact surfaces of friction units;

4. Establish correlation dependencies between equipment modes and quality parameters of the formed coatings;

5. To introduce the results of research into the practice of manufacturing friction units in the enterprise.

In the introduction, the choice of the topic of the dissertation and scientific tasks is substantiated, the purpose and tasks of research are formulated, the scientific novelty and practical value of the received results are defined, and also the information on approbation, structure and volume of work is resulted.

In the first chapter, the principle, equipment, detection method, treatment process and discharge mechanism of the electro-spark deposition technology will be comprehensively introduced. The effects of various process parameters on the mass transfer, surface roughness, elemental composition, microstructure and mechanical properties of the coating will be deeply studied. The effects of this treatment method on

the phase composition, material hardness and friction and wear properties of the coatings will be systematically analyzed. All this allowed to formulate the purpose and tasks of the dissertation.

In the second chapter, the basic principle of ESD technology is introduced in detail, the testing methods of surface roughness, surface morphology, element composition, phase composition, hardness and tribological properties are established, and the coatings performance index system is constructed, the principle of determining the weight by entropy method is derived, and the TOPSIS model is used for comprehensive evaluation. The experimental materials, experimental equipment and coatings preparation process involved in this paper are introduced.

In the third chapter, the mechanism of low friction coefficient and the formation process of the coatings are described. The mass transfer, surface roughness, microstructure and elemental composition of the coatings are studied. The effects of process parameters on the thickness, phase composition, hardness and tribological properties of the coatings were studied.

In the fourth chapter, the traditional processing and manufacturing process of plain bearing bush is briefly introduced, the test results of different running-in coatings are summarized and analyzed, the entropy method is used to determine the weight of running-in coatings index, and the TOPSIS model is used to comprehensively evaluate and sort the running-in coatings, and the best industrial application scheme is determined. The base material, coating material, processing technology and coating technology of bearing bush which affect the product quality are analyzed. A new environmental protection technology of constructing running-in coatings of tin bronze

bearing bush is put forward, and the technical design, manufacture, processing, installation and trial operation are described in detail. Finally, some technical suggestions for the application of running-in coatings process of tin bronze bearing are put forward.

In the fifth chapter, the full text is summarized, conclusions are drawn, and suggestions for future research are put forward.

According to the set purpose and tasks in work the following **results** are received:

1. The soft material coating of silver under the optimal process parameters, the mass transfer is 25.0 mg, the surface roughness of the Ag coating is 15.46 μm and the thickness is 15 μm. The minimum friction coefficient of the Ag coating is about 0.31. However, the performance of silver as antifriction material coating needs to be further improved.

2. Under the optimal process parameters of the soft material coatings of silver and Babbitt B83, the mass transfer is 125.2 mg, the surface roughness of the composite coatings is 19.43 μm and the maximum thickness of the layers is 80 μm. The minimum friction coefficient of the composite coatings is about 0.177 after running-in stage. The main wear mechanism of composite coatings prepared under optimal process parameters is plastic deformation and abrasive wear.

3. Under the optimal process parameters of the soft antifriction material of silver, copper and Babbitt B83, the mass transfer is 54.4 mg/cm^2, the surface roughness of the composite coatings is 32.3 μm. The coatings are dense, metallurgical fusion with the substrate and under the optimal parameters, the thickness of the coatings is about 100 μm and the maximum thickness is 160 μm. The hardness distribution from the coatings

surface to the substrate increases first, then decreases and then increases gradually. The surface microhardness of the composite coatings is 29 $HV_{0.01}$, which is about 82% lower than that of tin bronze substrate (161 $HV_{0.01}$). The surface friction coefficient of the composite coatings is 55.6% of the tin bronze substrate. The main wear mechanism of composite coatings is plastic deformation accompanied by slight polishing.

4. The running-in coatings on the tin bronze by electro-spark deposition (ESD) applying the antifriction material of silver, copper, Babbitt B83 and graphene oxide (GO). The results show that under the optimal process parameters, the mass transfer is 244.2 mg, the surface roughness of is 15.9 μm and the thickness of the layers is 160 μm. The modulus and the hardness of the running-in coatings is 24.9% and 14.2% of the substrate, and the deformation ratio of the coatings is 10.2% higher than that of the substrate. The friction coefficient of the running-in coatings is about 0.210 after running-in stage which is 64.8% of the substrate (0.324). The main wear mechanism of the running-in coatings is plastic deformation, scratching and slight polishing. The running-in coatings deformation under action of high specific loads provides parts automatic adjustment and compensation of manufacturing errors.

5. An evaluation indicator system for the characterization was constructed based on 6 factors including material price, time, mass transfer, roughness, thickness and friction coefficient of the coatings by electro-spark deposition. An integrated coatings characterization assessment approach is proposed here by combining a multi-criteria decision making technique, the technique for order preference by similarity to ideal solution (TOPSIS), with the Shannon entropy method.

6. Technical recommendations for the manufacture of rotary machinery involving tin bronze bushes for plain bearings have been formulated and implemented, with an expected economic benefit of 216 thousand UAH for environmentally friendly methods.

Scientific novelty of the obtained results:

1. For the first time, Tin bronze QSn10-1 is selected as the substrate material, and silver, copper, B83, GO are selected as the coating materials. The substrate and the coatings have a good metallurgical bonding, a new Ag_3Sn phase is formed, the grain size is refined, the surface hardness is reduced, and the friction coefficient is greatly reduced. It is very suitable for running-in coatings.

2. For the first time, according to the selected substrate material and coatings materials, the process parameters of electro-spark deposition were studied, and the equipment DZ-4000III was selected as the deposition equipment to find out the optimal electro-spark deposition parameters.

3. For the first time, the index evaluation system of electro-spark deposition coatings was established, the weight of each index was determined by entropy method, and the TOPSIS model was used to comprehensively evaluate different coatings.

The practical significance of the obtained results is to provide technical suggestions for the manufacture of tin bronze Bush of sliding bearing in rotating machinery. Adapt to that technical cycle of sliding bearing in rotating machinery and the operating conditions of friction unit using tin bronze bushes for the rotating running of the core components.

Keywords: alloy, coating, electro-spark deposition, electrospark alloying, wear resistance, coefficient of friction, surface layer, layer thickness, microstructure, hardness of surfacing, bearing, pump, hardness.

АНОТАЦІЯ

Чжан Чженчуань. Технологічне забезпечення входження вузлів тертя в період нормальної експлуатації формуванням припрацювальних покриттів. Кваліфікаційна наукова робота за рукописом.

Дисертація на здобуття наукового ступеня доктора філософії з галузі знань 13 – Механічна інженерія за спеціальністю 133 – Галузеве машинобудування. – Сумський національний аграрний університет, Суми, 2023.

Дисертація присвячена вирішенню актуальної науково-технічної проблеми в галузі галузевого машинобудування: розробці інноваційної, енергоефективної та екологічно безпечної технології покращення робочого стану поверхні тертя для сприяння режимам припрацювання, деформації під час роботи. високе питоме навантаження забезпечує автоматичне регулювання і компенсацію похибок виготовлення бронзових втулок підшипників. Вирішення цієї проблеми підвищить надійність роторних машин, збільшить ресурс їх робочих органів, зменшить споживання енергії, що дуже важливо для сучасної України.

Об'єкт дослідження – Технологічний процес формування функціональних покриттів на поверхні елементів машин з бронзовими втулками підшипників

ковзання механізмів обертання.

Предмет дослідження – Припрацьовані покриття на поверхні втулок олов'яної бронзи, утворені методом електроіскрового легування (ЕІЛ) з нанесенням антифрикційного матеріалу срібла, міді, бабіту Б83 або оксиду графену (ГО).

Метою дослідження є забезпечення надійності та довговічності вузлів тертя механізмів обертання шляхом підвищення якості трибоповерхонь на етапі введення в експлуатацію шляхом формування спеціального обкаткового покриття.

Для досягнення поставленої мети необхідно вирішити такі завдання:

1. Проаналізувати технологію виготовлення та особливості роботи вузлів тертя;

2. Проаналізувати конструктивно-технологічні прийоми підвищення надійності та довговічності вузлів тертя;

3. Розробити систему спрямованого вибору технологічних параметрів формування обкатування покриттів на різних контактних поверхнях вузлів тертя;

4. Встановити кореляційні залежності між режимами обладнання та параметрами якості сформованих покриттів;

5. Впровадити результати дослідження в практику виготовлення вузлів тертя на підприємстві.

У вступі обґрунтовано вибір теми дисертації та наукових завдань, сформульовано мету та завдання дослідження, визначено наукову новизну та практичне значення отриманих результатів, а також подано відомості про апробацію, структуру та обсяг роботи.

У першому розділі було всебічно представлено принцип, обладнання, метод виявлення, процес обробки та механізм розряду технології електроіскрового легування. Було досліджено вплив різних параметрів процесу на масообмін, шорсткість поверхні, елементний склад, мікроструктуру та механічні властивості покриття. Було системно проаналізовано вплив цього методу обробки на фазовий склад, твердість матеріалу та властивості покриття на тертя та зношування. Усе це дозволило сформулювати мету та завдання дисертації.

У другому розділі детально представлено основний принцип технології ЕІЛ, встановлено методи випробування шорсткості поверхні, морфології поверхні, елементного складу, фазового складу, твердості та трибологічних властивостей, а також побудовано систему індексу ефективності покриттів, принцип виведено визначення ваги ентропійним методом, а для комплексної оцінки використано модель TOPSIS. У цьому документі представлені експериментальні матеріали, експериментальне обладнання та процес приготування покриттів.

У третьому розділі описано механізм зниження коефіцієнта тертя та процес утворення покриттів. Досліджено масообмін, шорсткість поверхні, мікроструктуру та елементний склад покриттів. Досліджено вплив технологічних параметрів на товщину, фазовий склад, твердість і трибологічні властивості покриттів.

У четвертому розділі коротко представлено традиційний процес обробки та виготовлення втулки підшипника ковзання, узагальнено та проаналізовано результати випробувань різних покриттів для обкатки. Використано ентропійний метод для визначення ваги індексу обкатки покриттів, а також модель TOPSIS для всебічної оцінки та сортування покриттів для припрацювання та визначення

найкращої схеми промислового застосування. Проаналізовано основний матеріал, матеріал покриття, технологію обробки та технологію покриття втулки підшипника, які впливають на якість продукції. Запропоновано нову екологічнобезпечну технологію створення припрацювальних покриттів втулки підшипника з олов'яної бронзи, детально описано технічний проєкт, виготовлення, обробку, монтаж і дослідну експлуатацію. Запропоновано ряд технічних рекомендацій щодо застосування процесу формування припрацювальних покриттів підшипників з олов'яної бронзи.

У п'ятому розділі узагальнено повний текст, зроблено висновки та надано пропозиції щодо подальших досліджень.

Відповідно до поставленої мети та завдань у роботі отримано наступні результати:

1. М'яке покриття зі срібла за оптимальних параметрів процесу нанесення має масопередачу 25,0 мг, шорсткість поверхні становить 15,46 мкм, а товщина становить 15 мкм. Коефіцієнт поверхневого тертя стабілізується після обкатки, а мінімальний коефіцієнт тертя покриття Ag становить близько 0,31. Однак характеристики срібла як покриття антифрикційного матеріалу потребують подальшого вдосконалення.

2. За оптимальних параметрів процесу формування м'якого покриття зі срібла та бабіту Б83 масопередача становить 125,2 мг, шорсткість поверхні композитного покриття 19,43 мкм і максимальна товщина шару 80 мкм. Мінімальний коефіцієнт тертя композитних покриттів після стадії припрацювання становить близько 0,177. Основним механізмом зношування композиційних

покриттів, виготовлених за оптимальних технологічних параметрів, є пластична деформація та абразивне зношування.

3. При оптимальних технологічних параметрах формування м'якого антифрикційного покриття зі срібла, міді та бабіту Б83 масопередача становить 54,4 мг/см^2, шорсткість поверхні композиційних покриттів 32,3 мкм. Покриття щільні, металургійне сплавлення з підкладкою і при оптимальних параметрах товщина покриттів становить близько 100 мкм, а максимальна товщина – 160 мкм. Елементний склад трьох характерних областей (гладка поверхня, шорстка поверхня та пори) на поверхні композитних покриттів значно змінюється через різні способи виробництва. Розподіл твердості від поверхні покриття до основи спочатку збільшується, потім зменшується, а потім поступово збільшується. Поверхнева мікротвердість композиційних покриттів становить 29 $HV_{0,01}$, що приблизно на 82% нижче, ніж у підкладки з олов'яної бронзи (161 $HV_{0,01}$). Коефіцієнт поверхневого тертя композитних покриттів становить 55,6% підкладки олов'яної бронзи. Основним механізмом зношування композиційних покриттів, виготовлених за оптимальних технологічних параметрів, є пластична деформація та легке полірування.

4. Досліджено припрацювальні покриття на основі олов'янистої бронзи, що отримані електроіскровим легуванням (ЕІЛ) з нанесенням антифрикційного матеріалу срібла, міді, бабіту В83 та оксиду графену (ГО). Результати показують, що обкаткові покриття є щільними, зернистість подрібнена, рівномірно розподілена та металургійно сплавлена з підкладкою. За оптимальних параметрів процесу масопередача становить 244,2 мг, шорсткість поверхні – 15,9 мкм,

товщина шару – 160 мкм. Модуль і твердість покриттів при обкатці становить 24,9% і 14,2% підкладки, а коефіцієнт деформації покриттів на 10,2% вище, ніж у підкладки. Коефіцієнт тертя обкатуваних покриттів становить близько 0,210 після етапу обкатки, що складає 64,8% основи (0,324). Основним механізмом зношування припрацьованих покриттів за оптимальних параметрів процесу є пластична деформація, подряпини та легке полірування. Деформація покриттів при обкатці під дією високих питомих навантажень забезпечує автоматичне регулювання деталей і компенсацію похибок виготовлення.

5. Система оцінки показників для характеристики була побудована на основі 6 факторів, включаючи ціну матеріалу, час, масопередачу, шорсткість, товщину та коефіцієнт тертя покриттів електроіскровим легуванням. Запропоновано інтегральний підхід до оцінки характеристик покриттів, який поєднує багатокритеріалий метод прийняття рішень, максимально близьких до ідеального рішення (TOPSIS) і метод ентропії Шеннона. Для врахування неоднорідності значень показників використовується метод ентропії Шеннона. Модель TOPSIS було застосовано для узагальненої рейтингової оцінки характеристик припрацювальних покриттів, отриманих методом електроіскрового легування.

6. Розроблено та впроваджено технологічні рекомендації щодо виготовлення роторних машин із застосуванням втулок олов'яної бронзи для підшипників ковзання, отриманих екологічно безпечними методами, з очікуваним економічним ефектом 216 тис. грн.

Наукова новизна отриманих результатів:

1. Вперше в якості матеріалу підкладки обрано олов'янисту бронзу QSn10-1, а срібло, мідь, Б83, ОГ – як матеріали покриття. Основа і покриття мають хороше металургійне зв'язування, утворюється нова фаза Ag_3Sn, розмір зерен зменшується, поверхнева твердість знижується, а коефіцієнт тертя суттєво знижується. Дуже добре підходить для припрацювальних покриттів.

2. Вперше, відповідно до обраних матеріалів підкладки та матеріалів покриттів, було вивчено параметри процесу електроіскрового легування, а обладнання DZ-4000III було обрано для визначення оптимальних параметрів електроіскрового легування.

3. Вперше було створено систему оцінки індексу електроіскрового легування покриттів, вагу кожного індексу було визначено ентропійним методом, а модель TOPSIS було використано для комплексної оцінки різних покриттів.

Практичне значення отриманих результатів полягає у наданні технологічних пропозицій щодо виготовлення з олов'янистої бронзи втулки підшипника ковзання обертових машин. Виконано апробацію технологічного процесу виготовлення підшипників ковзання до умов роботи вузла тертя в обертових машинах.

Ключові слова: сплав, покриття, електроіскрове напилення, електроіскрове легування, зносостійкість, коефіцієнт тертя, поверхневий шар, товщина шару, мікроструктура, поверхнева твердість, підшипник, насос, твердість.

LIST OF THE APPLICANT'S PUBLICATIONS ON THE TOPIC OF THE DISSERTATION

Articles in scientific professional publications of Ukraine

1. **Zhang Zhengchuan**, Liu Guanjun, Viacheslav Tarelnyk, Ievgen Konoplianchenko. Application of Electro-Spark Deposition Technology to Functional Coatings Create. Compressor and Power Engineering. 2019, 4(58), 14-16. (PhD participant in carrying out of experimental researches, processing of results, preparation of article for printing).

2. **Zhang Zhengchuan**, Liu Guanjun, Ie. Konoplianchenko, V. Tarelnyk, Ge Zhiqin, Du Xin. A review of the electro-spark deposition technology. Bulletin of Sumy National Agrarian University, The Series: Mechanization and Automation of Production Processes. 2021, 2(44), 45-53. (PhD participant in carrying out of experimental researches, processing of results, preparation of article for printing).

https://doi.org/10.32845/msnau.2021.2.10

3. **Zhang Zhengchuan**. The characterization of silver coating on the surface of tin bronze by electro-spark deposition. Bulletin of Sumy National Agrarian University, The Series: Mechanization and Automation of Production Processes. 2021, 4(46), 60-66. (PhD participant in carrying out of experimental researches, processing of results, preparation of article for printing).

https://doi.org/10.32845/msnau.2021.4.9

4. **Zhang Zhengchuan**, Ievgen Konoplianchenko, Viacheslav Tarelnyk, Liu Guanjun, Du Xin, Ju Yao, Song Zhaoyang. Industry Application of the Coatings on the Bearing Bush by Electro Spark Alloying Technology. Scientific Bulletin of

Ivano-Frankivsk National Technical University of Oil and Gas. 2022, 1(52), 15-23. (PhD participant in carrying out of experimental researches, processing of results, preparation of article for printing).

https://doi.org/10.31471/1993-9965-2022-1(52)-15-23

Articles in scientific journals of other countries

5. **Zhang Zhengchuan**, Ievgen Konoplianchenko, Viacheslav Tarelnyk, Liu Guanjun, Du Xin, Yu Hua. The Characterization of Running-In Coatings on the Surface of Tin Bronze by Electro-spark Deposition. Coatings. 2022, 12(7), 930-945. (PhD participant in carrying out of experimental researches, processing of results, preparation of article for printing).

https://doi.org/10.3390/coatings12070930　　**(Web of Science)**

6. **Zhang Zhengchuan**, Ievgen Konoplianchenko, Viacheslav Tarelnyk, Liu Guanjun, Du Xin, Yu Hua. The Characterization of Soft Antifriction Coating on the Tin Bronze by Electro-spark Alloying. Materials Science (Medžiagotyra). 2023, 29(1), 40-47. (PhD participant in carrying out of experimental researches, processing of results, preparation of article for printing).

http://dx.doi.org/10.5755/j02.ms.30610　　**(Web of Science)**

7. **Zhang Zhengchuan**, Viacheslav Tarelnyk, Ievgen Konoplianchenko, Liu Guanjun, Du Xin，Ju Yao. Characterization of Tin Bronze Substrates Coated by Ag+B83 through Electro-spark Deposition Method. Surface Engineering and Applied Electrochemistry. 2023, 59(2), 220-230. (PhD participant in carrying out of experimental researches, processing of results, preparation of article for printing).

https://doi.org/10.3103/S1068375523020187　　**(Web of Science)**

8. **Zhang Zhengchuan**, Viacheslav Tarelnyk, Ievgen Konoplianchenko, Liu Guanjun, Wang Hongyue, Du Xin，Ju Yao, Li Zongxi. New Evaluation Method for the Characterization of Coatings by Electroerosive Alloying. Materials Research Express. 2023, 10(3), 036401. (PhD participant in carrying out of experimental researches, processing of results, preparation of article for printing).

https://doi.org/10.1088/2053-1591/acc15b   **(Web of Science)**

Theses of scientific reports

9. **Zhang Zhengchuan**, Viacheslav Tarelnyk, Ievgen Konoplianchenko. The use of electro-spark technologies in the formation of running-in coatings. Youth and Agricultural Machinery in the XXI Century. April 4-5th, 2019. (PhD participant in carrying out of experimental researches, processing of results, preparation of article for printing).

10. Ie. Konoplianchenko, **Zhang Zhengchuan**. Improving the running-in conditions quality of sliding bearing by the formation of running-in coatings. Технології XXI сторіччя: Збірник тез за матеріалами 25-ої міжнародної науково-практичної конференції (15-20 вересня 2019 р.). Ч.3. – Суми: СНАУ, 2019 – С. 53-54. (PhD participant in carrying out of experimental researches, processing of results, preparation of article for printing).

11. **Zhang Zhengchuan**, Viacheslav Tarelnyk, Ievgen Konoplianchenko. Application of electro-spark deposition technology to functional coatings create. Sumy National Agrarian University. April 18th, 2019. (PhD participant in carrying out of experimental researches, processing of results, preparation of article for printing).

12. Konoplianchenko, I., Tarelnyk, V., Martsynkovskyy, V., Gaponova, O., Lazarenko, A., Sarzhanov, A., Mikulina, M., **Zhengchuan, Z.**, Pirogov, V. New technology for restoring Babbitt coatings (2021) Journal of Physics: Conference Series, 1741 (1), art. no. 012040. (PhD participant in carrying out of investigation, preparation of article for printing).

https://doi.org/10.1088/1742-6596/1741/1/012040   **(SCOPUS)**

13. Konoplianchenko, I., Tarelnyk, V., Gaponova, O., Bondarev, S., Vasilenko, O., Belous, A., Smolyarov, G., Semirnenko, Y., **Zhang, Z.**, Mikulina, M., Kutakh, A., Semirnenko, S., Gerasimenko, V. Increasing the Efficiency of Running-In the Titanium Nitride Nanostructures Formed on R6M5 and 12KH18N10T Steels by Sulphidizing with Electric Spark Alloying Method (2020) Proceedings of the 2020 IEEE 10th International Conference on "Nanomaterials: Applications and Properties", NAP 2020, art. no. 9309700. (PhD participant in carrying out of investigation, preparation of article for printing).

https://doi.org/10.1109/nap51477.2020.9309700   **(Web of Science, SCOPUS)**

14. **Zhang Zhengchuan**, Viacheslav Tarelnyk, Ievgen Konoplianchenko, Liu Guanjun, Du Xin, Yu Hua. Research on the Characterization of Ag+Cu+B83 Composite Coatings on the Surface of Tin Bronze by Electro-spark Deposition (2021) Proceedings of the 2021 IEEE 11th International Conference on "Nanomaterials: Applications and Properties", NAP 2021, pp. 1-8. (PhD participant in carrying out of experimental researches, processing of results, preparation of article for printing).

https://doi.org/10.1109/NAP51885.2021.9568514   **(SCOPUS)**

15. **Zhang Zh.**, Konoplianchenko Ie.V., Tarelnyk V.B., Du X. The future research direction of the ESD deposition technology. Машинобудування очима молодих: прогресивні ідеї – наука – виробництво: матеріали XX Міжнародної науково-технічної конференції (м. Суми, 29 вересня – 1 жовтня 2021 року) / редкол.: В. О. Залога, В. О. Іванов. – Суми: Сумський державний університет, 2021. – С. 21-23. (PhD participant in carrying out of experimental researches, processing of results, preparation of article for printing).

16. Ju Yao, Ie. Konoplianchenko, **Zhang Zhengchuan**. AlCoNiFeCrSi high-entropy alloy coating on the surface of H13 steel by laser cladding. ТехнологіїXXI сторіччя: Збірниктеззаматеріалами 27-ої міжнародної науково-практичної конференції (24-26 листопада 2021 р.). Ч.1. – Суми: СНАУ, 2021 – С. 214-215. (PhD participant in carrying out of experimental researches, review and editing).

17. Ju Y., Konoplianchenko Ie., **Zhang Zh.** Practical application of high-entropy alloy obtained on the H13 steel by laser cladding technology. Машинобудування очима молодих: прогресивні ідеї – наука – виробництво: матеріали XX Міжнародної науково-технічної конференції (м. Суми, 29 вересня – 1 жовтня 2021 року) / редкол.: В. О. Залога, В. О. Іванов. – Суми: Сумський державний університет, 2021. – С. 12-14. (PhD participant in carrying out of experimental researches, review and editing).

Patents

18. **Zhang Zhengchuan,** Li Bo, Meng Fanlei, Wang Long, Wei Yangqi, Wang Mingyi, Yang Shulong, Ge Yong. A composite coatings process on the surface of the crane bearing bush by electro-spark deposition.   **(202211543478.X, China)**

19. **Zhang Zhengchuan,** Li Bo, Wang Long, Meng Fanlei, Wei Yangqi, Wang Mingyi, Yang Shulong, Ge Yong. A process of soft antifriction coatings on tin bronze bearing bush surface by electro-spark alloying.   **(202211348829.1, China)**

LIST OF SYMBOLS

ESD - electro-spark deposition

GO - graphene oxide

FU - friction units

TOPSIS - technique for order preference by similarity to an ideal solution

SEM - scanning electron microscopy

EDS - energy dispersion spectrum

XRD - X-ray diffractometer

C_1 - Material price, Yuan

C_2 - Time, min

C_3 - Mass Transfer, mg

C_4, R_a - Roughness, μm

C_5 - Thickness, μm

C_6 - Friction coefficient

e_j - the entropy value

d_j - the information utility value of indicator

w_j - the weighting value of the jth indicator

D_i^+ - the Euclidean distance between the evaluation value and the best solution

D_i^- - the Euclidean distance between the evaluation value and the worst solution

C_i - the relative closeness of the object i

INTRODUCTION

Justification of the choice of research topic.

Gas turbine works under the conditions of high load, high speed and high temperature, but it is also affected by corrosive and abrasive working environment. Sliding bearing is one of the key components of large gas turbine unit, which supports the weight of the rotor and ensures the high-speed and stable operation of the rotor. The bearing bush material is used in pairs with the steel journal. The shaft is an important part, the manufacturing process is complex, the cost is high, and the replacement is difficult, so in the case of inevitable wear, the shaft should be ensured to be subjected to minimum wear, and the bearing bush can be replaced if necessary to continue to use the shaft.

The main requirements for the materials of sliding bearings are mutual material compatibility, low friction coefficient, high pressure resistance, strong fatigue resistance, high thermal stability, good corrosion resistance, strong wear resistance, good shock resistance, low cost, structural stability and recoverability of performance after forced contact. These materials should be hard enough without excessive wear on the shaft. They should be relatively easy to plastically deform under the influence of local stresses and should have the ability to store lubricating oil on the surface. Steam turbine bearing support rotor is a kind of heavy load and high speed sliding bearing. The material of bearing is tin-base Babbitt alloy which has small friction coefficient, good wear resistance and high enough compressive strength. Babbitt alloy is a kind of antifriction alloy with good performance. Compared with other bearing materials, tin-based bearing alloy has small expansion coefficient, good embeddability and antifriction, excellent

toughness and corrosion resistance, and good adhesion to the back of the bearing. Its main disadvantage is that its fatigue strength is poor, and its mechanical strength decreases sharply with the increase of temperature. The maximum operating temperature should generally be less than 110 ℃.

In the actual work of the bearing, tin bronze bearing has good mechanical properties and thermal conductivity, but the friction is slightly higher, Babbitt alloy bearing has less friction, but the performance at high temperature is poor, which further affects the reliability and stability of the bearing. The addition of a small amount of silver in the Babbitt alloy can play a role in grain refinement, so that the strength and the hardness of the alloy are improved. Copper can provide the preferential crystallization center of Babbitt alloy, refine the grain, and improve the microstructure and mechanical properties of alloy.

Electro-spark deposition technology is a new environmental protection method to repair and strengthen the surface of metal materials. The method has the advantages of simple equipment, convenient operation, safety, environmental protection and wide application range. The alloy coatings have high wear resistance, good corrosion resistance, good friction performance, high fatigue strength, high temperature resistance and other special properties, and have good practical value and wide application prospect. Widely used in mold, agricultural machinery, aerospace, nuclear industry, ships, turbines, electric drive and other industries, mechanical parts of the surface strengthening and local material addition manufacturing.

Usually, the surface layer carries the largest load and is affected by the external environment, so the surface performance directly determines the working life and

stability of the parts. Machine parts and components are worn from the surface, so to improve the performance of machines and machinery, it is necessary to improve the surface quality of parts. Through the application of special coatings, the most effective surface quality and component handling performance improvements are provided. To a large extent, the reliability of plain bearings depends on the quality of bearing manufacturing, coating application, installation and maintenance work. In the manufacturing process, there are always deviations from the ideal shape geometry; Additional errors are introduced during part installation, and the reduction of the actual contact area is the cause of the increased surface layer load, especially during running-in. With improved conditions and improved friction surface handling during later operation, it is possible to improve the bearing surface properties by coating with a soft metal by means of the electro-spark deposition (ESD) technique. Deformation of the soft coating (Ag, Cu, B83 or composite coating) under high loads provides the possibility of automatic part adjustment and compensation for manufacturing errors.

Therefore, the purpose of this work is to establish a functional coating of tin-bronze bearing by using environmental-friendly electro-spark deposition technology, to improve the surface properties, wear resistance and fatigue resistance of bearings, to reduce the wear between bearings and bearing bushes, and to improve the manufacturing quality, stability and durability of tin-bronze bearing bushes of rotating machines, which is of great significance to the development of the world economy.

Relationship with academic programs, plans, themes.

The dissertation is a fragment of scientific programs of research work of the Ministry of Education and Science of Ukraine "Scientific methodology of parts working

surfaces maintenance properties providing by energy-efficient environmentally friendly methods" (№ 0116U002756).

The purpose and objectives of the study. Ensuring the reliability and durability of the rotating mechanisms friction units by improving the tribosurfaces quality at commissioning stage the special running-in coating formation.

For the purpose were assigned the following tasks:

1. To analyze the manufacturing technology and features of the friction units operation;

2. To analyze structural and technological methods of increasing the reliability and durability of friction units;

3. Develop a system of directional selection of technological parameters for forming running-in coatings on various contact surfaces of friction units;

4. Establish correlation dependencies between equipment modes and quality parameters of the formed coatings;

5. To introduce the results of research into the practice of manufacturing friction units in the enterprise.

Object of research - Technological process of formation of functional coatings on the surface of elements of machines with bronze bushes for sliding bearings of rotating mechanisms.

Subject of research - The running-in coatings on the surface of tin bronze bushes that was formed by electro-spark deposition (ESD) applying the antifriction material of silver, copper, Babbitt B83 or graphene oxide (GO).

Research methods - The experimental research method is consisted to adapt existing technology for producing running-in coatings, based on the ESD method, to the working conditions, design and technological features of FU parts. Thus, there is a need for complex research aimed at definition the quality parameters of the formed surface layers (microstructure, microhardness, roughness, composition, nanoindentation and tribological properties): metallographic, durometer, X-ray structural research; definition of the surface layer topography; study of residual stresses and fatigue strength; research of wear resistance.

Scientific novelty of the obtained results.

1. For the first time, Tin bronze QSn10-1 is selected as the substrate material, and silver, copper, B83, GO are selected as the coating materials. The substrate and the coatings have a good metallurgical bonding, a new Ag_3Sn phase is formed, the grain size is refined, the surface hardness is reduced, and the friction coefficient is greatly reduced. It is very suitable for running-in coatings.

2. For the first time, according to the selected substrate material and coatings materials, the process parameters of electro-spark deposition were studied, and the equipment DZ-4000III was selected as the deposition equipment to find out the optimal electro-spark deposition parameters.

3. For the first time, the index evaluation system of electro-spark deposition coatings was established, the weight of each index was determined by entropy method, and the TOPSIS model was used to comprehensively evaluate different coatings.

The practical significance of the obtained results is to provide technical suggestions for the manufacture of tin bronze Bush of sliding bearing in rotating

machinery. Adapt to that technical cycle of sliding bearing in rotating machinery and the operating conditions of friction unit using tin bronze bushes for the rotating running of the core components.

Personal contribution of PhD.

Setting goals and objectives, discussing the results, forming conclusions were carried out together with the scientific supervisor. The author analyzed the literature and patent search on the topic of dissertation. Conducted experimental studies using modern methods Co-authors of scientific papers are the supervisor and scientists with whom the research was carried out. In scientific works published in co-authorship, the dissertation belongs to the actual material and the main creative work.

Publications. According to the results of research, 19 scientific papers were published, including: 4 articles in professional editions of Ukraine, 9 conferences, 2 patents; 4 articles - in foreign editions, which is in the Scopus or WOS scientific-metric publication, 1 methodical recommendation.

Structure and scope of the thesis. The dissertation is set out on 194 pages of computer text. It consists of an introduction, 4 sections, general conclusions, a list of sources used and 3 annexes. The main body of the dissertation is 129 pages of printed text. The work is illustrated with 30 tables, 52 figures. The list of references includes the name of 197 sources on 29 pages.

CHAPTER 1. LITERATURE REVIEW, THE PURPOSE AND THE TASKS OF RESEARCH

The electro-spark deposition (ESD) can be used as a surface strengthening method to strengthen the surface with the requirements of wear resistance, corrosion resistance and oxidation resistance, or to repair the surface through deposition, and also to prepare various special functional coatings [1-3].

1.1 The research on the mechanism of electro-spark deposition

Since the theory of electro-spark deposition was put forward in 1943, the new technology of electro-spark deposition has been developed rapidly [4-6]. With the development of the theory of electro-spark deposition, researchers have different views on the definition of this technology [7-9]. Some scholars believe that electro-spark deposition is a process of surface strengthening by direct use of high energy density of electric energy [10-12]. Through spark discharge, conductive materials as electrodes are infiltrated into the surface of metal workpieces to form alloyed surface deposits, which can improve the physical, chemical and mechanical properties of workpieces [13-15]. Another part of researchers connect the electric spark deposition with the traditional electric arc welding, and think that the electric spark deposition is a kind of pulse electric arc micro-welding technique, which utilizes the short time big electric current pulse produced by the electric capacity discharge to form the high temperature plasma arc with the temperature as high as 5000~25000℃, melting or vaporizing the electrode material and transiting to the work piece [16-18].

Researchers put forward two theories to explain the mechanism of electric spark deposition discharge. One is the principle of non-contact discharge, the other is the

principle of contact discharge [19]. The physical process of non-contact discharge is that the electric field strength increases when the electrodes are close to each other, when the distance is close enough, the gap between the electrode and the workpiece is broken down to generate spark discharge, through the discharge channel, the electron beam bombards the surface of the anode and converts into heat energy, the surface of the anode is heated and melted to generate metal droplets [20-22]. The droplets move from the front of the moving anode to the cathode and are heated in the process of separating from the anode, and the temperature rises until boiling and explosion occur, forming a large area of particle flow. The molten particles reach the cathode, adhere to the cathode and partially infiltrate into the surface of the cathode. The electrode moving behind these particles mechanically strikes the workpiece and moves upward away from the workpiece, leaving a layer of anode material on the cathode surface.

At the same time, some researchers also questioned the non-contact discharge theory, thinking that it cannot reasonably explain the discharge mechanism of electro-spark deposition, they think that under normal conditions, when the discharge voltage of electro-spark deposition cannot reach the air breakdown voltage, non-contact discharge mode is difficult to occur. For example, in iron cathode, the minimum breakdown voltage of air is 270V, while in electro-spark deposition, the bipolar voltage is less than 100V. Therefore, the theory of contact discharge is put forward, and the discharge process can be divided into three stages: (1) the formation stage of low voltage breakdown condition; (2) spark discharge stage; (3) separate that electrode from the workpiece. The condition of low voltage breakdown is that high current density is generated instantaneously under the condition of contact resistance discharge and the

energy is highly concentrated, so that thermal emission and thermal ionization are generated, the concentration of free electrons, ions and other charged particles between electrodes is greatly increased, the number of collisions between electrons and atoms or molecules meeting the requirement of gas breakdown is realized and the gas low voltage breakdown condition is formed.

In [23], the formation mechanism of micro-nano coating was described, the main reason for the improvement of hardness and wear resistance of cladding layer were analyzed. The addition of nanocrystalline hard phase and focused on the formation reason of nanocrystalline structure in micro-nano coating. The metal surface layer was quenched at ultra-high speed in the cladding process of rapid cooling and rapid heating.

In another report [24], the phenomenon of arc drift in spark discharge during the study of automatic strengthening of electric spark was observed and explained this phenomenon by using the principle of welding arc. But there are essential differences between welding arc and electric spark deposition arc. Welding arc is continuous discharge, but electric spark deposition arc is intermittent discharge controlled by high frequency pulse.

Single point gap discharge, single point contact discharge and continuous discharge with rotary electrode tests were conducted in order to study the discharge mechanism of electro-spark deposition with rotary electrode, as in research [25]. The results show that the medium between electrode and substrate can be broken down and result in gap discharge under certain voltage and gap conditions. Contact discharge mainly consists of two stages: short circuit discharge and gap discharge. During the discharge process, there exists not only non-contact discharge phenomena, but contact discharge and short

circuit discharge phenomena. Most of them are contact discharge phenomena.

At present, the research on the mechanism of electro-spark deposition is still continuing.

1.2 The research on the electro-spark deposition equipment

In 1944, the former Soviet Union made the world's first electric spark perforating machine according to the deposition process proposed by Lazarenko and his wife. In 1950, the former Soviet Union Central Institute of Electrical Science developed the yHP series of electro-spark deposition equipment and also developed the series of electro-spark deposition equipment. In 1964, the Institute of Applied Physics of the Academy of Sciences of Moldavia of the former Soviet Union developed 3H series equipment according to the theory of deposition technology of Lazarenko and his wife and widely used in industrial departments. The Kishinev Experimental Factory of the Institute of Applied Physics of the Academy of Sciences of Moldavia produced the new equipment for electro-spark deposition using thyristors and transistors in the 1970s which has greatly improved the quality of deposited layers and manual operability. According to records, in 1978 to 1979, the former Soviet Union used 37 such sedimentation equipment to save about 400000 rubles.

European and American countries began to study and use this deposition process in the 1950s and mostly used in mould parts while Japan began to study and use it in the 1960s. These devices are typically manually operated devices with a power of within 200W. After entering the 1990s, Japan's electro-spark deposition technology has been great development, they developed the SparkDepo deposition equipment power is bigger, can obtain a more uniform coating, coating thickness also increased a lot and the

current use of SparkDepo Model 300 electro-spark deposition equipment. ASAP (Advanced Surface and Processes Inc.) of the United States is the authority on the spark deposition, is the most advanced spark deposition system manufacturers and it has also the successful applied ESD to the aviation, marine, military, medical, automotive and food processing industries.

The research of electro-spark deposition technology in China started very early and the research of electro-spark deposition equipment began in the 1950s, but due to the theoretical knowledge and technical conditions at that time, this technology was not applied in a large area. In 1977, Suzhou Electro-machining Machine Tool Research Institute developed D9 series of deposition equipment which has been widely used in the deposition strengthening and surface repair of dies, measuring tools and mechanical parts and achieved good economic benefits. In the 1990s, with the progress of science, this enhancement technology has been further developed. Xi'an Qing'an Group Co Ltd of Aviation First Group has developed the ZS-116 type electro-spark deposition equipment which is characterized by a wide range of deposition current and can be used for a variety of electro-spark deposition processes. Some institutions of higher learning and scientific research units in China have done a great deal of work on the development of the deposition equipment and have developed a series of new-type electro-spark deposition equipment. For example, some scientific research units such as Tsinghua University have developed the pulse electric spark deposition equipment. Because a set of control circuit is designed on this series equipment, the discharge energy is greatly increased, thus the quality and thickness of the deposition layer are improved and the surface roughness is reduced. The Institute of Metal Research of

Chinese Academy of Sciences has developed the 3H-ES series of electric spark surface strengthening and repairing machine, high energy micro-arc pulse cold welding processing equipment which is characterized by small thermal effect, no deformation of the workpiece, metallurgical bonding between the deposit and the substrate and on-line surface deposition and repair, thus greatly saving production costs. At present, the DZ-4000III electric spark surfacing machine produced by the Institute of Surface Engineering Technology of China Academy of Agricultural Mechanization Science and Technology is widely used.

The electro-spark deposition equipment and the parameters (model, power, voltage, capacitance and frequency) are shown in Table 1.1and Figure 1.1.

Table 1.1 – The parameters of the electro-spark deposition equipment

Model	Power	Voltage (V)	Capacitance (μF)	Frequency (Hz)
Elitron22A	500W	15-70	360	---
Elitron52A	3500W	35-210	120-2040	---
Depo150	500W	50/100/150	---	60-1400
Depo300	2000W	50/100/150	---	60-2000
DZ-4000III	4000W	20-200	30-420	1300-6000
SZ08	1500W	20-100	---	50-500
SZHCS07	3800W	20-100	---	50-500
SW1500	1500W	20-100	---	50-500
VC400DHF	1500W	20-100	---	50-500

Figure 1.1 – The ESD equipment: a - Elitron22A; b - Elitron52A; c - Depo150; d - Depo300; e - SZ08; f - SZHCS07

1.3 The research on the electro-spark deposition process

The equipment and process of electro-spark deposition have a significant impact on the efficiency and quality of deposition [26-28]. There are many process parameters affecting the electro-spark deposition which are systematically studied and classified as follows:

(1) Electrode and its movement. Electrode materials (material composition, density,

microstructure), manufacturing technology (machining, powder metallurgy, 3D printing), shape, speed of movement, specific deposition time, contact force, cycle times, deposition angle and so on [29-31]. According to the application, the electrode materials used can be divided into three categories [32-34]. The first is wear resistance material that include hard carbides (carbides of W, Ti, Cr, Ta, Mo, Hf, Zr, Nb, V, etc.), hardfacing alloys (Stellite, high nickel chromium alloy), Ti, Zr, Ta and other borides, intermetallic compounds and cermets [35-37]. The second is corrosion resistance material that include stainless steel, special alloys (Hastelloy, Inconel, etc.), intermetallic compounds of Fe, Ni and Ti with Al, multicomponent alloys FeCrAlY, NiCrAlY, CoCrAlY [38-40]. The third is repair or modification material that include nickel-based or cobalt-based superalloy, noble metals such as Au, Ag, Pt, Ir, Pd and Rh, refractory metal such as W, Mo, Ta, Re, Nb and Hf and alloys thereof and alloys of Fe, Ni, Cr, Co, Al, Ti, Cu, Zr, Zn, V, Sn and Er [41-43]. Because the electrical resistivity, melting heat, thermal conductivity, ductility, wetting angle and other characteristics of materials are very different and considering the instability of the electro-spark deposition process, the influence of process parameters on the preparation and performance of coatings is uncertain.

(2) Substrate material. Material, surface roughness, cleanliness, shape, temperature [44-46].

(3) Power supply. Electric spark energy and frequency, voltage, current, capacitance, discharge time of electric spark, inductance [47-49].

(4) Environment. Gas or liquid composition, fluid properties, gas flow rate and mode, temperature [50-52].

(5) Electro-spark deposition composite process. Sometimes it cannot achieve the desired effect by using a single electro-spark deposition technology for deposition, some scholars combine the electro-spark deposition technology with other processes to achieve better results [53-55]. And other process combined with that electro-spark deposition technology include magnetron sputter, ultrasonic treatment, laser treatment, chemical heat treatment, shot peening treatment and rolling treatment [56-58].

The research scope of electro-spark deposition by scholars is narrow and the thickness of deposition layer is often used as the basis for evaluating performance and selecting process parameters [59-61]. And the research of electro-spark deposition mostly focused on how to determine the relationship between process parameters and deposit thickness and how to increase the deposit thickness, and the research of deposition process parameters mainly focused on the limited ceramic or cemented carbide deposition materials, spark capacitance, voltage, frequency and specific deposition time [62-64]. There are obvious deficiencies in the research of deposition materials, electrode motion and automatic control.

In [65], NiCrAlY coatings with different Al contents on GH4169 superalloy by electro-spark deposition were prepared. There was a coating thickness limit for the NiCrAlY coating with high Al content. The coating thickness could be further increased by coating again after annealing treatment. The low aluminum content NiCrAlY coating was not applied to the limit thickness after being applied to the 130 layers. Different element content of the alloy coating on the thickness of the coating is also a great impact.

In another paper [66], a new method of ESD is proposed to improve the wear

resistance of copper alloysurface. The results show that the coating is mainly composed of TiN hard phase with a thickness of about 85 μm. The microhardness of the coating can reach 890 $HV_{0.05}$, which is about 4.8 times of the substrate (185 $HV_{0.05}$). The friction coefficient of the coating is 0.125-0.2, which is much smaller than that of the substrate (0.23-0.35) and the fluctuation is small. The wear rate of the TiN coating is about 49.6% of that of the substrate.

In other work [67], electro-spark deposition process was used to prepare the Mo_2FeB_2-based cermet coatings in Ar and in air. The coating prepared in Ar has better wear resistance, whose wear mass is about 1/7 that of the coating produced in air. The abrasion mechanism of the two coatings is fatigue wear and abrasive wear and the coating produced in Ar is mainly fatigue wear, whereas the coating prepared in air is primarily abrasive wear.

In [68], In order to investigate the effects of pulse energy on microstructure and properties of Mo^2FeB^2-based ceramet coatings, three kinds of coatings were prepared under different pulse energy (1.35 J, 6.41 J and 17.81 J) by electro-spark deposition. The results show that all the coatings are consisted of amorphous, martensite and Fe_3B. The coating deposited at pulse energy of 6.41 J has a maximum peak microhardness of 1395 $HV_{0.05}$, the minimum mean friction coefficient (0.313) in the steady state and the minimum wear mass (0.7mg) after 1h of abrasion, indicating its better friction and wear performance.

In the present study [69], the effects of process parameters (voltage, nitrogen flux and specific strengthening time) on the microstructure and wear resistance properties of TiN coatings prepared by electro-spark deposition (ESD) were investigated

systematically. The results show that the variation of wear mass loss by the variation of the voltage and nitrogen flux is attributed to the change of wear mechanisms of TiN coatings. The main wear mechanism of TiN coating prepared under optimal process parameters is micro-cutting wear accompanied by micro-fracture wear.

The most recently [70], aiming at the defects such as pores, microcracks, loose surface structure, poor continuity and poor surface quality in the ESD layer, a machining method of "ESD-remelting and rolling" was proposed. The results show that the electrode has great extrusion and rolling effect on the deposited surface during remelting and rolling. Remelting and rolling can effectively eliminate the defects such as pores, microcracks and loose microstructure in the sediment layer.

In order to determine the temperature field of WC-12Co coating, mathematical model of heat conduction was established by utilizing suitable heat source and the thermal boundary conditions [71]. Numerical simulation was carried out by commercial finite element code ANSYS, and iso-surface, the temperature distribution curve and temperature variation curve were derived. The areas of melting and gasification zone were measured by setting of contour lines of temperature field. Furthermore, the influence of process parameters on the areas of melting and gasification zone was researched and the optimized process parameters were predicted. To verify the prediction, electro spark deposition experiments were carried out and the optimized process parameters were determined.

Through the optimization of different process parameters, analysis of the various parameters on the deposition layer quality and deposition efficiency to obtain stable and reliable process parameters in order to achieve quality and efficiency of double

excellent is one of the research directions of the electro-spark deposition process scholars and experts.

1.4 The research on the surface characteristics of electro-spark deposition

Electro-spark deposition technology can effectively improve the physical and chemical properties, mechanical properties and tribological properties of the surface, so that the surface has high hardness, high wear resistance, high fatigue strength, high corrosion resistance and oxidation resistance, high temperature resistance, ablation resistance and other special properties [72-74].

The composite coatings of the tin bronze surface that was formed by alternately ESD applying the soft antifriction material of silver, copper and babbitt B83. The investigation of the tribological properties of the coatings in dry friction show that the lower resistance is exhibited by the composite coatings deposited using the soft antifriction material. The surface friction coefficient of the composite coatings is 55.6% of the tin bronze substrate. The surfaces of wear traces were analysed in order to understand the friction and wear resistance mechanisms of the coatings. The wear scars of the tin bronze substrate with and without the soft antifriction composite coatings after tribological testing are shown in Figure 1.2 and Figure 1.3. It was found from analysis of wear scars in Figure 1.2 that the wear mechanism of the tin bronze substrate is dominated by severe ploughing wear and fatigue delamination. A lamellar structure can be distinguished on the surface of the worn tin bronze substrate. This can be responsible for low friction under these conditions. However, it can be seen in Figure 1.3 that the soft antifriction composite coatings may effectively restrain fatigue delamination, showing plastic deformation and slight polishing. Plastic deformation dominated on the

relatively soft composite coatings. The initial surface microgeometry was changed during load application and its surface became smooth with fine shallow scratches observed after the wear test. After the smooth surface was formed, the friction and wear stabilized.
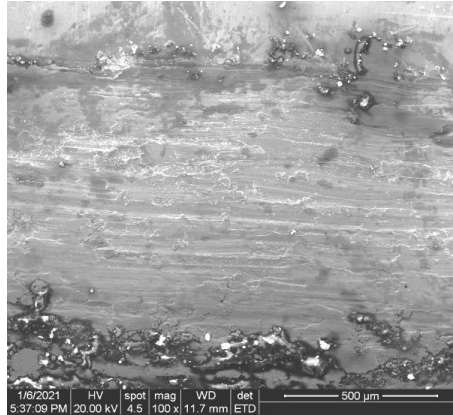

Figure 1.2 –The wear scars of the tin bronze substrate after tribological testing
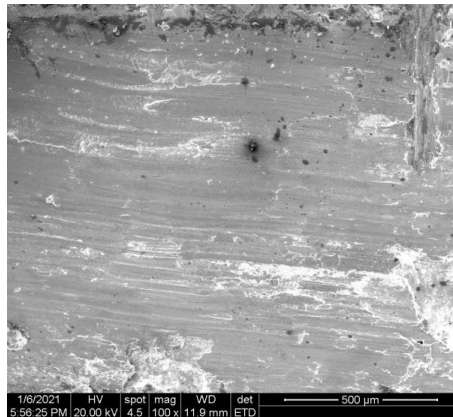
Figure 1.3 –The wear scars of the tin bronze substrate with the composite coatings after tribological testing

In [75], indium, tin, copper and silver soft wear-resistant coatings were deposited on the axial surface of Babbitt alloy by electro-spark deposition technology, which can reduce the requirements for the assembly standards of friction units and reduce the formation of SnSb crystals on the surface of Babbitt alloy.

In other research [76], a new method was proposed to improve the surface properties of titanium alloy TC4 by synthesizing TiN coating with flexible titanium

electrode. In that process, the flexible titanium electrode and the titanium alloy TC4 surface are subjected to electric spark discharge, nitrogen is introduced into a processing area through the interior of the titanium electrode at the same time, and the TiN coating is generated on the surface of a workpiece by utilizing the electro spark discharge energy. The results show that the TiN strengthening coating is prepared on the surface of TC4 workpiece and the coating is compact, uniform and continuous.

WC-Cu coating was deposited on the surface of C45 carbon steel by using laser technology and electro-spark deposition technology and good anti-corrosion effect was obtained [77].

In another report [78], the tribological properties of electro-spark deposited bronze were studied, Molybdenum, chromium, composite T15K6 and bronze on C45 steel under boundary lubrication conditions. The results showed that the molybdenum coating was the most stable, but the bronze coating had a lower friction coefficient in low load applications.

In more recent work [79], it was found that a metallic glass coating was uniformly formed on the stainless steel substrate. The samples with optimized coating were shown to exert lower cytotoxicity, better cell attachment, and higher blood compatibility than the stainless steel substrates.

In other work [80], the impact of laser modification on the morphology and mechanical properties of carbide/copper coatings produced by electro-spark treatment was analyzed. The laser beam machining of ESD coatings led to the homogenization of chemical composition, fragmentation of the structure, and elimination of microcracks. Laser processing proved to have a positive effect on improving the adhesion of coatings

and reducing their porosity. This paper also presents a simulation model of heat transfer processes for the case of laser radiation impact on a WC-Cu coating. The developed numerical model, describing the influence of laser treatment on the distribution of temperature fields in the heated material (at a given depth) is of significant importance in the development of treatment technologies. Laser-modified ESD coatings perform anti-wear and protective functions, which enable their potential application in means of transport such as rolling stock.

1.5 The future research direction of the ESD deposition technology

The electro-spark deposition technology is a new technology with special strengthening effect and unique technical value which has great potential in the future. The application of electro-spark deposition in the prevention, protection and repair of surface coatings has obvious effect on improving production efficiency and reducing cost [81-83].

At present, the scientific research worker has done the massive research work in the electro-spark deposition technology mechanism research, equipment development and application and has obtained many research results, but along with the modern industry development of the high speed and heavy load, the mechanical components service condition is worse, the surface damage form and the degree are complex serious day by day [84-86]. Electro-spark deposition technology needs to be applied in a wide range. But the problem of thin deposition layer, large surface roughness, low deposition efficiency, poor process stability and reliability also need to be solved [87-89]. The existence of these problems greatly limits the expansion of the application field of this technology, so the future research direction of electro-spark deposition technology will

mainly focus on the following aspects:

(1) To strengthen the research on the mechanism of electro-spark deposition technology which will play an important role in guiding the basic research, equipment manufacturing and application development of ESD. At present, the existing mechanism of electro-spark deposition still has great limitations, including the mechanism of electro-spark deposition discharge and electrode material transfer mechanism. Scholars have not yet reached a unified conclusion on this which requires researchers to further overcome the difficulties and form a complete theoretical system as soon as possible to support the promotion and application of electro-spark deposition technology [90-92].

(2) The new types of electro-spark deposition automatic equipment are needed to develop and improve the quality and stability of the coating and the deposition efficiency.

(3) Strengthen the research of ESD process parameters. The strengthening process of different electrode and matrix materials, multi-electrode strengthening process, the strengthening process of multi-electrode materials on the same surface and composite strengthening process were studied [82, 93, 94].

(4) The research of coating materials is mainly focused on cemented carbide and ceramic materials, but other materials with excellent performance are also worth to be studied.

(5) Combining other technologies with the electro-spark deposition technology and developing the composite treatment technology to prepare the deposits with excellent performance may become the preferred process in the process of the development of this technology [95-97]. Electro-spark deposition technology combines with ultrasonic

technology, nano-technology, laser technology, plasma technology, magnetron sputtering, chemical heat treatment, thermal spraying, electroplating, brush plating, chemical plating, physical meteorology deposition, ion implantation and other technical means to deposit coatings with better performance. Electro-spark deposition technology combines with computer simulation, artificial neural network, fuzzy control, expert system, intelligent control, pattern recognition, genetic algorithm, ant colony algorithm, particle swarm algorithm and other advanced technologies to promote the continuous progress of electro-spark technology.

1.6 The purpose and the tasks of the research

The purpose of the research is ensuring the reliability and durability of the rotating mechanisms friction units by improving the tribosurfaces quality at commissioning stage the special running-in coating formation.

To achieve this goal, it is necessary to solve the following **tasks:**

1. To analyze the manufacturing technology and features of the friction units operation;

2. To analyze structural and technological methods of increasing the reliability and durability of friction units;

3. Develop a system of directional selection of technological parameters for forming running-in coatings on various contact surfaces of friction units;

4. Establish correlation dependencies between equipment modes and quality parameters of the formed coatings;

5. To introduce the results of research into the practice of manufacturing friction units in the enterprise.

CHAPTER 2. BASIC THEORY AND METHODOLOGY OF RESEARCH

The experimental research was consisted of adapt existing technology for producing coatings, based on the ESD method, to the working conditions, design and technological features of bearing bush.

2.1 The basic principle of electro-spark deposition (ESD) technology

The electro-spark deposition (ESD) technology is that the material to be deposited is used as the electrode, the electrode is operated on the surface of the substrate, the pulse frequency of the power supply is 100Hz-6000Hz and a high-density current (10^5-10^6A/cm2) is instantaneously (10^{-6} to 10^{-5}s) passed through the power supply, produce high temperature of 5000 ~ 25000°C in a very small scope, make the material in the discharge area ionize with high energy, the electrode transfers to the surface of the substrate at a high speed and diffuses to the surface of the substrate, thus forms the deposit coating with metallurgy combination (Figure 2.1) [98-100]. The process can really realize the metallurgical bonding of the coating and the substrate and simultaneously can keep the temperature of the substrate at room temperature and prevent the thermal deformation of the substrate metal [101-103]. This process can be used not only for the repair of local areas of parts, but also for surface coating. The thickness of a single layer of deposited metal is limit, the electro-spark deposition is carried out again and again on the previous deposited layer, and finally a deposited layer with a certain thickness is obtained [104-106]. Because the electric spark discharge of the latter deposit layer will make the former deposit metal re-melt, and the micro-cracks in its surface layer will also be eliminated, so only the last surface deposit layer has micro-cracks. At the end of deposition, the deposited layer is slightly higher than the

required size of the workpiece, and the remaining layer can be grinded to eliminate the micro-cracks on the surface layer.
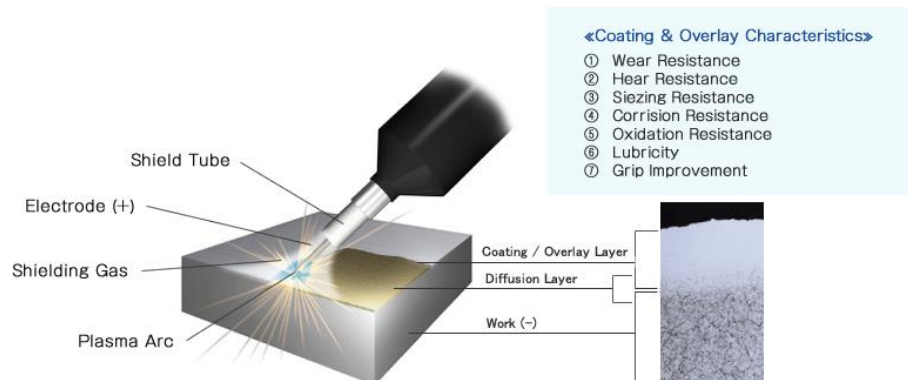

Figure 2.1 – Electro-spark deposition technologies

The electro-spark deposition technology can effectively improve the physical and chemical properties, mechanical properties and tribological properties of the surface of mechanical parts, so that the surface of mechanical parts has high hardness, high wear resistance, high fatigue strength, high corrosion resistance and oxidation resistance, high temperature resistance, ablation resistance and other special properties. Widely used in tools, molds, cutting tools, agricultural machinery, military, medicine, automotive, food, mining, metallurgy, aerospace, nuclear industry, marine vessels, turbines, electric power generation, electrical transmission and other industries of mechanical parts of the surface strengthening and the surface repair of failure parts, especially for precision parts of the surface strengthening and local material addition manufacturing. Compared with other surface treatment technologies, electro-spark deposition has the following advantages.

(1) No temperature rise or very low temperature rise in parts, no change in organizational structure and performance, parts will not anneal and deform.

(2) Fast heating and rapid cooling can easily obtain fine crystal and even

amorphous structure. When the material is heated and cooled rapidly, it is easy to obtain fine grain structure, even amorphous structure under high temperature gradient, so as to improve the mechanical properties, wear resistance and corrosion resistance of the material surface.

(3) The ESD coating and the substrate are metallurgically bonded and the bonding strength is high.

(4) The ESD coating is dense and has good uniformity.

(5) Only a small amount of pre-treatment and post-treatment is needed and sometimes even no need. The final machining allowance of the deposited layer is small and the subsequent machining cost of a workpiece is saved.

(6) The ESD device is simple and convenient to carry and operate. It is suitable for online repair (good equipment mobility), which is very important for the repair of large workpieces or online equipment.

(7) Wide application range, suitable for all conductive, fusible metal and ceramic materials.

(8) The surface of the deposition layer is orange peel-like with a large number of tiny pores and pits, which is quite beneficial to the lubrication of the workpiece.

(9) There are some other advantages of electro-spark deposition, such as economic and practical, safe and environmental protection, easy to automate. It can be used in places that can't be seen, such as inner holes and grooves of parts.

However, there are also some shortcomings in the process, such as thin surface layer (generally less than 1 mm), slow deposition rate and low efficiency, so it is not suitable for large area and complex surface [3, 107, 108].

The electro-spark deposition technology can make the surface have high hardness, high wear resistance, high fatigue strength, high corrosion resistance and oxidation resistance, high temperature resistance, ablation resistance and other special properties [92, 109, 110]. It is believed that with the development of this new surface treatment technology, more and more people will devote themselves to the research of this technology and this technology will be widely used and play an important role in surface treatment. The research on the new technology of electro-spark deposition is an innovative and challenging research work which not only enriches the connotation of electro-spark deposition, but also has great significance for improving the processing and application level of advanced composite materials [111-113].

2.2 Properties investigation

The mass transfer data were constructed in weighing the specimens on a Mettler Toledo AL204 balance with an accuracy of 0.1 mg.

Surface roughness and topography measurements were made using 3D optical profilometers of Bruker Contour GT-k1.

Samples for the microstructural analysis were prepared from the cross sections of the running-in coatings block and mounted in bakelite. After polishing and cleaning, in order to reveal elements of the granular structure, the surfaces of the samples were subjected to etching with 4% nitric acid alcohol and exposure time of 10s. ESD treated surface morphology, cross section morphology and wear scars of the running-in coatings were analysed using scanning electron microscopy (SEM) of FEI Quanta 200 and metallographic microscopy LECIA DMi8 M. The element composition on the surface and the cross section of the coatings were characterized by energy dispersion

spectrum (EDS) built into SEM.

The phase composition of the coatings under investigation was analyzed by X-ray diffraction method using a D8 Advance A25 of Bruker X-ray diffractometer in Cu-Kα radiation.

The micro-hardness of the composite coatings was determined by a VHL VMH-002V Vickers indenter. The micro-hardness measurements were conducted at a load of 10g with a dwell time of 12s.

The nanoindentation properties of the running-in coatings were determined by a Nano Indenter G200 of KLA-Tencor. The nanoindentation measurements were conducted at a load of 500mN with a dwell time of 1s.

An assessment of tribological properties was performed in the ball-on-plate reciprocating rig on the MWF-500 tribometer. The study is to investigate tribological properties of ESD layers under dry friction conditions. The test temperature was 25°C. The low sliding velocity of 20mm/s was chosen to ensure boundary lubricating conditions and was maintained constant for all the stripes. The track length was 6 mm. The 8 mm diameter bearing steel (GCr15) ball was used as counter-face. The applied loads were 5N, 10N and 15N. For the initial 600 seconds, the applied load was 5N, the following 600 seconds, have more load of 10N, and then to 15N for the final 600 seconds.

2.3 Evaluation methods

In this research, multi-attribute decision-making methods of Shannon's Entropy and TOPSIS have been used as quantitative attitude in the assessment of the characterization of the coatings by electro-spark deposition.

2.3.1 Construction of the characterization indicators system of the coatings

On the basis of analyzing and sorting out the characterization indicators system of relevant scholars and institutions, according to the connotation requirements of the coatings by electro-spark deposition, combined with the availability of data, according to the four principles of scientific, systematic, practical and operational, 6 indicators are selected. The indicators system of influencing factors of the characterization of the coatings by electro-spark deposition is constructed in Table 2.1.

Table 2.1 – The indicator system of the comprehensive evaluation of the characterization of the coatings

Target	Indicators	Unit	Attribute
The comprehensive assessment of the characterization of the coatings	Material price C_1	Yuan	negative
	Time C_2	min	negative
	Mass Transfer C_3	mg	positive
	Roughness C_4	μm	negative
	Thickness C_5	μm	positive
	Friction coefficient C_6	/	negative

It can be seen from Table 2.1 that the factors affecting the characterization of the coatings by electro-spark deposition include material price, time, mass transfer, roughness, thickness and friction coefficient, which constitute the six decision-making of the indicators system. The selection basis of each aspect is described as follows.

(1) Material price

Almost any conductive material can be used as an electrode for electro-spark deposition, but the price of different materials varies widely. The price of the deposited material has a great influence on the cost of the deposited coating. Researchers need to find cheaper materials to achieve better performance.

(2) Time

A single discharge formed a very small discharge micro area, the material melting amount is less, and the electro-spark deposition process is accompanied by the erosion of workpiece material, resulting in a long deposition time, low deposition efficiency. In addition, current electro-spark deposition equipment is mostly hand-held, and manual operation under low efficiency increases labor intensity. Therefore, the deposition time is a very important factor of electro-spark deposition.

(3) Mass transfer

The electro-spark deposition running-in coatings are the result of gradual accumulation through multiple discharge and a large number of deposition points. The mass transfer is usually regarded as an important index to evaluate ESD [114-116]. At the beginning of deposition, the coating mass increases most obviously. With the increase of deposition time, the mass transfer of electrode to substrate gradually decreases. Finally, with the increase of deposition time, the mass of substrate stops increasing. This is because with the increase of deposition time, the content of oxide or nitride on the surface of the coating increases, the residual stress on the surface increases, the binding force decreases, and the material is more likely to splash during discharge, which impedes the mass transfer in the process of ESD [117-119].

(4) Roughness

Surface roughness has a great influence on the use of parts. Generally speaking, the surface roughness value is small, will improve the fit quality, reduce wear, prolong the service life of parts and the rougher the surface, the smaller the effective contact area between the mating surfaces, the greater the pressure, the greater the friction resistance, the faster the wear [120-122].

The surface roughness of the running-in coatings is not only affected by the deposition parameters, but also affected by the operation technology, the mechanical accuracy of the welding torch and the properties of the deposited materials.

(5) Thickness

The thickness of the running-in coatings is one the most important index of ESD. If the coating thickness is too small, the coating is easy to wear off, cannot play a running-in coating special performance. If the coating thickness is small, in strict working conditions (high speed and high specific pressure) run-in, bearing face may appear scratches.

(6) Friction coefficient

Electro-spark deposition technology can effectively change the surface of the physical and chemical properties, mechanical properties, so that the friction coefficient of the surface changes [123-125].

The friction coefficient of the deposited layer has an important influence on the practical application prospect of the workpiece, so a small friction coefficient should be selected. Material friction resistance should be relatively small, otherwise it will produce large friction power consumption.

2.3.2 Entropy method

Entropy used to be a thermodynamic concept: it was introduced into information theory in 1948 by C. E. Shannon who put forward the concept of information entropy to measure the level of system chaos or disorder [126-128]. Shannon information entropy, which is an objective and applicable method for the determination of weight value, was introduced into the comprehensive assessment [129-131]. In the application of the

Shannon information entropy method, the greater entropy weight indicates greater variation extent of relevant index, which enables much more information and has a greater effect [132-134]. The information entropy can clearly reveal the utility of each indicator and avoid the interference of subjective factors, which ensures that it is more objective and credible than the subjective methods for comprehensive evaluation of multivariate index.

The principles of the entropy method are as follows:

(1) Construct the original decision matrix

According to the original data, the indicators are taken as an $m \times n$ matrix, where m is defined as the number of evaluation objects and n indicates the number of indicators.

The performance matrix can be presented as follows:

$$X = \begin{bmatrix} x_{11} & x_{12} & \cdots & x_{1n} \\ \cdots & \cdots & \cdots & \cdots \\ \cdots & \cdots & \cdots & \cdots \\ x_{m1} & x_{m2} & \cdots & x_{mn} \end{bmatrix} \tag{2.1}$$

(2) Data normalization

It denotes that there are schemes and indicators in the research plan. Taking into account its differences in dimension and magnitude, the original data cannot be directly used for assessment. After collection of the original data, the process of data normalization is necessary. Based on appraisal target characteristics, the indicators are divided into two categories: the positive type and the negative type. The positive type indicators are the indicators for which bigger values are better. The negative type indicators refer to the indicators for which smaller values are better.

When x_{ij} is the positive indicator, the normalized value S_{ij} can be calculated as Equation (2.2):

$$S_{ij} = \frac{x_{ij} - \min x_{ij}}{\max x_{ij} - \min x_{ij}} \tag{2.2}$$

When x_{ij} is the negative indicator, the normalized value S_{ij} can be calculated as Equation (2.3):

$$S_{ij} = \frac{\max x_{ij} - x_{ij}}{\max x_{ij} - \min x_{ij}} \tag{2.3}$$

where x_{ij} is the value of the jth indicator of the ith object. $\max x_{ij}$ and $\min x_{ij}$ denote the maximum and minimum values of the jth indicator, respectively.

(3) Calculation of the entropy value of the indicators

To calculate the entropy value of each indicator, the standardized value of indicator j for object i must first be calculated, and is written as Equation (2.4):

$$p_{ij} = \frac{S_{ij}}{\sum\limits_{i=1}^{m} S_{ij}} \tag{2.4}$$

Then, calculate the entropy value of the indicator by the following Equation (2.5):

$$e_j = -\frac{1}{Inm} \sum\limits_{i=1}^{m} p_{ij} In p_{ij} \tag{2.5}$$

(4) Calculate the indicator weight

To calculate the weighting value of each indicator, the information utility value of indicator must first be calculated, and is written as Equation (2.6):

$$d_j = 1 - e_j \tag{2.6}$$

The weighting value of the jth indicator is defined as Equation (2.7):

$$w_j = \frac{d_j}{\sum\limits_{j=1}^{n} d_j} \tag{2.7}$$

2.3.3 TOPSIS model

The TOPSIS method (Technique for Order Preference by Similarity to an Ideal Solution) was first proposed by C.L. Hwang and K. Yoon in 1981. It is an ordering method based on the degree of closeness between limited appraisal objects and

idealization objects, and it is a kind of relative advantages and disadvantages evaluation in the existing appraisal objects [135-137]. It is a comprehensive evaluation based on distance and is widely used for multiple attribute decision making [138-140]. This model can objectively and comprehensively reflect the characterization of the coatings by calculating the closeness degree between an evaluation value and its ideal solution. Specific steps are as follows:

(1) Construct the weighted standardized matrix

The weighted standardized matrix is established as Equation (2.8):

$$a_{ij} = w_j \bullet p_{ij}(i = 1, 2, \cdots, m; j = 1, 2, \cdots, n) \qquad (2.8)$$

(2) Determine the positive ideal solution and the negative ideal solution

The positive ideal solution and the negative ideal solution are two basic concepts in the TOPSIS method. The positive ideal solution is supposed as the optimal solution, all attribute values of which achieve the best value in all schemes. The negative ideal solution is supposed as the worst solution, all attribute values of which achieve the worst value.

In the step, the positive ideal solution A^+ and the negative ideal solution A^- were obtained.

$$A^+ = \left\{\max A_{ij} \mid i=1, 2,\cdots, m\right\} = \left\{A_1^+, A_2^+, \cdots, A_n^+\right\} \qquad (2.9)$$

$$A^- = \left\{\min A_{ij} \mid i=1, 2,\cdots, m\right\} = \left\{A_1^-, A_2^-, \cdots, A_n^-\right\} \qquad (2.10)$$

(3) Calculate the distance

Calculate the Euclidean distance D_i^+ between the evaluation value and the best solution A_j^+, and the Euclidean distance D_i^- between the evaluation value and the worst solution A_j^-:

$$D_i^+ = \sqrt{\sum_{j=1}^{n}\left(A_j^+ - A_{ij}\right)^2}\ (i=1,2,\cdots,m) \tag{2.11}$$

$$D_i^- = \sqrt{\sum_{j=1}^{n}\left(A_j^- - A_{ij}\right)^2}\ (i=1,2,\cdots,m) \tag{2.12}$$

(4) Calculate the relative closeness

To compare the distance between the evaluation value and two ideal solutions, calculate the relative closeness of the object *i* using Equation (2.13):

$$C_i = \frac{D_i^-}{D_i^+ + D_i^-}\ (i=1,2,\cdots,m) \tag{2.13}$$

The value of relative closeness reflects the relative superiority of the alternatives. Larger C_i indicates that the alternative *i* is relatively better, whereas smaller C_i indicates this alternative is relatively poorer.

2.4 The experiment materials

(1) The substrate material

The substrate material is tin bronze QSn10-1 commonly used bearing material provided by Zhejiang Shenfa Bearing Co., LTD. The material QSn10-1(Cu 89.10%, Sn 9.38%, P 0.72%, Others 0.80%) was cut into size 25mm * 29mm * 4mm as the substrate by electro-spark CNC wire-cutting machine DK77-40.

The surfaces of the substrates were ground on silicon carbide grinding papers of different grain size (400, 600, 800, 1200 and 1500 grit) by Rotary swing gravity grinding and polishing machine ZYP300 and the roughness of the surface is not greater than 1μm (Figure 2.2). Before coatings deposition, the substrates were cleaned in anhydrous ethanol with an ultrasonic cleaning machine for 20 minutes to remove the oil and impurities on the surface, and the substrate was dried with a hair dryer, and then the weight of the substrate was weighed by an electronic balance.

Figure 2.2 – grinding and polishing

(2) The electrodes materials

Silver (Ag 99.99%), copper (Cu 99.99%) and Babbitt B83 (SnSb11Cu6, Sn 83.10%, Sb 11.02%, Cu 5.83%, Others 0.05%) materials were used to make 3mm in diameter for electro-spark deposition electrodes, respectively (Figure 2.3). Graphene oxide was a dispersible solution of 4mg/ml with water as the solvent. The surfaces of the electrodes were ground on silicon carbide grinding papers of different grain size (400, 600, 800, 1200 and 1500 grit) and the roughness of the surface is not greater than 1μm. Prior to deposition of the coatings, the electrodes were cleaned in anhydrous ethanol for 20 minutes by ultrasonic cleaner, removed grease and impurities on the surface, and dry the substrates with a hair dryer.

Figure 2.3 – Electrodes bar

2.5 Experiment equipment

The experimental equipment: electro-spark CNC wire-cutting machine DK77-40, Rotary swing gravity grinding and polishing machine ZYP300, Electro-Spark Deposition machine DZ-4000III, optical microscope Leica DM2500M, ultrasonic cleaner PS-20, metallographic cutter TQG250 of TIME, pointing machine XQ-1.

The analyses of deposition on mass transfer, roughness, thickness, morphology, composition, Vickers hardness, nanoindentation and tribological properties of the coatings were investigated by electronicscales AL204 of Mettler Toledo, 3D optical profilometers GT-k1, scanning electron microscopy (SEM) with energy dispersion spectrum (EDS) Quanta 200, metallographic microscopy Lecia DMi8 M, X-ray diffractometer (XRD) D8 Advance A25, Vickers Microhardness tester VMH-002V of UHL, Nano Indenter G200 and MWF-500 tribometer.

(1) The Electro-Spark Deposition machine

The Electro-Spark Deposition machine DZ-4000III has a control panel to change the electrical parameters including ESD voltage, capacitance and frequency (Figure 2.4). The ESD machine has the ground attachment, the shielding gas outlet and he applicator attachment. The rotation speed and direction can be controlled on the applicator, shielding gas is Argon gas. The parameters range of the Electro-Spark Deposition machine DZ-4000III was shown in Table 2.2.

The measurement error of output voltage is $\pm$ 1%.

The measurement error of discharge frequency is $\pm$ 1%.

Figure 2.4 – The ESD machine DZ-4000III

Table 2.2 – The Electro-Spark Deposition machine DZ-4000III parameter range

Parameter	Power	Voltage	Capacitance	Frequency	rotation speed
Range	4000W	20V-250V	30-420μF	1300Hz-6000Hz	2600r/min

(2) The 3D optical profilometers

The 3D Optical Profilometers model is Bruker Contour GT-k1 (Figure 2.5). The Contour GT-k1 is a stand-alone optical surface-profiling system in its standard-footprint configuration. It measures surface topography with high accuracy in a range from fractions of a nm up to approximately 10mm. The system contains motorized x/y, tip/tilt and z stages to enable automated production monitoring. Magnification selection is also motorized so complex measurement sequences can be programmed. Additional capability is offered to enable continuous calibration, film measurements and field-of-view stitching (to extend the effective measurement area).
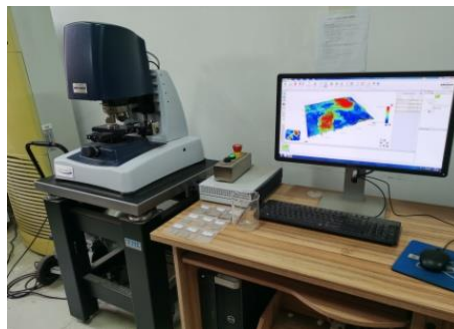
The vertical measurement error of the device is ± 3nm.

Figure 2.5 – The 3D Optical Profilometers GT-k1

(3) The Metallographic microscope

The metallographic microscope model is Lecia DMi8 M (Figure 2.6). Leica Microsystems introduces the modular Leica DMi8 inverted microscope platform for industrial applications. Sample preparation for the inverted microscope is less time-consuming as compared to upright microscopes. The microscope's optics are located below the stage, which offers the advantage of accommodating large sample sizes. The stage carries up to 30 kg in weight and sample height is not restricted. Leica Microsystems' exclusive macro objective for the Leica DMi8 offer a field of view of 35 mm. This is four times more than a standard objective. To see even more details of the sample surface in high contrast, users can also use the new Ultra Contrast 3D Illumination, another Leica Microsystems exclusive technology.

Figure 2.6 – The metallographic microscope

(4) The scanning electron microscopy (SEM)

The Scanning electron microscopy (SEM) model is Quanta 200 of FEI (Figure 2.7). The Quanta 200 Scanning Electron Microscope is a flexible, general purpose, simple-to-use instrument that can be operated in either regular high-vacuum or low-vacuum modes, enabling users to image a wide variety of samples.

The electron beam in this instrument is generated by a conventional tungsten filament electron source, which, under optimal conditions, is capable of resolving

features as small as 3 nm. The Quanta is equipped with standard Secondary Electron (SE) and Back Scatter Electron (BSE) detectors, in addition to an Energy Dispersion Spectrum (EDS) detector and an internal TV camera.

Figure 2.7 – The SEM equipment

(5) The X-ray diffractometer (XRD)

The X-ray diffractometer (XRD) model is D8 Advance A25 of Bruker (Figure 2.8). The D8 ADVANCE is based on the unique D8 diffractometer family platform and is perfectly designed for all X-ray powder diffraction and scattering applications including: traditional X-ray powder diffraction (XRD), Pair Distribution Function (PDF) analysis, small and wide angle X-ray scattering. The minimum step angle of the device is 0.0001°.

Analysis of thin films and coatings is based on the same principles of XRPD, but with further beam conditioning and angular control. Typical examples include, but are not limited to, phase identification, crystalline quality, residual stress, texture analysis, thickness determination and composition vs strain analysis. Analysis of thin films and coatings is focusing on properties of layered materials with nm to μm thickness, ranging from amorphous and poly-crystalline coatings to epitaxially grown films. The D8 ADVANCE and the DIFFRAC.SUITE software enable high quality analyses of thin films including: Grazing incidence diffraction, X-Ray Reflectometry, High resolution

X-ray diffraction and Reciprocal space mapping.

Figure 2.8 – The X-ray diffractometer (XRD)

(6) The Microhardness tester

The Microhardness tester model is VMH-002V of Walter UHL technische Mikroskopie (Figure 2.9). The instrument offer 12 steps of test force: 1, 5, 10, 15, 25, 50, 100, 200, 300, 500, 1000, 2000 p (gf) covering the range of test forces required by the standards ASTM E-384, EN ISO 6507 and EN ISO 4545. The test force can also be changed by the computer when running automated measurement cycles and as a consequence allowing different test forces in the inspection.

For specific applications depending on elastic and plastic properties of the material, the approach velocity of the indenter can be selected between 25 and 60µm/s.

The infinity corrected Leica Plan objectives 10x and 50x are used according to International Standards, Objectives 2.5X and 100x are optional. The measuring eyepiece with field of view 16 mm offers an optimized, ergonomic working position.

For each test, the measured diagonal lengths and the hardness value with test force are given as well as tolerance judgement, statistics (mean value, maximum/minimum, standard deviation).

The measuring error of distance: ±0.01µm

Figure 2.9 – The Microhardness tester

(7) The Nano Indenter

The Nano Indenter model is G200 of KLA-Tencor (Figure 2.10). The Nano Indenter G200 system is designed for nanoscale measurements during characterization and development of a wide range of materials.

The G200 measures Young's modulus and hardness, including measurement of deformation over six orders of magnitude, from nanometers to millimeters. The Nano Indenter G200 system can perform scratch and wear testing on a variety of materials.

The Nano Indenter G200 system can accurately perform ISO standardized nanoindentation testing and measure elastic modulus and hardness of the coating without influence from the substrate. The Nano Indenter G200 nanoindenter is also capable of measuring scratch hardness and wear resistance. In the case of high surface roughness coatings, the Nano Blitz 3D option can be used to quickly and quantitatively assess material properties.

Nano Indenter G200 systems can initiate the interfacial fracture and measure the adhesion and residual stress properties of the multiple-layer thin film.

The measuring errors of the device are:

The measuring error of pressure: ±0.001mN

The measuring error of distance: ±0.001nm

The measuring error of modulus: ±0.001GPa

The measuring error of hardness: ±0.001GPa

Figure 2.10 – The Nano Indenter

(8) The tribological tester

The tribological tester model is MWF-500 of Ji'nan Huaxing Test Equipment Co., Ltd (Figure 2.11). The tester is mainly used for the research of friction performance to carry out reciprocating friction and wear experiments, with high test accuracy (1%) and strong reliability. The main machine is composed of reciprocating motion table reciprocating motion servo system test force automatic loading system and friction automatic measurement system. The servo driving mechanism drives the friction pair to carry out linear reciprocating motion. The test force is automatically applied to the relatively static friction pair sample by the servo system, the size of the test force is adjusted and set by the servo system and the force sensor to be loaded on the friction pair sample. The pressure intensity can be arbitrarily set within the range of 5-500N, and the servo driving mechanism drives the friction pair to carry out reciprocating motion. A friction process is carried out through a test measurement and control system, thereby measuring the friction force (1-100 N) under certain conditions of pressure and

its coefficient of friction. Friction force, friction coefficient, friction time and other test parameters can be arbitrarily set by the operator on the computer interface and controlled and displayed by the computer in real time, and the corresponding parameter curves can be drawn, saved and printed out test reports.

The main machine of the testing machine consists of a reciprocating motion worktable, a servo mechanism, a reciprocating motion stroke adjusting device, an automatic test force applying system and a friction force measuring system. The servo motor rotates through the servo driving mechanism so as to drive the reciprocating motion worktable to do reciprocating linear motion along the linear motion guide rail. The test force is applied to the relatively static friction couple by the automatic loading system. The size of the test force is measured by the force sensor and can be freely set by an operator through the servo system and control software, and is automatically loaded. Another friction couple part, namely a reciprocating motion system, is driven by a servo system to do reciprocating linear motion so as to generate friction force, and that coefficient of friction can be calculated. The operator can freely set the test time or the number of times and automatically stop the machine. One cycle of reciprocation is one time, and the maximum reciprocating stroke is 20mm.

The measuring errors of the equipment are:

the measuring error of test force: $\pm 1\%$

the measuring error of friction force: $\pm 1\%$

the measuring error of friction coefficient: $\pm 1\%$

Figure 2.11 – Tribological tester

2.6 Coating preparation

(1) Treatment before coating preparation

Before the coatings are deposited by electro-spark, the substrate sample is clamped by a bench, and the electrode material to be deposited is installed on the welding gun. Connect the power supply and argon to the electric spark deposition equipment, firmly connect the cathode power supply to the bench, and adjust the argon flow to prepare for the deposition of the coating.

(2) Coating preparation methods

Adjust the experimental parameters of ESD machine according to the voltage, capacitance and specific deposition time designed. The electrode moving speed in both cases was 2 mm/s, and the electrode moving speed should be uniform when working (Figure 2.12). Moving according to the small ring track or the broken line network track can ensure the corresponding pressure, as far as possible to ensure the stability of the discharge voltage and the arc stability of the workpiece surface, and the excellent quality of the sediment layer can be obtained (Figure 2.13). The frequency of the first layer was 3 kHz, the frequency of the second layer was 4 kHz and the frequency of the third and the fifth layers were 5 kHz. Deposition was carried out using a hand-held gun

at room temperature with the argon gas (Ar 99%) protection (10 L/min flow rate), which avoids contamination of the deposit zone by interstitial elements such as oxygen or nitrogen. And that work angle between the rotary electrode and the substrate is about 45 degrees.

Figure 2.12 – The ESD operation

Figure 2.13 – The sample after ESD

(3) Treatment of coatings after preparation

After the base material is deposited, wash it in anhydrous ethanol with an ultrasonic cleaner for 20 minutes to remove the oil and impurities on the surface (Figure 2.14), dry the base material with a hair dryer, and then weigh the weight after deposition with an electronic balance (Figure 2.15). The surface morphology, roughness,

microstructure, phase composition, element distribution and surface hardness of the electro-spark deposited coatings were measured.

Samples of the electro-spark deposited tin bronze were cut into two pieces by a metallographic cutting machine TQG250 of TIME, and then ground and cleaned respectively. One of them was used to detect the phase composition, surface hardness and friction and wear properties of the coating. And another Sample for the microstructural analysis were prepared from the cross sections of the running-in coatings block and mounted in Bakelite by the pointing machine XQ-1 of Shanghai metallographic machine (Figure 2.16). After polishing and cleaning, in order to reveal elements of the granular structure, the surfaces of the samples were subjected to etching with 4% nitric acid alcohol and exposure time of 10 s, clean with anhydrous ethanol and air dry (Figure 2.17). And that it is used for detecting the cross section morphology, the microstructure, the element distribution and the cross section hardness distribution of the coatings.

Figure 2.14 – Ultrasonic cleaning

Figure 2.15 – Weigh

Figure 2.16 – inlay

Figure 2.17 – sample

2.7 Summary

In this chapter, the basic principle of electro-spark deposition (ESD), the application fields of electro-spark deposition in surface strengthening or surface repair, and the advantages and disadvantages of electro-spark technology are described in

detail. The methods of performance investigation and research are introduced in detail. A new method was proposed to construct the evaluation index system of the comprehensive properties of the electro-spark deposited coatings. The principles of entropy method and TOPSIS model are introduced, and the calculation method is derived in detail.

The composition and processing method of the matrix material and the composition and processing method of the electrode material are introduced in detail. The types, functions, parameters, characteristics, usage and precautions of the main experimental equipment are introduced. The preparation work before coatings preparation, the specific process and operation method of coatings preparation, and the processing methods after coatings preparation are described.

CHAPTER 3. EXPERIMENT RESEARCH RESULTS AND ANALYSIS

3.1 The characterization of Ag coatings

The bearing tin bronze based alloys exhibit better mechanical properties as compared with the Babbitt. Analyzing of their work has shown that the damageability of the bronze pads is exposed in the form of constrained running, high wear and high probability of scoring [141-143]. Thus, there is need to provide for the bronze bearing pads with special coatings improving the running conditions.

Tin bronze has good thermal conductivity and can effectively eliminate the heat generated by friction as a substrate material [144-146]. Soft metal silver is used in the design of bearings bearing high loads and high speeds and has good lubrication performance, mechanical properties and corrosion resistance [147-149]. Silver and copper have very good wettability, which is conducive to improving the metallurgical bonding performance between metals during ESD.

There are many methods to prepare the related coatings, but there are few reports on how to deposit the Ag coatings on the surface of tin-bronze bearing bush by electro-spark deposition (ESD) technology to improve the operating conditions.

The coatings of the tin bronze surface that was formed by ESD applying the soft antifriction material of silver. The analysis of morphology, composition and properties of the coatings were investigated.

3.1.1 Deposition process parameters

The ESD machine HMT-9500 has a control panel to change the electrical parameters including ESD voltage (20 V - 100 V), duty cycle (20% - 100%), rotation speed (150 r/min – 880 r/min) and frequency (50 Hz – 500 Hz). The ESD machine has

the ground attachment, the shielding gas outlet and the applicator attachment. The rotation direction can be controlled on the applicator.

Travel speed in both cases was 2 mm/s. The rotation speed of the layers was 550 r/min and the frequency was 400 Hz. Deposition was carried out using a hand-held gun at room temperature with the argon gas (Ar 99%) protection (10 L/min flow rate), which avoids contamination of the deposit zone by interstitial elements such as oxygen or nitrogen.

The electro-spark deposition process parameters (electrodes, voltage, duty cycle and efficiency) are shown in Table 3.1.

Table 3.1 – The ESD parameters of the Ag coatings

Specimens	Electrodes	Voltage (V)	Duty cycle (%)	Efficiency (min/cm^2)
1#	Ag	40	20	1
2#	Ag	60	25	1
3#	Ag	80	30	1

3.1.2 The mass transfer, roughness and thickness characteristics of the coatings

In this study, the analysis of deposition on mass transfer, roughness, and thickness of the Ag coatings were investigated, as shown in Table 3.2.

The deposition coatings are the result of gradual accumulation through multiple discharge and a large number of deposition points [81, 150, 151]. The mass transfer is usually regarded as an important index to evaluate ESD. At the beginning of deposition, the coating mass increases most obviously. With the increase of deposition time, the mass transfer of electrode to substrate gradually decreases. Finally, with the increase of deposition time, the mass of substrate stops increasing. This is because with the increase of deposition time, the content of oxide or nitride on the surface of the coating increases, the residual stress on the surface increases, the binding force decreases, and the material

is more likely to splash during discharge, which impedes the mass transfer in the process of ESD.

In this study, a precision electronic balance with an accuracy of 0.1mg was used to measure the samples and calculate the mass added to the substrate after ESD, as shown in Table 3.2. From the point of spark discharge rule, the larger of the discharge energy, the mass of the more increase, and Table 3.2 shows that the increase of the mass as the energy increases. When the voltage is 40 V, the duty cycle is 20%, the efficiency is 1 min/cm^2, the minimum value of mass transfer is 16.8 mg. When the voltage is 80 V, the duty cycle is 30%, the efficiency is 1 min/cm^2, the maximum value of mass transfer is 32.3 mg.

The Bruker Contour GT-K1 3D optical profilometers was used to observe the surface of the deposition layer and measure the surface roughness. As can be seen from Table 3.2, the roughness increases with the increase of deposition energy. When the voltage is 40 V, the duty cycle is 20%, the efficiency is 1 min/cm^2, the minimum value of the surface roughness is 11.09 μm. When the voltage is 80 V, the duty cycle is 30%, the efficiency is 1 min/cm^2, the maximum value of the surface roughness is 23.84 μm.

The surface roughness of the composite coatings is not only affected by the deposition parameters, but also affected by the operation technology, the mechanical accuracy of the welding torch and the properties of the deposited materials.

The measured results of the coating surface topography and profile are shown in Figure 3.1. It can be seen from the figure that, Figure 3.1(a), Figure 3.1(b) and Figure 3.1(c), the surface topography gradually becomes rough, and the change of surface profile curve gradually increases.

The thickness of the composite coatings is the most important index of ESD. As can be seen from Table 3.2, the coating thickness increases with the increase of deposition energy. When the voltage is 40 V, the duty cycle is 20%, the efficiency is 1 min/cm^2, the minimum value of the thickness is 9 μm. When the voltage is 80 V, the duty cycle is 30%, the efficiency is 1 min/cm^2, the maximum value of the thickness is 21 μm.

Table 3.2 – The mass transfer, roughness and thickness characteristics of the Ag coatings

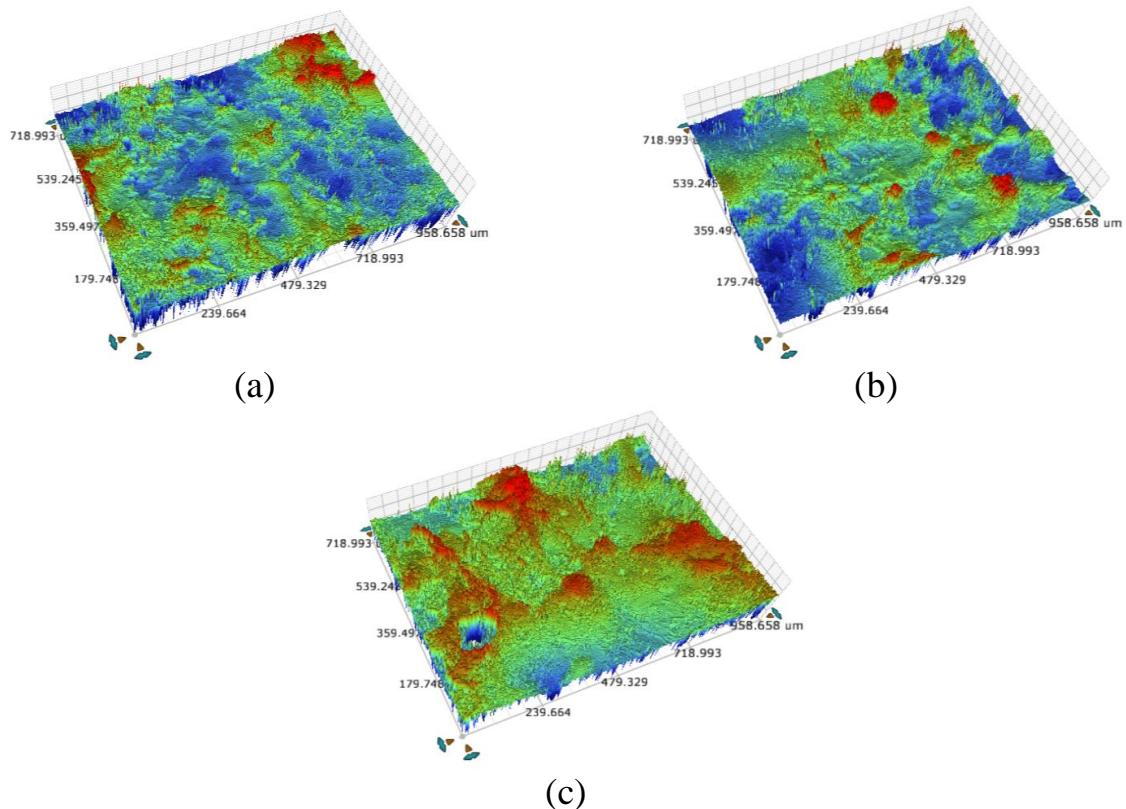| Specimens	Electrodes	Mass transfer (mg)	Roughness R_a (μm)	Thickness (μm)
1#	Ag	16.8	11.09	9
2#	Ag	25.0	15.46	15
3#	Ag	32.3	23.84	21

(a)

(b)

(c)

Figure 3.1 – The surface topography and profile of the Ag coatings: a - specimen 1#; b - specimen 2#; c - specimen 3#

3.1.3 The morphology and element composition of the composite coatings surface

The morphology of the Ag coatings surface is shown in Figure 3.2. It can be seen from the figure that the surface of the deposited coatings is sputtering stacking, which is formed by the superposition of many irregular small droplet spots melted by continuous pulse discharge. There are a few microcracks on the surface of the composite coatings, which tend to propagate along the direction perpendicular to the surface of the coatings. This is due to the rapid heating and cooling in the process of spark discharge, the residual thermal stress in the coatings will exist, leading to the initiation of micro-cracks, and Ag with good plasticity can play a role in relieving the thermal stress, thus reducing the number of cracks. The multilayer structure with a low modulus ratio contributed to reduced stress concentration in harder sub-layer, thereby inhibiting crack initiation.

After deposition, only simple grinding is needed to meet the requirements of surface roughness. The prepared coatings surface has a small amount of ferrous metal oxides due to oxidation, which is caused by the oxidation of copper in bronze alloy. It can also be seen from Figure 3.2 that the surface of specimen 1# in Figure 3.2(a) has dense discharge spots and more rough surfaces. With the increase of discharge energy, discharge spots and smooth surfaces increase. That's because the higher the energy, the more molten the metal at the interface, the more fluid it is.

The element composition on the surface of the Ag coatings was characterized by energy dispersion spectrum (EDS) in Table 3.3. As can be seen from the table, with the increase of discharge energy, the content of elements on the surface of the sample changes little and the copper content is relatively high which indicates that the coatings thickness is not too thick, and the good wettability between silver and copper can make

the metallurgical combination better.
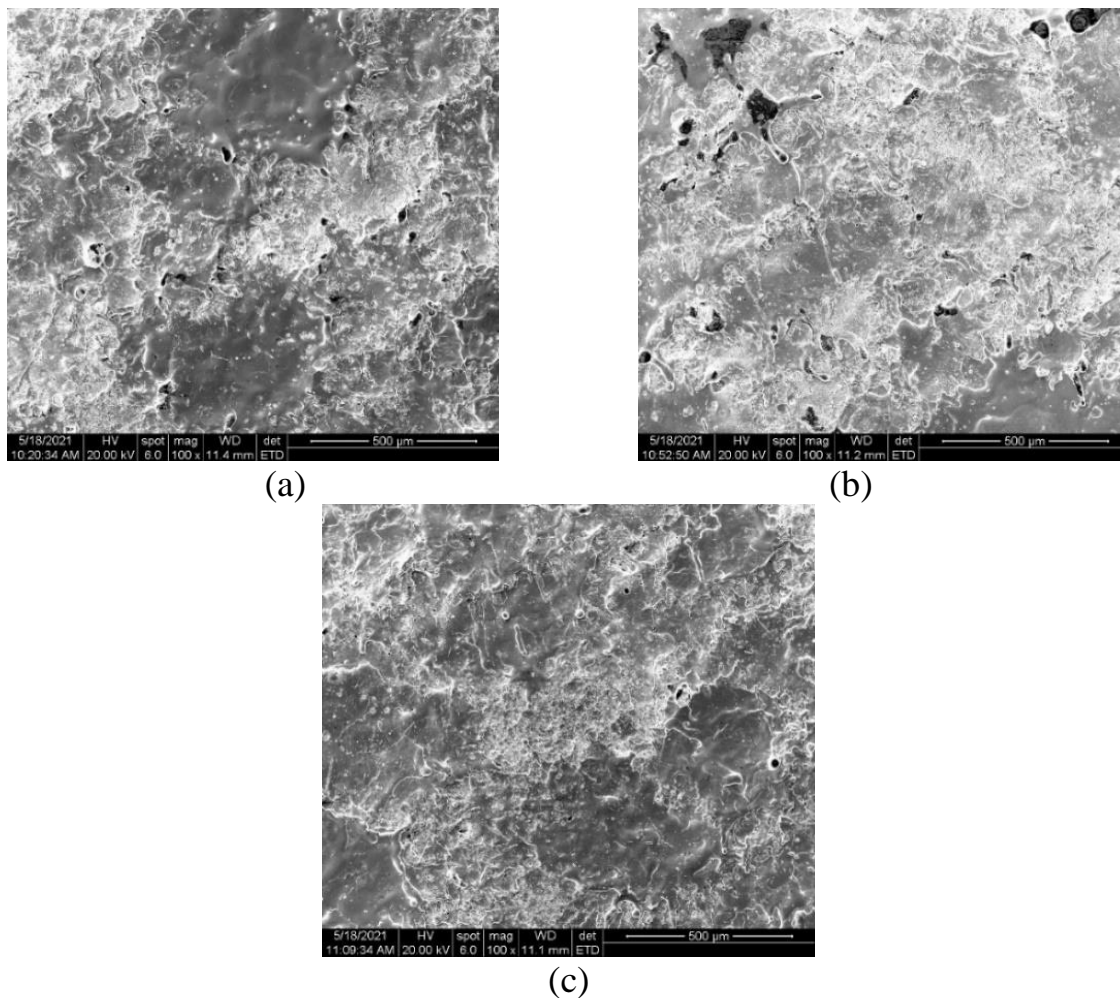

(a)

(b)

(c)

Figure 3.2 – The morphology of the Ag coatings surface: a - specimen 1#; b - specimen

2#; c - specimen 3#

Table 3.3 – The elemental composition of the Ag coatings surface

Specimens	P (%)	Cu (%)	Ag (%)	Sn (%)
1#	0.29	40.74	56.46	2.51
2#	0.19	38.14	59.60	2.06
3#	0.18	45.31	51.09	3.41

3.1.4 Tribological properties of the Ag coatings

Electro-spark deposition technology can effectively change the surface of the physical and chemical properties, mechanical properties, so that the tribological properties of the surface changes, which has special properties [152-154].

Table 3.4 compares the evolution of the coefficient of friction at the applied loaded

of 5 N, 10 N and 15 N of the ESD modified samples sliding against a GCr15 steel ball in air. For the initial 600 seconds at load of 5 N of specimen 1#, the friction coefficient with an average value of about 0.33. The following 600 seconds at load of 10 N, the friction coefficient is about 0.24. And then to 15 N for the final 600 seconds, the friction coefficient is about 0.35. The friction coefficient of the coatings after running-in is slightly larger mainly because of the thinner coatings. For the initial 600 seconds at load of 5 N of specimen 2#, the friction coefficient with an average value of about 0.69. The following 600 seconds at load of 10 N, the friction coefficient is about 0.36. And then to 15 N for the final 600 seconds, the friction coefficient is about 0.31. The friction coefficient of the coatings is slightly larger at the beginning of the run-in mainly because of the increase of the surface roughness of the coatings. For the initial 600 seconds at load of 5 N of specimen 3#, the friction coefficient with an average value of about 0.20. The following 600 seconds at load of 10 N, the friction coefficient is about 0.22. And then to 15 N for the final 600 seconds, the friction coefficient is about 0.31. The reason why the friction coefficient of the coating is small at the beginning of run-in is that the coatings thickness increases and the surface is more prone to plastic deformation. The investigation of the tribological properties of the coatings in dry friction show that the lower resistance is exhibited by the coatings deposited using the soft antifriction material.

From the evolution of the coefficient of friction of the tin bronze substrate with the Ag coatings, it is clear that wear process indicated is rather complicated because of the influence of different surface topography and chemical composition during running-in phase. For ESD layers, at the beginning of steady stage its friction coefficient shows to

some extent direct response to surface roughness and the coatings thickness. Because GCr15 with high hardness produce material loss of soft antifriction composite coatings counterpart (with relative low hardness) through dominant abrasion mechanism. With the generation of tribofilm, abrasion of coatings-GCr15 sliding couples is transferred to interfacial sliding. Similar to other sliding couples, the steady-state fiction coefficients become more or less independent of surface roughness. The friction coefficient stabilizes after running-in, and becomes stable throughout the test.

The surfaces of wear traces were analyzed in order to understand the friction and wear resistance mechanisms of the coatings. The wear scars of the tin bronze substrate with the Ag coatings after tribological testing are shown in Figure 3.3. It was found from analysis of wear scars in Figure 3.3 (a) that the wear mechanism of the specimen 1# is dominated by abrasive wear and fatigue delamination. The friction surface of specimen 1# is smooth, the wear marks are fine and shallow, and some materials are spalling and forming spalling pits. The wear mechanism of the specimen 2# is dominated by abrasive wear and slight fatigue delamination that was found from analysis of wear scars in Figure 3.3 (b). However, it can be seen in Figure 3.3 (c) that the soft antifriction coatings may effectively restrain fatigue delamination, showing plastic deformation, abrasive wear and slight polishing. Plastic deformation and abrasive wear dominated on the relatively soft composite coatings. The initial surface microgeometry was changed during load application and its surface became smooth with fine shallow scratches observed after the wear test. After the smooth surface was formed, the friction and wear stabilized.

The elemental composition of the Ag coatings surfaces after tribological testing are

shown in Table 3.5. By comparing Table 3.3 and Table 3.5, it can be found that copper content on the surface of specimen 1# decreases from 40.74% to 38.29%, silver content decreases from 56.46% to 46.52%. The tin content on the surface changed little before and after the friction test. In addition, carbon and oxygen elements were detected on the surface, indicating the formation of carbides and oxides after surface wear.

By comparing Table 3.3 and Table 3.5, it can be found that after friction test, copper content on the surface of specimen 2# increases from 38.14% to 45.45%, silver content decreases from 59.60% to 46.32%. The tin content on the surface changed little before and after the friction test. In addition, the low content of carbon and oxygen detected on the surface indicates that due to the good stability of silver, less carbides and oxides are produced after surface wear.

By comparing Table 3.3 and Table 3.5, it can be found that copper content on the surface of specimen 3# decreases from 45.31% to 41.48%, silver content decreases from 51.09% to 34.72%. The contents of tin on the surface of specimen 3# have little change after friction test. In addition, the higher carbon and oxygen elements content detected on the surface indicates that due to the poor stability of tin and copper, more oxides are generated after ESD. However, due to the large surface roughness, the oxides and carbides on the surface have not been completely removed.

Table 3.4 – The friction coefficient during coatings tests at loads of 5 N, 10 N, and 15 N

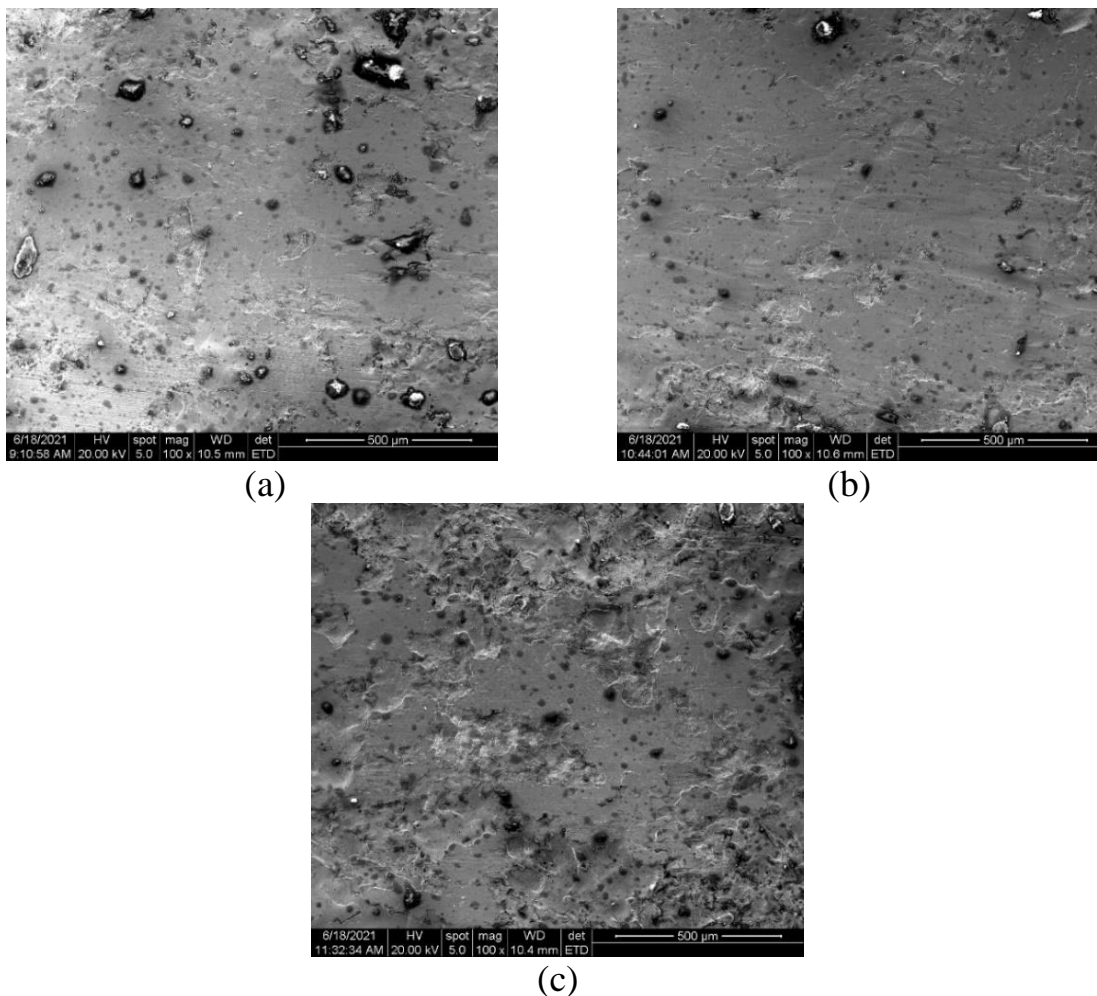| Specimens	5 N	10 N	15 N
1#	0.33	0.24	0.35
2#	0.69	0.36	0.31
3#	0.20	0.22	0.31

(a)

(b)

(c)

Figure 3.3 – The wear scars of the tin bronze substrate with the coatings after

tribological testing: a - specimen 1#; b - specimen 2#; c - specimen 3#

Table 3.5 – The elemental composition of the Ag coatings surface after tribological

testing

Specimens	C (%)	O (%)	Cu (%)	Ag (%)	Sn (%)
1#	7.63	4.76	38.29	46.52	2.81
2#	1.03	5.52	45.45	46.32	1.68
3#	11.27	11.05	41.48	34.72	1.48

3.2 The characterization of Ag+B83 composite coatings

Most responsible parts and assembly units of centrifugal compressors, pumps,

turbines and other machines work under conditions of heavy loads, high speeds, high

temperatures, and also of corrosive, abrasive and other types of influence of working

environments [155-157]. With the large variety of the operation conditions of the parts,

their surface layers are considered as the most loaded portions [158-160]. Therefore, the real working resource of the machine operation directly depends on the part surface bearing capacity being determined by the quality of its surface layer [161-163]. The bearing materials operate in pairs with steel or cast iron shaft journals. The cost of a shaft is usually higher than the cost of bearing pads, so they should wear less than the bearing pads [164-166]. The main general requirements to the materials of sliding bearings are as follows: mutual materials compatibility, low coefficient of friction, high pressure properties, high thermal stability, high corrosion and erosion resistance, resistance toleration, low cost, high dimensional and structural stability, conformability, and recoverability of properties after forced contact [167-169]. These materials should have sufficient hardness, but not as high as to cause excessive wear of the shaft; they should be relatively easy to form under the influence of local stresses and also they should keep the lubricant on the surface. The bearing copper based alloys exhibit better mechanical properties as compared with the Babbitt and also the alloys on the base of zinc and aluminum [170-172]. Babbitt B83 could not withstand a short term rise in temperature up to 250°C and the B83 bearings were replaced by the bearings wherein there was used bronze [173-175]. Analyzing of their work has shown that the damageability of the bronze pads is exposed in the form of constrained running, high wear and high probability of scoring. Thus, there is need to provide for the bronze bearing pads with special coatings improving the running conditions.

Tin bronze has good thermal conductivity and can effectively eliminate the heat generated by friction as a substrate material. Soft metal silver is used in the design of bearings bearing high loads and high speeds and has good lubrication performance,

mechanical properties and corrosion resistance. Silver and copper have very good wettability, which is conducive to improving the metallurgical bonding performance between metals during ESD. However, the performance of silver as anti-wear metal coating needs to be further improved. Therefore, based on the above factors, silver is suitable as the transition coating. Tin-base Babbitt B83 has good embedding and compliance, and plays the role of anti-friction and anti-bite in actual working conditions which is particularly beneficial to the running-in at the early stage of operation, and is very suitable for operation as the coating. In the actual work of bearing bush, tin bronze bearing bush has good thermal conductivity but slightly higher friction force, while Babbitt alloy bearing bush has small friction force but poor mechanical performance at high temperature, which further affects the reliability and stability of bearing bush. There are many methods to prepare the related coatings, but there are few reports on how to deposit the Ag+B83 composite coatings on the surface of tin-bronze bearing bush by electro-spark deposition (ESD) technology to improve the operating conditions.

The composite coatings of the tin bronze surface that was formed by alternately ESD applying the soft antifriction material of silver and Babbitt B83. The analysis of morphology, composition and properties of the coatings were investigated.

3.2.1 Deposition process parameters

The ESD machine HMT-9500 has a control panel to change the electrical parameters including ESD voltage (20 V – 100 V), duty cycle (20% - 100%), rotation speed (150 r/min – 880 r/min) and frequency (50 Hz – 500 Hz).

Travel speed in both cases was 2 mm/s. The rotation speed of the layers was 550 r/min and the frequency was 400 Hz. Deposition was carried out using a hand-held gun

at room temperature with the argon gas (Ar 99%) protection (15 L/min flow rate), which avoids contamination of the deposit zone by interstitial elements such as oxygen or nitrogen.

The electro-spark deposition process parameters (electrodes, voltage, duty cycle and efficiency) are shown in Table 3.6.

Table 3.6 – The ESD parameters of the Ag+B83 composite coatings

Specimens	Electrodes	Voltage (V)	Duty cycle (%)	Efficiency (min/cm^2)
1#	Ag-B83	40/20	20/20	1/3
2#	Ag-B83	50/25	25/25	1/3
3#	Ag-B83	60/30	30/30	1/3

3.2.2 The mass transfer, roughness and thickness characteristics of the composite coatings

In this study, the analysis of deposition on mass transfer, roughness, and thickness of the Ag+B83 composite coatings were investigated, as shown in Table 3.7.

The electro-spark deposition composite coatings are the result of gradual accumulation through multiple discharge and a large number of deposition points [176-178]. The mass transfer is usually regarded as an important index to evaluate ESD. At the beginning of deposition, the coating mass increases most obviously. With the increase of deposition time, the mass transfer of electrode to substrate gradually decreases. Finally, with the increase of deposition time, the mass of substrate stops increasing. This is because with the increase of deposition time, the content of oxide or nitride on the surface of the coating increases, the residual stress on the surface increases, the binding force decreases, and the material is more likely to splash during discharge, which impedes the mass transfer in the process of ESD.

In this study, a precision electronic balance with an accuracy of 0.1 mg was used to

measure the samples and calculate the mass added to the substrate after ESD, as shown in Table 3.7. From the point of spark discharge rule, the larger of the discharge energy, the mass of the more increase, and Table 3.7 shows that the increase of the mass as the energy increases. When the voltage is 40 V and 20 V, the duty cycle is 20% and 20%, the efficiency is 1 min/cm^2 and 3 min/cm^2, the minimum value of mass transfer is 27.6 mg. When the voltage is 60 V and 30 V, the duty cycle is 30% and 30%, the efficiency is 1 min/cm^2 and 3 min/cm^2, the maximum value of mass transfer is 125.2 mg.

The Bruker Contour GT-K1 3D optical profilometers was used to observe the surface of the deposition layer and measure the surface roughness. The surface roughness of the Ag+B83 composite coatings are shown in Table 3.7. As can be seen from Table 3.7, the roughness increases with the increase of deposition energy. When the voltage is 40 V and 20 V, the duty cycle is 20% and 20%, the efficiency is 1 min/cm^2 and 3 min/cm^2, the minimum value of the surface roughness is 5.97 μm. When the voltage is 60 V and 30 V, the duty cycle is 30% and 30%, the efficiency is 1 min/cm^2 and 3 min/cm^2, the maximum value of the surface roughness is 19.43 μm.

The measured results of the coating surface topography and profile are shown in Figure 3.4. It can be seen from the figure that, Figure 3.4 (a), Figure 3.4 (b) and Figure 3.4 (c), the surface topography gradually becomes rough, and the change of surface profile curve gradually increases.

The thickness of the composite coatings is the most important index of ESD, followed by the surface roughness of the coatings, and the mass of the coatings directly affects the thickness of the coatings. The thicknesses of the Ag+B83 composite coatings are shown in Table 3.7. As can be seen from Table 3.7, the coating thickness increases

with the increase of deposition energy. When the voltage is 40 V and 20 V, the duty cycle is 20% and 20%, the efficiency is 1 min/cm^2 and 3 min/cm^2, the minimum value of the thickness is 30 μm. When the voltage is 60 V and 30 V, the duty cycle is 30% and 30%, the efficiency is 1 min/cm^2 and 3 min/cm^2, the maximum value of the thickness is 80 μm.

Table 3.7 – The mass transfer, roughness and thickness characteristics of the Ag+B83 composite coatings

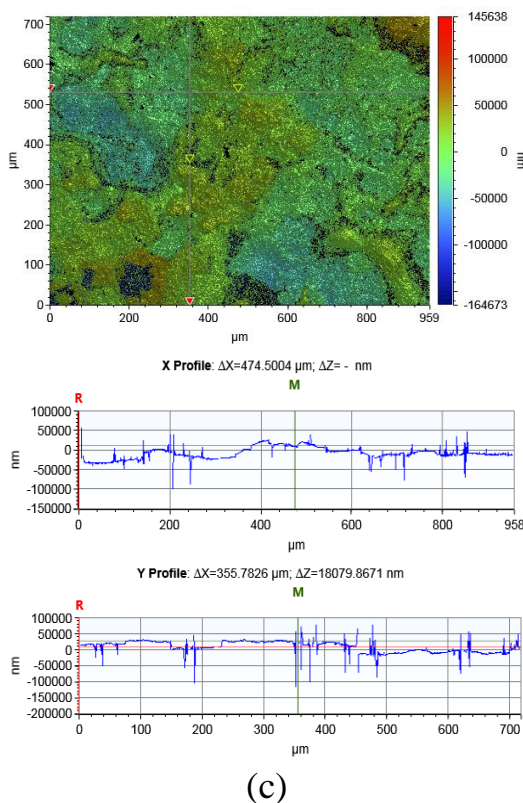| Specimens	Electrodes	Mass transfer (mg)	Roughness R_a (μm)	Thickness (μm)
1#	Ag-B83	27.6	5.97	30
2#	Ag-B83	73.2	6.66	50
3#	Ag-B83	125.2	19.43	80

(a)   (b)

(c)
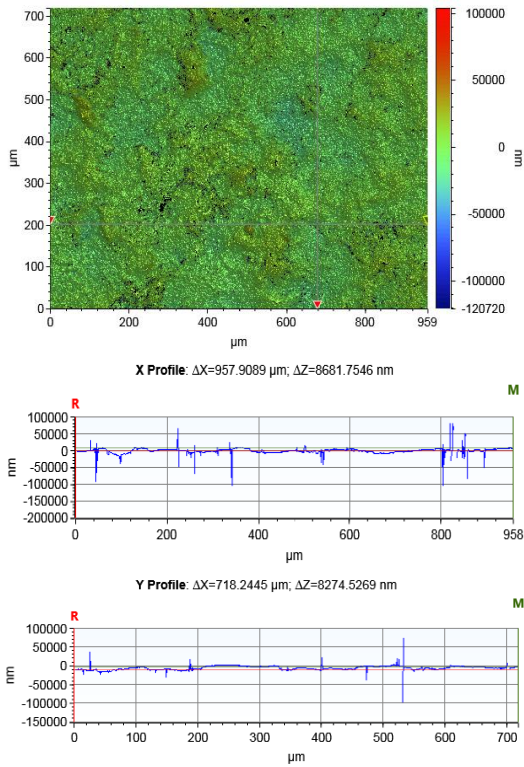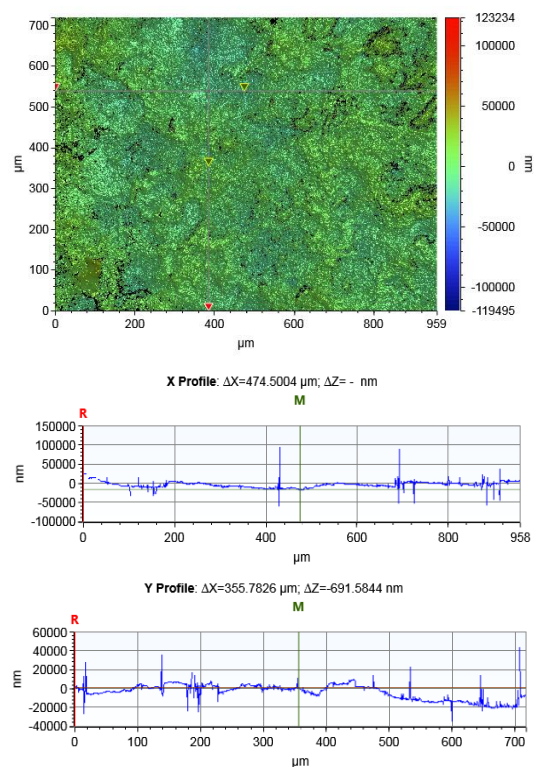
Figure 3.4 – The surface topography and profile of the Ag+B83 coatings: a -
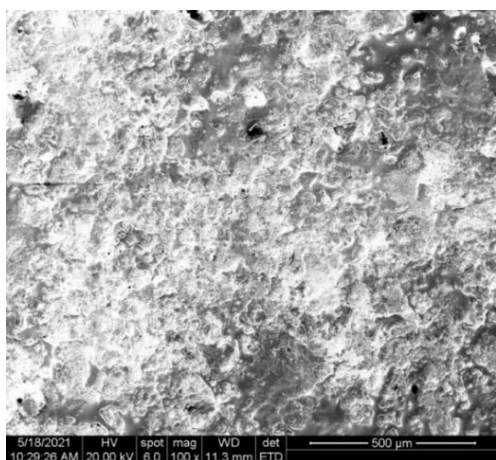
specimen 1#; b - specimen 2#; c - specimen 3#

3.2.3 The morphology and element composition of the composite coatings surface

The morphology of the Ag+B83 composite coatings surface is shown in Figure 3.5. It can be seen from the figure that the surface of the deposited coatings is sputtering stacking, which is formed by the superposition of many irregular small droplet spots melted by continuous pulse discharge. There are a few microcracks on the surface of the composite coatings, which tend to propagate along the direction perpendicular to the surface of the coatings. This is due to the rapid heating and cooling in the process of spark discharge, the residual thermal stress in the coatings will exist, leading to the initiation of micro-cracks, and the transition layer of Ag with good plasticity can play a role in relieving the thermal stress, thus reducing the number of cracks. The multilayer structure with a low modulus ratio contributed to reduced stress concentration in harder

sub-layer, thereby inhibiting crack initiation.

The microtexture on the surface of the polished composite coatings is conducive to the storage of abrasive particles and lubricating oil during the operation of the bearing bush, reducing the wear of abrasive particles on the surface of the bearing bush, reducing the friction coefficient and improving the self-lubricating performance. The prepared coatings surface has a small amount of ferrous metal oxides due to oxidation, which is caused by the oxidation of tin in Babbitt alloy. It can also be seen from Figure 3.5 that the surface of Specimen 1# in Figure 3.5 (a) has dense discharge spots and more rough surfaces. With the increase of discharge energy, discharge spots and smooth surfaces increase. That's because the higher the energy, the more molten the metal at the interface, the more fluid it is.

The element composition on the surface of the Ag+B83 composite coatings was characterized by energy dispersion spectrum (EDS) in Table 3.8. As can be seen from the table, with the increase of discharge energy, the content of copper on the sample surface gradually decreases, while the content of tin and antimony gradually increases, which also indicates that the composite coating gradually thickens.
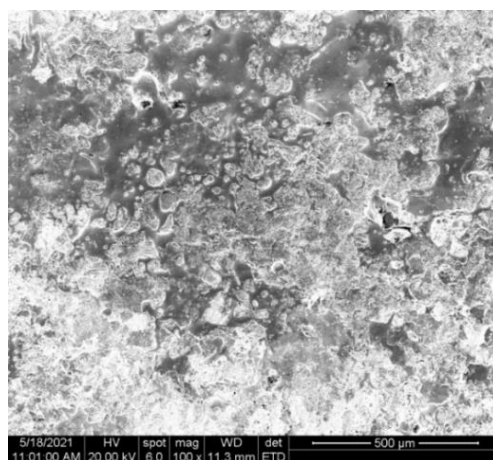
(a)   (b)
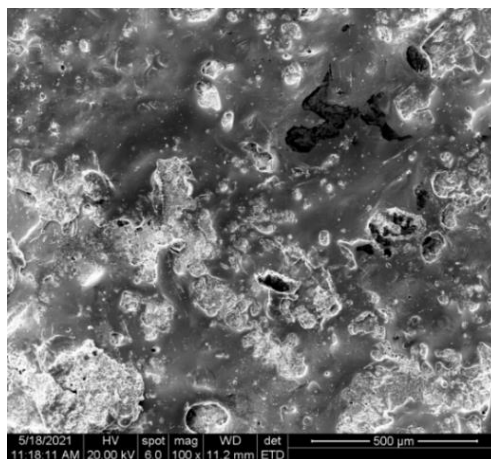
(c)

Figure 3.5 – The morphology of the Ag+B83 composite coatings surface: a - specimen

1#; b - specimen 2#; c - specimen 3#

Table 3.8 – The elemental composition of the Ag+B83 composite coatings surface

Specimens	Cu (%)	Ag (%)	Sn (%)	Sb (%)
1#	28.58	24.15	44.14	3.13
2#	20.14	27.10	44.27	8.49
3#	9.67	10.24	64.61	15.48

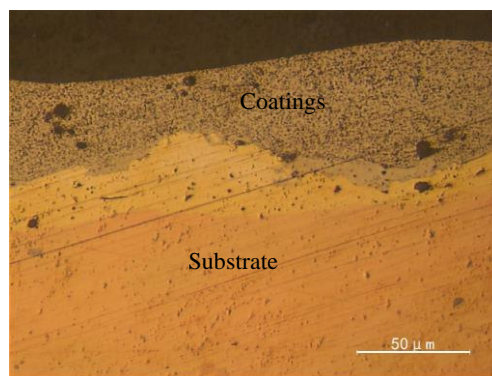3.2.4 The cross section morphology of the composite coatings

The Ag+B83 ESD treated cross section morphology of the composite coatings was analyzed using metallographic microscopy LECIA DMi8 M. Figure 3.6 (a), Figure 3.6 (b) and Figure 3.6(c) shows the cross section morphology of the Ag+B83 ESD composite coatings. It can be seen that the composite coatings have a good metallurgical combination with the substrate, the microstructure of the deposition layer is compact, and the continuous interface is formed at the joint. The thickness of the composite coatings is about 30 μm in Figure 3.6 (a), 50 μm in Figure 3.6 (b) and 80 μm in Figure 3.6 (c), but there are some defects such as micro-cracks and holes in some places. The composite coatings are tin-base Babbitt B83 and silver from the surface to the substrate. However, because the wettability of silver and copper is very good, the silver-white silver coating can rarely be observed and the coating is completely fused together

during the electro-spark deposition, forming the alloy layer. Since the ESD is a process of continuous superposition of the deposited materials, the thickness of the deposited layer increases with the increase of the electrode materials deposited on the surface. During ESD, the instantaneous high temperature generated by high frequency pulse discharge melts and vaporizes the materials in the discharge area, and melts, diffuses and alloys occur on the deposited surface. Then the substrate surface is rapidly cooled and solidified, resulting in large cyclic thermal stress and microstructure stress in the deposited layer, resulting in micro-cracks or pores on the surface of the deposition. In the process of layer by layer covering, a small number of micro-cracks or pores on the surface of the coating cannot be completely filled by the molten material, forming holes.

Figure 3.6 (d) is the metallographic diagram of electrode material B83, from which it can be seen that the square or rectangle with bright color is SnSb, the dark color is α-Sn, and the chain or elongated needle is Cu_6Sn_5. However, we can see from Figure 3.6 (a), Figure 3.6 (b) and Figure 3.6 (c) that the grains in the deposition layer are very dense, refined and uniformly distributed which is due to the rapid heating and cooling of the electrode and substrate by ESD technology.

(a)
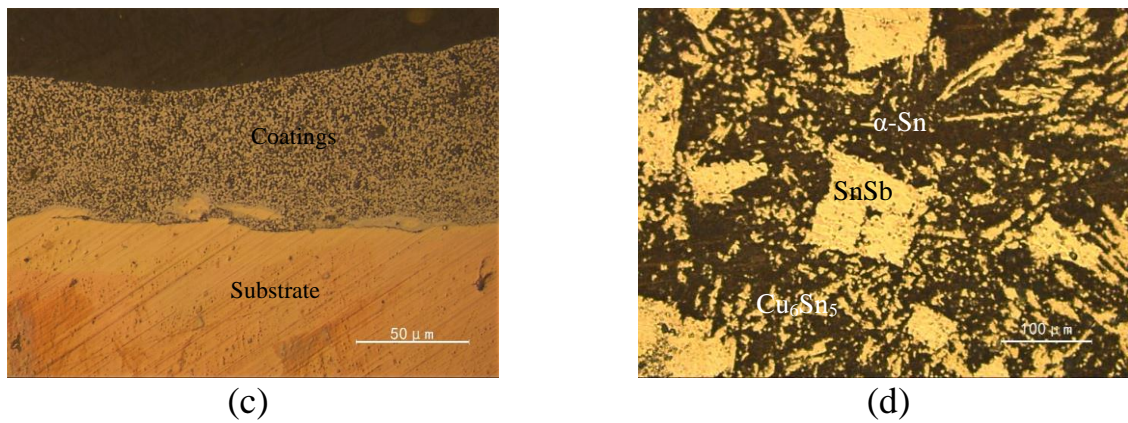

(b)

(c)   (d)
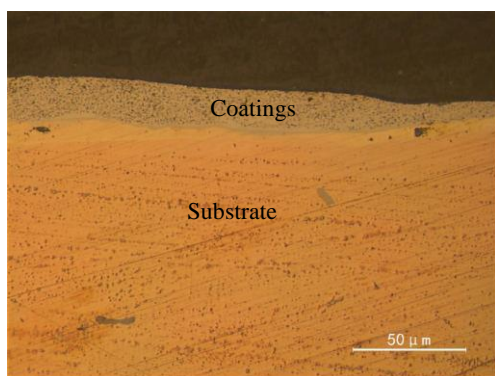
Figure 3.6 – The cross section morphology of the composite coatings and electrode B83:

a - specimen 1#; b - specimen 2#; c - specimen 3#; d - electrode B83

3.2.5 Tribological properties of the composite coatings

Electro-spark deposition technology can effectively change the surface of the physical and chemical properties, mechanical properties, so that the tribological properties of the surface changes, which has special properties [179-181].

Table 3.9 compares the evolution of the coefficient of friction at the applied loaded of 5 N, 10 N and 15 N of the ESD modified samples sliding against a GCr15 steel ball in air. For the initial 600 seconds at load of 5 N of specimen 1#, the friction coefficient with an average value of about 0.341. The following 600 seconds at load of 10 N, the friction coefficient is about 0.344. And then to 15 N for the final 600 seconds, the friction coefficient is about 0.265. For the initial 600 seconds at load of 5 N of specimen 2#, the friction coefficient with an average value of about 0.324. The following 600 seconds at load of 10 N, the friction coefficient is about 0.245. And then to 15 N for the final 600 seconds, the friction coefficient is about 0.288. For the initial 600 seconds at load of 5 N of specimen 3#, the friction coefficient with an average value of about 0.340. The following 600 seconds at load of 10 N, the friction coefficient is about 0.167. And then to 15 N for the final 600 seconds, the friction coefficient is about 0.177. The

investigation of the tribological properties of the coatings in dry friction show that the lower resistance is exhibited by the composite coatings deposited using the soft antifriction material. The surface friction coefficient of the specimen 3# is the minimum of the composite coatings after running-in stage.

From the evolution of the coefficient of friction of the tin bronze substrate with the Ag+B83 composite coatings of the specimen 3#, it is clear that wear process indicated is rather complicated because of the influence of different surface topography and chemical composition during running-in phase. For ESD layers, at the beginning of steady stage its friction coefficient shows to some extent direct response to surface roughness. And for the initial 600 seconds at load of 5 N, the friction coefficient is about 0.340 influenced by the surface roughness. Because GCr15 with high hardness produce material loss of soft antifriction composite coatings counterpart (with relative low hardness) through dominant abrasion mechanism. With the generation of tribofilm, abrasion of composite coatings-GCr15 sliding couples is transferred to interfacial sliding. Similar to other sliding couples, the steady-state fiction coefficients become more or less independent of surface roughness. After the first running-in stage, the soft antifriction composite coatings demonstrated a relatively stable friction coefficient with an average value of about 0.167 after the following 600 seconds at load of 10 N. After the second running-in stage, the friction coefficient with an average value of about 0.177 at load of 15 N. The friction coefficient stabilizes after running-in, and becomes stable throughout the test.

The surfaces of wear traces were analyzed in order to understand the friction and wear resistance mechanisms of the coatings. The wear scars of the tin bronze substrate
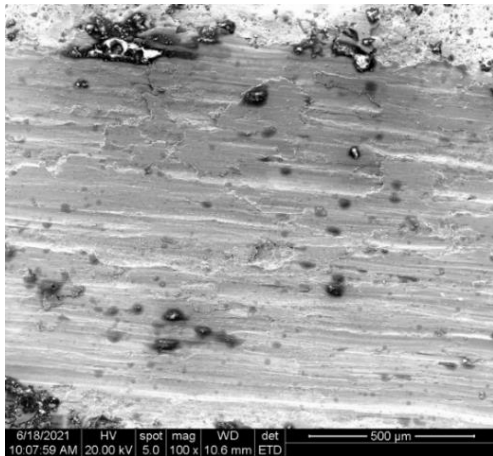
with the Ag+B83 composite coatings after tribological testing are shown in Figure 3.7. It was found from analysis of wear scars in Figure 3.7 (a) that the wear mechanism of the specimen 1# is dominated by severe ploughing wear and fatigue delamination. A lamellar structure can be distinguished on the surface of the worn specimen 1#. This can be responsible for low friction under these conditions. The wear mechanism of the specimen 2# is dominated by abrasive wear and slight plastic deformation that was found from analysis of wear scars in Figure 3.7 (b). However, it can be seen in Figure 3.7 (c) that the soft antifriction composite coatings may effectively restrain fatigue delamination, showing plastic deformation, abrasive wear and slight polishing. Plastic deformation and abrasive wear dominated on the relatively soft composite coatings. The initial surface microgeometry was changed during load application and its surface became smooth with fine shallow scratches observed after the wear test. After the smooth surface was formed, the friction and wear stabilized.

The elemental composition of the Ag+B83 composite coatings surfaces after tribological testing are shown in Table 3.10. By comparing Table 3.8 and Table 3.10, it can be found that copper content on the surface of specimen 1# increases from 28.58% to 74.31%, silver content decreases from 24.15% to 4.14%, tin content decreases from 44.14% to 4.75%, and antimony content decreases from 3.13% to 0 after friction test. This indicates that the composite coating on the surface of specimen 1# has been almost completely worn away, exposing the tin bronze substrate. In addition, carbon and oxygen elements were detected on the surface, indicating the formation of carbides and oxides after surface wear. By comparing Table 3.8 and Table 3.10, it can be found that after friction test, copper content on the surface of specimen 2# increases from 20.14%

to 50.19%, silver content decreases from 27.10% to 20.92%, tin content decreases from 44.27% to 16.71%, and antimony content decreases from 8.49% to 0. This indicates that the B83 coating on the surface of specimen 2# has been almost completely worn away, exposing the silver coating or substrate. In addition, the low content of carbon and oxygen detected on the surface indicates that due to the good stability of silver, less carbides and oxides are produced after surface wear. By comparing Table 3.8 and Table 3.10, it can be found that the contents of copper, silver, tin and antimony on the surface of specimen 3# have little change after friction test. This indicates that the composite coatings on the surface of specimen 3# are thick and stable. In addition, the higher oxygen content detected on the surface indicates that due to the poor stability of tin, more oxides are generated after surface wear.

Table 3.9 – The friction coefficient during composite coatings tests at loads of 5 N, 10 N, and 15 N
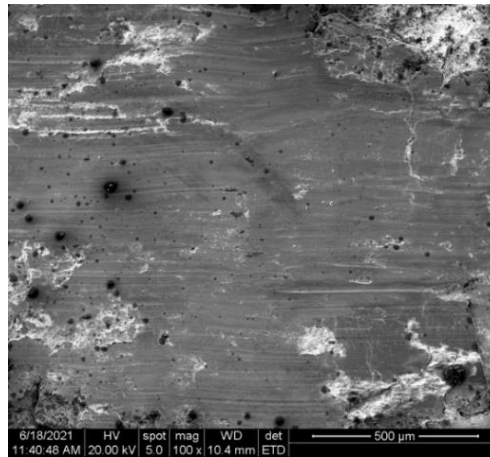
Specimens	5 N	10 N	15 N
1#	0.341	0.344	0.265
2#	0.324	0.245	0.288
3#	0.340	0.167	0.177

(a)
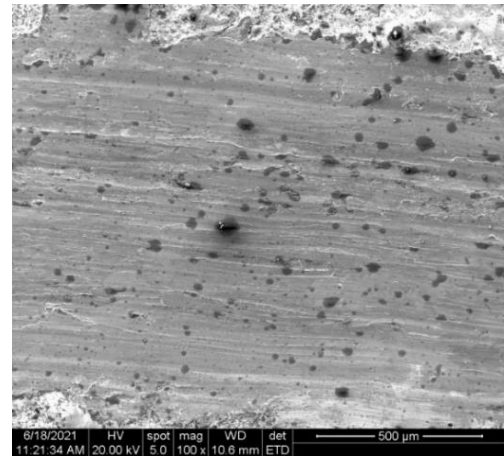
(b)

(c)

Figure 3.7 – The wear scars of the tin bronze substrate with the composite coatings after tribological testing: a - specimen 1#; b - specimen 2#; c - specimen 3#

Table 3.10 – The elemental composition of the Ag+B83 composite coatings surface after tribological testing

Specimens	C (%)	O (%)	Cu (%)	Ag (%)	Sn (%)	Sb (%)
1#	12.27	4.54	74.31	4.14	4.75	0
2#	3.57	8.61	50.19	20.92	16.71	0
3#	2.71	21.48	8.03	7.74	51.80	8.24

3.3 The characterization of Ag+Cu+B83 composite coatings

Silver and copper have very good wettability, which is conducive to improving the metallurgical bonding performance between metals during ESD. However, the performance of silver as anti-wear metal coating needs to be further improved. Therefore, based on the above factors, silver is suitable as the first transition coating. Pure copper is soft and has better wettability with silver. The copper in the coating can form ε-phase (Cu_6Sn_5) with the tin in the Sn-based Babbitt alloy, which is conducive to ensuring the metal bonding of the coating, so the copper is suitable for the second layer of transition coating. Tin-base Babbitt B83 has good embedding and compliance, and plays the role of anti-friction and anti-bite in actual working conditions, which is particularly beneficial to the running-in at the early stage of operation, and is very

suitable for operation as the coating [182, 183].

The combined coatings of the tin bronze surface that was formed by alternately ESD applying the soft antifriction material of silver, copper and Babbitt B83. The analysis of morphology, composition and properties of the coatings were investigated.

3.3.1 Deposition process parameters

The ESD machine DZ-4000III has a control panel to change the electrical parameters including ESD voltage (20 V – 250 V), capacitance (30 μF – 420 μF) and frequency (1300 Hz – 6000 Hz).

Travel speed in both cases was 2 mm/s. The frequency of the first layer is 3 kHz, the frequency of the second layer is 4 kHz and the frequency of the third layer is 5 kHz. Deposition was carried out using a hand-held gun at room temperature with the argon gas (Ar 99%) protection (10 L/min flow rate), which avoids contamination of the deposit zone by interstitial elements such as oxygen or nitrogen.

The electro-spark deposition process parameters (electrodes, voltage, capacitance and efficiency) are shown in Table 3.11.

Table 3.11 – The ESD parameters of the Ag-Cu-B83 composite coatings

Specimens	Electrodes	Voltage (V)	Capacitance (μF)	Efficiency (min/cm^2)
1#	Ag-Cu-B83	40/40/20	90/90/30	1/1/2
2#	Ag-Cu-B83	40/40/20	150/150/90	2/2/3
3#	Ag-Cu-B83	40/40/20	240/240/150	3/3/4
4#	Ag-Cu-B83	60/60/30	90/90/30	2/2/3
5#	Ag-Cu-B83	60/60/30	150/150/90	3/3/4
6#	Ag-Cu-B83	60/60/30	240/240/150	1/1/2
7#	Ag-Cu-B83	50/50/25	90/90/30	3/3/4
8#	Ag-Cu-B83	50/50/25	150/150/90	1/1/2
9#	Ag-Cu-B83	50/50/25	240/240/150	2/2/3

3.3.2 Analysis of orthogonal test results

The electro-spark deposition composite coatings are the result of gradual

accumulation through multiple discharge and a large number of deposition points. Mass transfer is usually regarded as an important index to evaluate ESD.

At the beginning of deposition, the coating mass increases most obviously. With the increase of deposition time, the mass transfer of electrode to substrate gradually decreases. Finally, with the increase of deposition time, the mass of substrate stops increasing. This is because with the increase of deposition time, the content of oxide or nitride on the surface of the coating increases, the residual stress on the surface increases, the binding force decreases, and the material is more likely to splash during discharge, which impedes the mass transfer in the process of ESD. In this study, a precision electronic balance with an accuracy of 0.1 mg was used to measure the samples and calculate the mass added to the substrate after ESD, as shown in Table 3.12.

Table 3.12 – The mass added of substrate after ESD

Specimens	1#	2#	3#	4#	5#	6#	7#	8#	9#
mg/cm^2	11.5	10.2	12.7	34.1	54.4	16.2	23.9	10.0	15.4

Orthogonal analysis shows that voltage has the greatest effect on the mass of the coatings, followed by specific deposition time, and capacitance has the least effect on the mass of the coatings. When the voltage is 60 V, 60 V, 30 V, capacitance is 150 μF, 150 μF, 90 μF, efficiency is 3 min/cm^2, 3 min/cm^2, 4 min/cm^2, the optimal value of unit coating weight is 54.4 mg/cm^2.

The energy of ESD discharge is shown in Formula (3.1):

$$W = \mathrm{k} \cdot \frac{CU^2}{2} \tag{3.1}$$

In the formula, W is the discharge energy, the unit is J. k is the circuit loss coefficient (k is 0.6-0.7), C is the capacity of the energy storage capacitor in F, U is the voltage in V. It can be seen from the energy formula of ESD discharge that the higher of the voltage, the higher of the energy and the higher of the capacitance, the higher of the energy.

From the point of spark discharge rule, the larger of the discharge energy, the mass of the more increase, but the experiment shows that the increase of the quality and not as the capacitance increases, this is mainly because the bigger the voltage, the easier to discharge, thereby affect the discharge frequency, increased the influence of the voltage, the influence of the capacitance is too small and concealed by the test error.

The Bruker Contour GT-K1 3D optical profilometers was used to observe the surface of the deposition layer and measure the surface roughness. The surface roughness of the Ag+Cu+B83 composite coatings is shown in Table 3.13:

Table 3.13 – The surface roughness of the Ag+Cu+B83 composite coatings

Specimens	1#	2#	3#	4#	5#	6#	7#	8#	9#
Ra/μm	14.8	13.5	26.3	32.6	32.3	36.6	23.5	20.0	31.2

The orthogonal analysis shows that the effects of voltage, capacitance and efficiency on the surface roughness of the composite coatings are in descending order. The optimal value was obtained when the voltage was 40 V, 40 V, 20 V, capacitance was 150 μF, 150 μF, 90 μF, and efficiency was 1 min/cm^2, 1 min/cm^2, 2 min/cm^2, respectively.

Through the analysis can also be found in the parameter of capacitance was 150 μF, 150 μF, 90 μF and capacitance was 90 μF, 90 μF, 30 μF, there is little difference in coating surface roughness, so the voltage respectively, 40 V, 40 V, 20 V, capacitance respectively 90 μF, 90 μF, 30 μF, and efficiency was 1 min/cm^2, 1 min/cm^2, 2 min/cm^2, respectively. And composite coatings surface roughness 14.8 μm as the optimal values. The surface roughness of the composite coatings is not only affected by the deposition parameters, but also affected by the operation technology, the mechanical accuracy of the welding torch and the properties of the deposited materials.

The thicknesses of the composite coatings are shown in Table 3.14. The thickness of the composite coatings is the most important index of ESD, followed by the surface roughness of the coatings, and the mass of the coatings directly affects the thickness of the coatings. Therefore, the optimal process parameters of ESD are determined by comprehensive analysis: the voltage was 60 V, 60 V, 30 V, capacitance was 150 μF, 150 μF, 90 μF, and efficiency was 3 min/cm^2, 3 min/cm^2, 4 min/cm^2, respectively.

Table 3.14 – The thicknesses of the Ag+Cu+B83 composite coatings

Thickness	1#	2#	3#	4#	5#	6#	7#	8#	9#
μm	50	60	50	160	160	60	100	60	60

Orthogonal analysis shows that voltage has the greatest effect on the mass transfer of the coatings, followed by efficiency, and capacitance has the least effect on the mass transfer of the coatings. When the voltage is 60 V, 60 V, 30 V, capacitance is 150 μF, 150 μF, 90 μF, efficiency is 3 min/cm^2, 3 min/cm^2, 4 min/cm^2, the optimal value of mass transfer is 54.4 mg/cm^2. Under the optimal process parameters, the surface roughness of the composite coatings is 32.3 μm, and the maximum thickness is 160 μm.

The measured results of the coating surface roughness are shown in Figure 3.8.
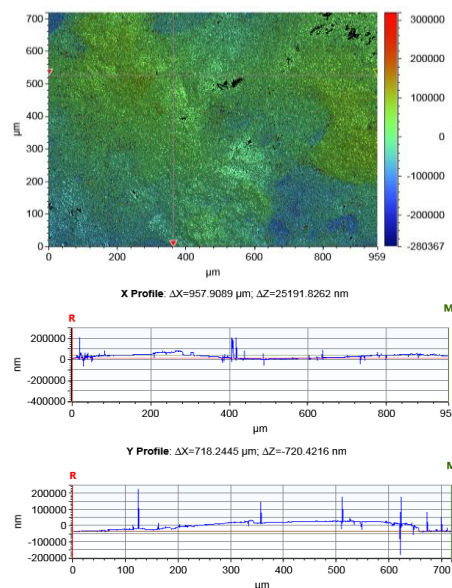

Figure 3.8 – The roughness of the Ag+Cu+B83 ESD coatings

3.3.3 The morphology of the surface and the cross section of the combined coatings

The morphology of the Ag+Cu+B83 ESD combined coatings surface is shown in Figure 3.9. It can be seen from the figure that the surface of the deposited coatings is sputtering stacking, which is formed by the superposition of many irregular small droplet spots melted by continuous pulse discharge. There are a few micro cracks on the surface of the composite coatings, which tend to propagate along the direction perpendicular to the surface of the coatings. This is due to the rapid heating and cooling in the process of spark discharge, the residual thermal stress in the coatings will exist, leading to the initiation of micro-cracks, and the transition layer of Ag and Cu with good plasticity can play a role in relieving the thermal stress, thus reducing the number of cracks [184]. The multilayer structure with a low modulus ratio contributed to reduced stress concentration in harder sub-layer, thereby inhibiting crack initiation.

Figure 3.10 shows the cross section morphology of the Ag+Cu+B83 ESD composite coatings. It can be seen that the composite coatings have a good metallurgical combination with the substrate, the microstructure of the sedimentary layer is compact, and the continuous interface is formed at the joint. The thickness of the composite coatings is about 100 μm, but there are some defects such as micro-cracks and holes in some places. The composite coatings are tin-base Babbitt B83, copper and silver from the surface to the substrate. However, because the wettability of silver and copper is very good, the silver-white silver coating can rarely be observed. In some areas, the copper coating is not obvious, because the coating is completely fused together during the electro-spark deposition, forming the alloy layer. Since the ESD is a process of

continuous superposition of the deposited materials, the thickness of the deposited layer increases with the increase of the electrode materials deposited on the surface. During ESD, the instantaneous high temperature generated by high frequency pulse discharge melts and vaporizes the materials in the discharge area, and melts, diffuses and alloys occur on the deposited surface. Then the substrate surface is rapidly cooled and solidified, resulting in large cyclic thermal stress and microstructure stress in the sedimentary layer, resulting in micro-cracks or pores on the surface of the deposition. In the process of layer by layer covering, a small number of micro-cracks or pores on the surface of the coating can not be completely filled by the molten material, forming holes.
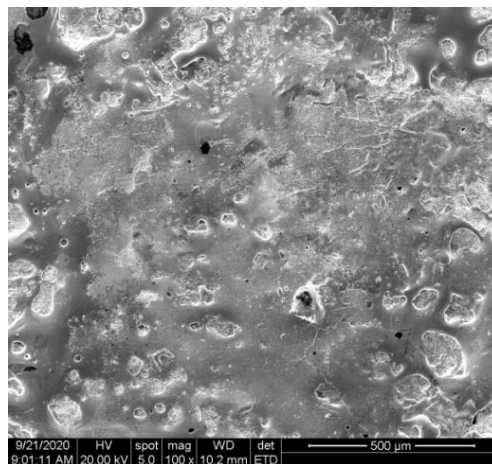

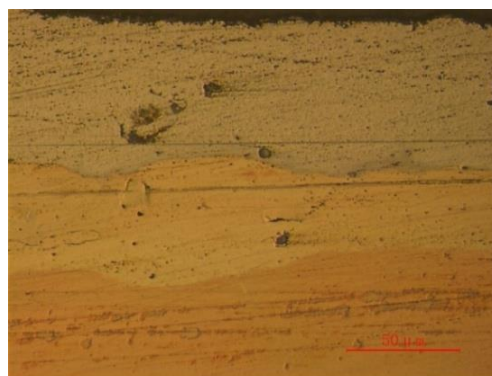Figure 3.9 – The morphology of the Ag+Cu+B83 composite coatings surface

Figure 3.10 – The cross section morphology of the Ag+Cu+B83 composite coatings

3.3.4 The region elemental composition of the surface and the cross section of the combined coatings

By observing the surface morphology of the composite coatings, three characteristic regions (smooth surface, rough surface and pore) can be selected on the coating surface, and the element composition of each characteristic region and a whole surface can be measured. The detection position of the element composition on the surface of the Ag+Cu+B83 composite coatings deposited by electric spark is shown in Figure 3.11. The elemental composition on the surface of the Ag+Cu+B83 composite coatings detected in different characteristic areas is shown in Table 3.15. As can be seen from Table 3.15, in addition to Sn, Sb and Cu elements, there are also some Ag and O elements in the surface coating, in which Cu content is also relatively high. This indicates that the ESD is not a simple process of transfer of the electrode material, but a dramatic diffusion and re-alloying of the atoms of the electrode and matrix material occurs during the deposition of each element, which makes the deposition layer and matrix realize metallurgical bonding. In spite of the argon protection, the surface of the composite coatings was oxidized by some air during the deposition of silver, copper and tin-base Babbitt alloy by electric spark. It can also be seen from Table 3.15 that the smooth surface coating has a low copper content, a high oxygen content and a certain oxidation phenomenon on the surface. The content of silver, copper and oxygen in the rough surface is relatively high, while the content of tin and antimony is relatively low, indicating that the B83 coating is relatively thin and oxidation phenomenon is more obvious. The content of copper and oxygen in the pores is relatively low, and the content of tin and antimony is relatively high, indicating that the pores may be left by

material splashing outward at high temperature. In the overall elemental composition of the surface, oxygen content is relatively low, copper content is relatively high, and there is a certain amount of silver, which indicates that the overall surface oxidation is less, and the diffusion is intense during deposition.

In the process of electro-spark deposition, between the electrode and substrate instantaneous discharge of high temperature enough to contact with the metal melting liquid metal molten pool formation, the liquid metal in the spark discharge of local physical explosion and the effect of rotating electrode, splash around and then cool and solidify sharply, in the process of solidification edge retained part of its flow marks, it also makes the sedimentary surface roughness is larger. Sn and Sb content of smooth surface area was obviously higher than that of rough surface area, but smooth surface area of Cu content is significantly lower than the rough surface area, the smooth surface area does not contain Ag element, while the rough surface area contains Ag element. the smooth surface area is due to the molten material in the electrode under the effect of rotating centrifugal force, splash from the electrode surface, because there is a certain kinetic energy, is deposited on the workpiece surface, after before completely frozen, due to the role of its kinetic energy, the surface flow in the sedimentary formation. Rough surface area is the high temperature generated by the spark discharge between the electrode and the matrix that melts the electrode and the matrix in the contact micro-area to form a liquid metal molten pool. These liquid metals splash around under the action of the local physical explosion and the rotating electrode, and the deposited surface metal molten pool area is left after the liquid metal splashes outward. The O content of the smooth surface region is obviously higher than that of the pore region,

but the content of Sn, Sb and Cu elements in the smooth surface region is basically the same as that in the pore region, and there is no Ag element in the smooth and pore regions, and the pores mainly exist on the smooth surface, which shows that the pore region is due to the rapid cooling and solidification of liquid metal melt at high temperature. Formed by the outward splashing of internally generated gases or refractory substances, And the outward splashing of the high temperature material impedes the oxidation of the nearby metal melt.

By scanning the Ag+Cu+B83 composite coatings surface to the substrate for many times, the element composition is analyzed in the composite coatings section, as shown in Figure 3.12. Table 3.16 shows the measured elemental composition at each position of the composite coatings section. From the SEM morphology of the composite coatings section in Figure 3.12, it can be seen that the internal structure of the Ag+Cu+B83 composite coatings deposited by electric spark is compact, the metallurgical bonding between the coatings and the substrate is good, and three different metal alloys can be distinguished. As can be seen from Table 3.16, from the surface of the composite coatings to the substrate, the content of the copper element gradually increases, the content of the tin element gradually decreases, only a relatively large amount of antimony is contained near the surface layer, a relatively large amount of silver is contained in the middle layer, and the phosphorus is contained near the substrate, which indicates that the thickness of the Ag+Cu+B83 composite coating is about 100 μm. In addition, no oxygen element was detected from the surface of the composite coatings to the substrate, indicating that the composite coating was not oxidized. It can also be seen from Table 3.16 that the contents of Sn, Sb and Cu in positions 1 to 4 of the cross

section of the composite coatings are close to the contents of Sn, Sb and Cu in the tin-based Babbitt alloy B83 electrode, indicating that this area is a Babbitt alloy B83 coating. The content of Cu element increases and the content of Sn element decreases from the position 5 to the position 8 of the cross section of the composite coatings, and the composite coatings contains the Ag element but does not contain the Sb element, which indicates that the metal copper and silver have very good wettability in the area, violent diffusion and re-alloying occur during electro-spark deposition, and the metal copper and silver coating form an alloy layer. The Cu, Sn and P elements in the position 9 of the composite coatings section are close to the contents of the Cu, Sn and P elements in the tin bronze substrate, but do not contain the Sb, Ag and O elements, which indicates that the area is the tin bronze substrate.
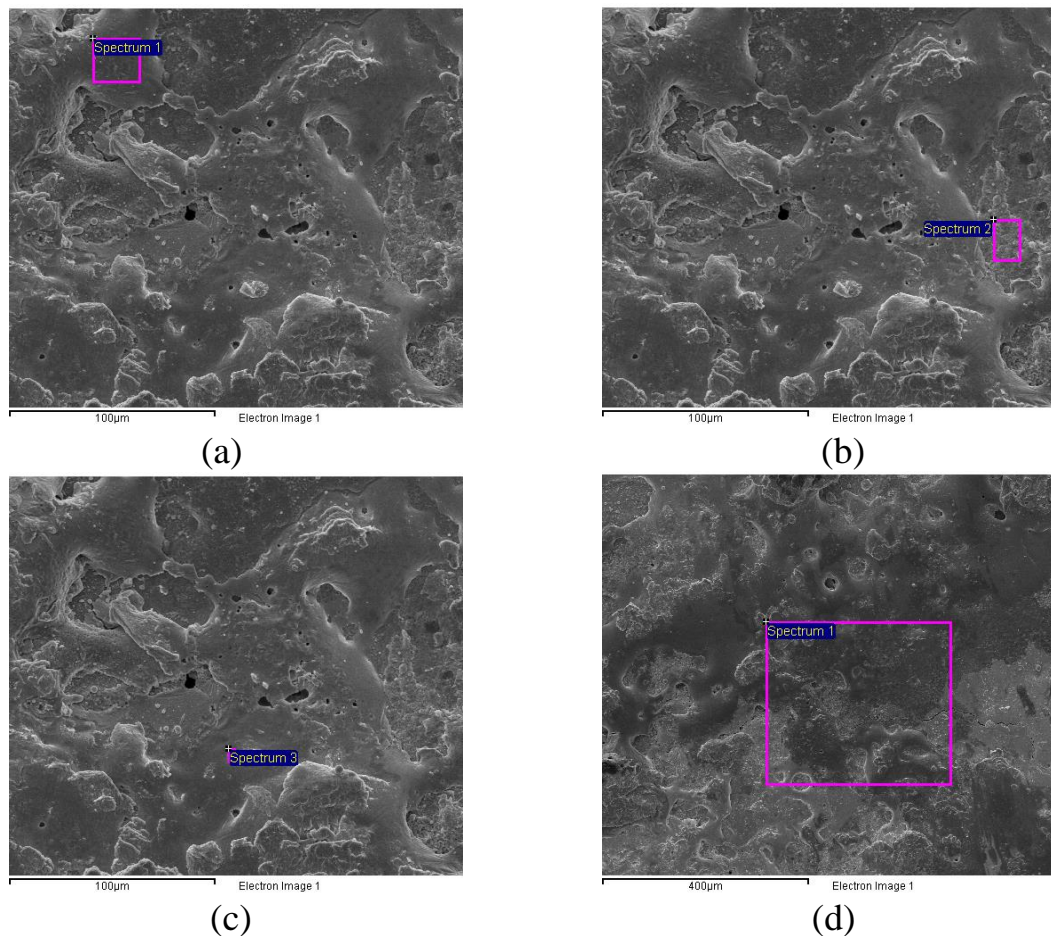

(a)

(b)

(c)

(d)

Figure 3.11 – The detection position of elemental composition of the Ag+Cu+B83

ESD composite coatings surface: a - smooth surfaces; b - rough surface; c - pore; d -

whole surface

Table 3.15 – The elemental composition of the Ag+Cu+B83 ESD composite coatings

surface

Research Area	O (%)	Cu (%)	Ag (%)	Sn (%)	Sb (%)
a	12.23	11.27	0	62.79	13.70
b	14.98	22.66	7.81	47.67	6.88
c	5.48	11.18	0	71.33	12.01
d	3.22	21.19	6.67	58.58	10.35
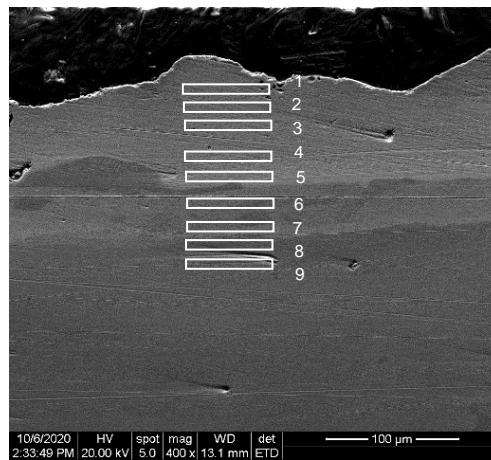
Figure 3.12 – The cross section SEM morphology of the Ag+Cu+B83 ESD

composite coatings at different position

Table 3.16 – The elemental composition of cross section of the Ag+Cu+B83 composite

coatings

Research Area	O (%)	P (%)	Cu (%)	Ag (%)	Sn (%)	Sb (%)
1	0	0	6.41	0	75.22	18.37
2	0	0	4.30	0	78.56	17.13
3	0	0	4.27	0	83.16	12.58
4	0	0	4.71	0	79.62	15.67
5	0	0	44.25	45.37	10.38	0
6	0	0	93.92	0	6.08	0
7	0	0	94.20	0.97	4.83	0
8	0	0	93.08	0.69	6.23	0
9	0	0.11	92.43	0	7.46	0

3.3.5 The line scan elemental composition of the cross section of composite coatings

By scanning the soft antifriction composite coatings surface to the substrate, the element composition is analyzed in the composite coatings section, as shown in Figure 3.13 (a). Figure 3.13 (b) shows the measured elemental composition at the line scanning position of the composite coatings section. From the SEM morphology of the composite coatings section in Figure 3.13 (a), it can be seen that the internal structure of the soft antifriction composite coatings deposited by electric spark is compact, the metallurgical bonding between the coatings and the substrate is good, and three different metal alloys can be distinguished. As can be seen from Figure 3.13 (b), from the surface of the composite coatings to the substrate, the content of the copper element gradually increases, the content of the tin element and the antimony element gradually decreases, a relatively large amount of the silver is contained in the middle layer, and a small amount of the phosphorus is contained, which indicates that the thickness of the soft antifriction composite coatings is about 160 μm. In addition, no oxygen element was detected from the surface of the composite coatings to the substrate, indicating that the composite coatings were not oxidized. It can also be seen from Figure 3.13 (b) that the contents of Sn, Sb and Cu in the surface to 70 μm of the cross section of the composite coatings are close to the contents of Sn, Sb and Cu in the babbitt B83 electrode, indicating that this area is the babbitt B83 coating. The content of Cu element and Ag element increases, the content of Sn element and Sb element decreases from 70 μm to 160 μm of the cross section of the composite coatings, which indicates that the metal copper and silver have very good wettability in the area, violent diffusion and

re-alloying occur during electro-spark deposition, and the metal copper and silver coatings form the alloy layer. The Cu, Sn and P elements in the depth over 160 μm of the composite coatings section are close to the contents of the Cu, Sn and P elements in the QSn10-1, which indicates that the area is the tin bronze substrate.

(a)   (b)
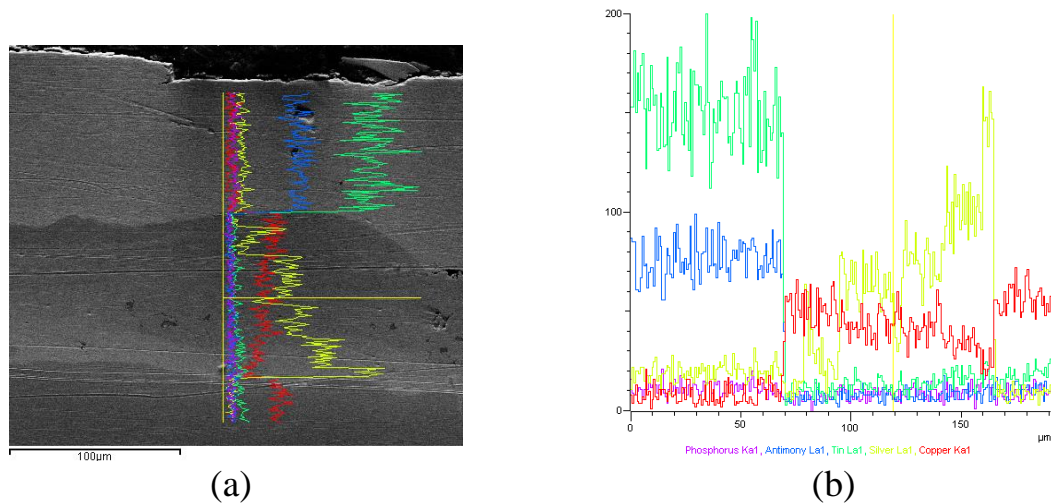
Figure 3.13 – The line scan elemental composition of the cross section of composite coatings: a - Line scanning position; b - All the elemental composition

3.3.6 The morphology and phase composition of the combined coatings surface after grind

After deposition, only simple grinding is needed to meet the requirements of surface roughness. The morphology of the soft antifriction composite coatings surface after grind is shown in Figure 3.14. The micro-texture on the surface of the polished composite coatings is conducive to the storage of abrasive particles and lubricating oil during the operation of the bearing bush, reducing the wear of abrasive particles on the surface of the bearing bush, reducing the friction coefficient and improving the self-lubricating performance. The prepared coatings surface has a small amount of ferrous metal oxides due to oxidation, which is caused by the oxidation of tin in babbitt alloy.

After alloying surfaces were grinded with 1000 grits sandpaper, the X-ray diffraction (XRD) analysis of the composite coatings surface was carried out. Figure 3.15 shows the X-ray diffractogram patterns of the soft antifriction composite coatings surface. The diffraction peaks observed for composite coatings surface in Figure 3.15 clearly indicate the phases corresponding to Sn, SbSn, Cu_6Sn_5 and Cu. The Sn phase shows strong diffraction intensity, suggest the content of Sn is relatively high of composite coatings. Moreover, in the case of soft antifriction composite coatings in addition a phase of Ag_3Sn was appeared which is conducive to ensuring the metal bonding of the coatings [185]. It is noted that oxide peaks, nitride peaks and carbide peaks were not observed. Maybe the content of these constitutions is too little to be detected by XRD.
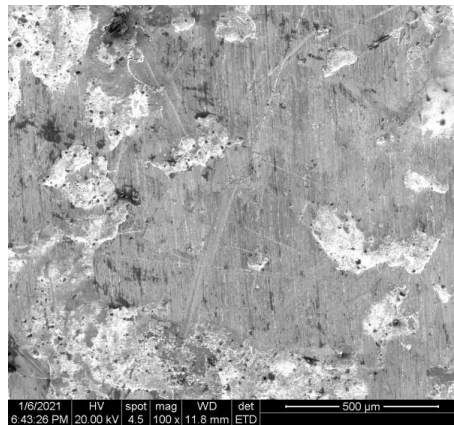

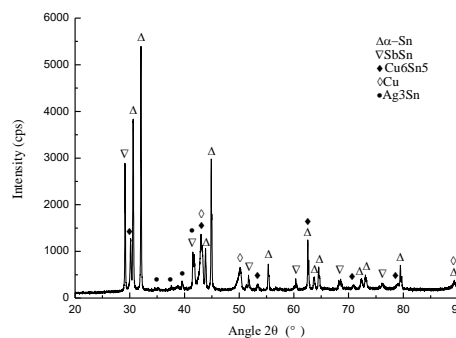Figure 3.14 – The morphology of the Ag+Cu+B83 ESD composite coatings surface after grind

Figure 3.15 – The X-ray diffraction patterns of the Ag+Cu+B83 ESD composite

coatings surface

3.3.7 The cross section microhardness distribution of the composite coatings

Electro-spark deposition technology can effectively change the surface of the physical and chemical properties, mechanical properties, so that the hardness of the surface changes, which has special properties. Figure 3.16 (a) is the cross section microhardness indentation of the composite coatings. Figure 3.16 (b) is the microhardness change curve from the surface of the composite coatings to the substrate, and the whole hardness curve presents obvious gradient distribution, which can be divided into four parts in turn: the tin-based Babbitt alloy B83 coatings area, the copper transition area, the silver transition area and the substrate. The material deposited on the surface of the composite coatings is tin-based Babbitt alloy B83, the thickness of the coating is about 50 micrometers, the coating is relatively soft, and the microhardness is 29 $HV_{0.01}$; The thickness of copper transition zone is about 25 μm, and the microhardness of the coating is 157 $HV_{0.01}$; The thickness of Ag transition zone is about 25 μm, and the microhardness of the coating is about 95 $HV_{0.01}$; And then the hardness of the composite coatings gradually increases and transits to the substrate, and the microhardness of the substrate is 161 $HV_{0.01}$. The microhardness of that composite coatings is gradually transferred from the surface to the substrate, which is beneficial to improve the bonding strength between metals and reducing crack. From the surface of the composite coatings to the substrate, the hardness of the composite coatings first increases, then decreases, and finally increases. The hardness of composite coatings is 82% lower than that of bronze substrate.
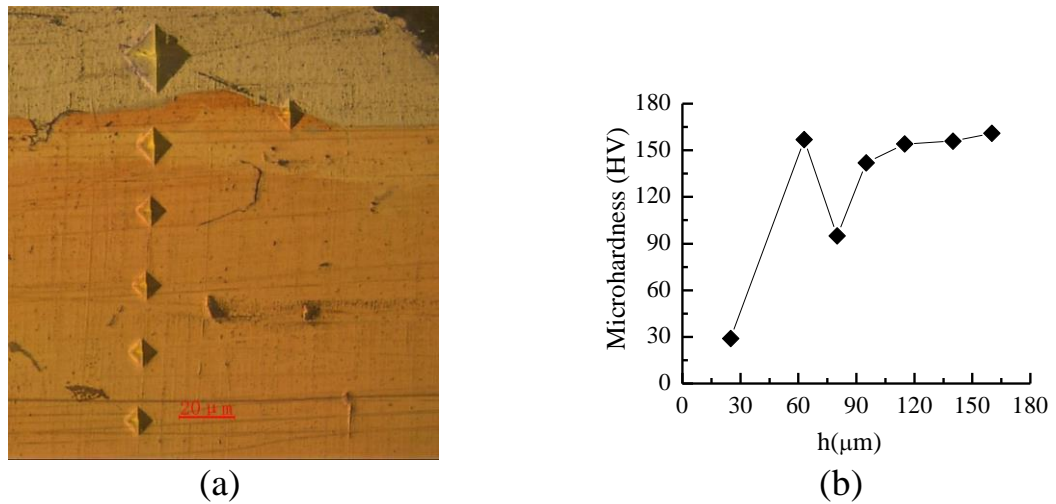
Figure 3.16 – The cross section microhardness distribution of the Ag+Cu+B83

ESD composite coatings: a - indentation; b - the microhardness change curve

3.3.8 Tribological properties of the combined coatings

Figure 3.17 compares the evolution of the friction coefficient variation during uncoating tests at loads of 5 N, 10 N and 15 N. For the initial 600 seconds at load of 5 N, the friction coefficient with an average value of about 0.333. The following 600 seconds at load of 10 N, the friction coefficient is about 0.330. And then to 15 N for the final 600 seconds, the friction coefficient is about 0.324.

Figure 3.18 compares the evolution of the coefficient of friction at the applied loaded of 5 N, 10 N and 15 N of the ESD modified samples sliding against a GCr15 steel ball in air. For the initial 600 seconds at load of 5 N, the friction coefficient with an average value of about 0.399. The following 600 seconds at load of 10 N, the friction coefficient is about 0.244. And then to 15 N for the final 600 seconds, the friction coefficient is about 0.180. The investigation of the tribological properties of the coatings in dry friction show that the lower resistance is exhibited by the composite coatings deposited using the soft antifriction material. The surface friction coefficient of the composite coatings is 55.6% of the tin bronze substrate.

From the evolution of the coefficient of friction of the tin bronze substrate with and without soft antifriction composite coatings, it is clear that wear process indicated is rather complicated because of the influence of different surface topography and chemical composition during running-in phase. For ESD layers, at the beginning of steady stage its friction coefficient shows to some extent direct response to surface roughness. And for the initial 600 seconds at load of 5 N, the friction coefficient is about 0.399 influenced by the surface roughness (Figure 3.18 (a)). Because GCr15 with high hardness produce material loss of soft antifriction composite coatings counterpart (with relative low hardness) through dominant abrasion mechanism. With the generation of tribofilm, abrasion of composite coatings-GCr15 sliding couples is transferred to interfacial sliding. Similar to other sliding couples, the steady-state fiction coefficients become more or less independent of surface roughness. After the first running-in stage, the soft antifriction composite coatings demonstrated a relatively stable friction coefficient with an average value of about 0.244 after the following 600 seconds at load of 10 N (Figure 3.18 (b)), after which it decreased to the level of 0.180 at load of 15 N (Figure 3.18 (c)). The friction coefficient stabilizes after running-in, and becomes stable throughout the test.

The surfaces of wear traces were analyzed in order to understand the friction and wear resistance mechanisms of the coatings. The wear scars of the tin bronze substrate with and without the soft antifriction composite coatings after tribological testing are shown in Figure 3.19.

It was found from analysis of wear scars in Figure 3.19 (a) that the wear mechanism of the tin bronze substrate is dominated by severe ploughing wear and

fatigue delamination. A lamellar structure can be distinguished on the surface of the worn tin bronze substrate. This can be responsible for low friction under these conditions.

However, it can be seen in Figure 3.19 (b) that the soft antifriction composite coatings may effectively restrain fatigue delamination, showing plastic deformation, abrasive wear and slight polishing. Plastic deformation and abrasive wear dominated on the relatively soft composite coatings. The initial surface microgeometry was changed during load application and its surface became smooth with fine shallow scratches observed after the wear test. After the smooth surface was formed, the friction and wear stabilized.

(a)

(b)

(c)
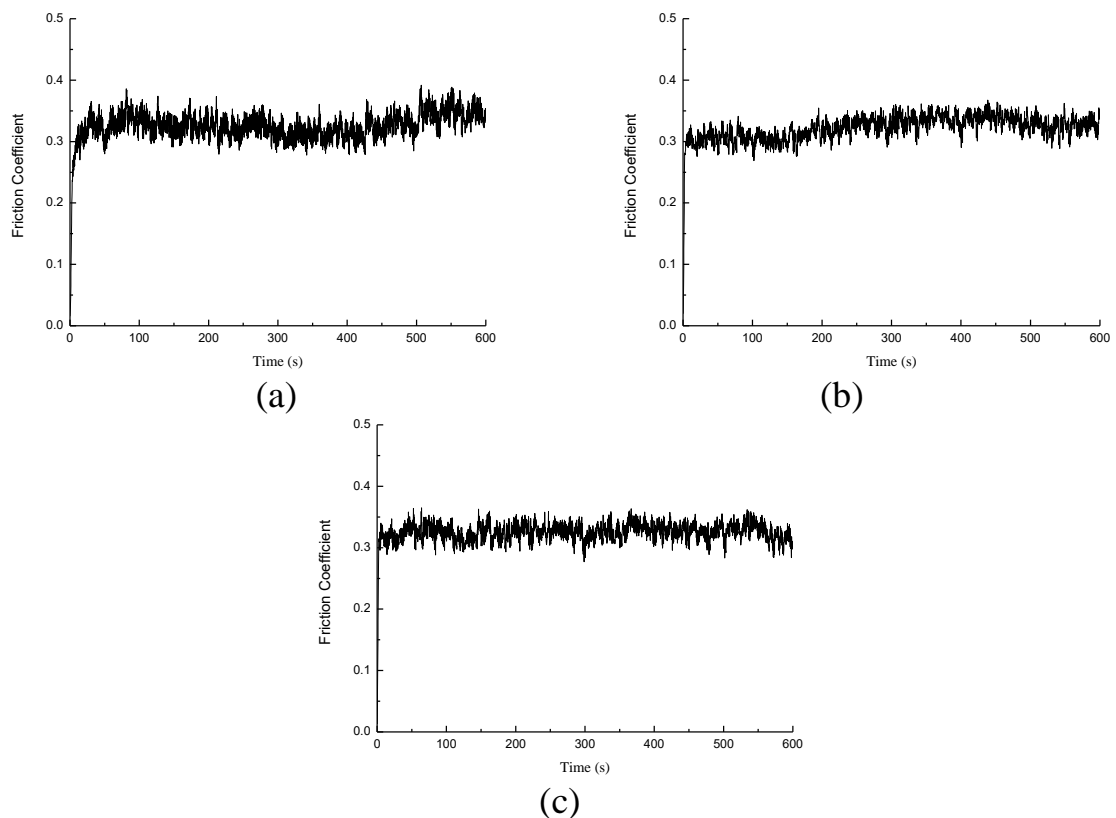
Figure 3.17 – Friction coefficient variation during uncoating tests at different loads:

a - 5 N; b - 10 N; c - 15 N

(a)

(b)

(c)
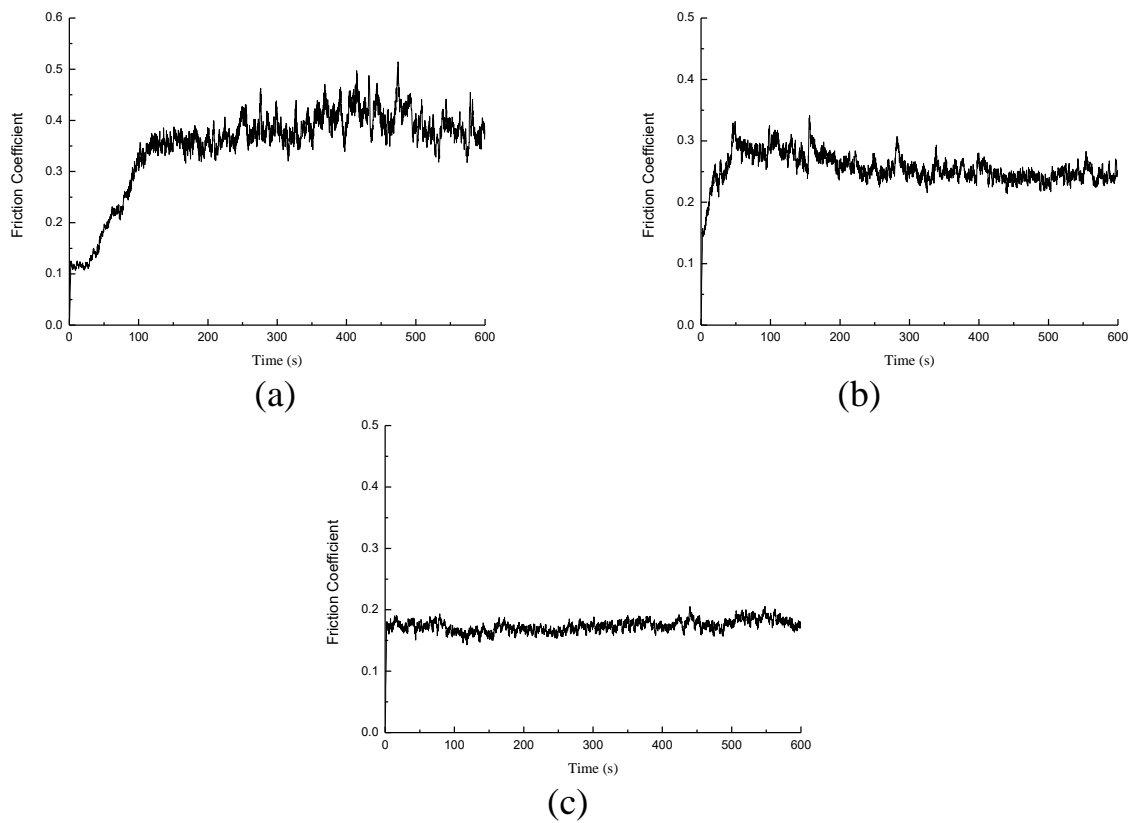
Figure 3.18 – Friction coefficient variation during composite coatings tests at

different loads: a - 5 N; b - 10 N; c - 15 N

(a)   (b)
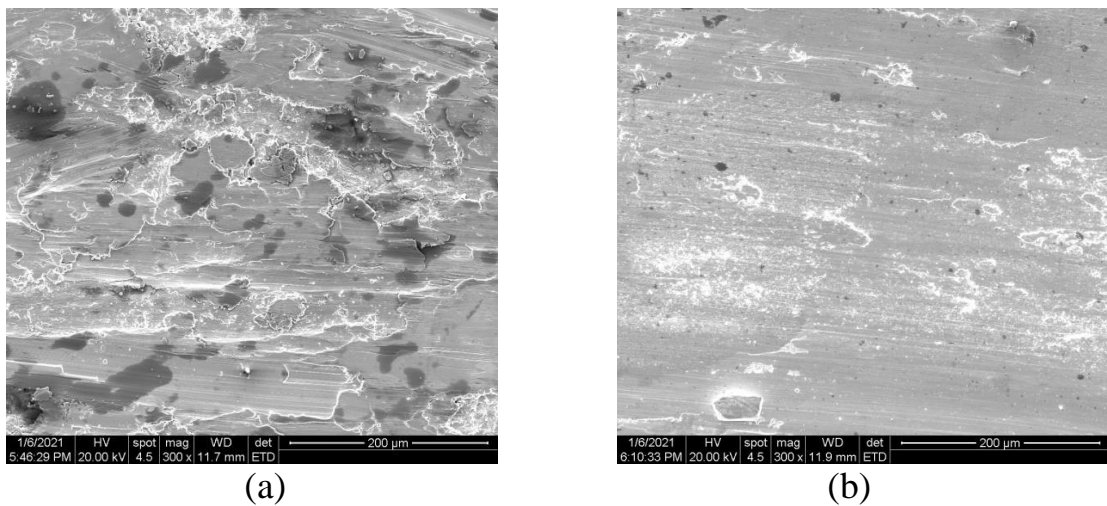
Figure 3.19 – The wear scars of the tin bronze substrate with and without the composite

coatings after tribological testing: a - Tin bronze; b - Tin bronze with the composite

coatings

3.4 The characterization of Ag+Cu+B83+GO+B83 composite coatings

With the large variety of the operation conditions of the parts, their surface layers

are considered as the most loaded portions. Therefore, the real working resource of the machine operation directly depends on the part surface bearing capacity being determined by the quality of its surface layer. Wear and breakdown of the machine components and mechanisms as a rule commence from a surface, and therefore in order to improve the operating properties of machines and mechanisms it is necessary to improve component surface quality. One of the most effective improvements of surface quality and component operating properties is provided by application of special coatings [186-188]. A functional coating for the friction units (FU) is used on curvilinear and flat surfaces various mechanisms, such as turbo-compressor units, electric motors, power engineering units, power transmission systems, etc. To a significant extent FU reliability depends on the quality of bearing manufacture, coating application quality, and assembly and repair work. During manufacture of FU there are always deviations from ideal shape geometry; additional errors are contributed during parts installation, which in combination a reduction in actual contact area is a reason an increased load on an antifriction layer, especially in the running-in period. Facilitation of running-in conditions and improvement of friction surface operating regime in the post running-in period may be provided by improving the FU and more close fitting to "beds" by applying to contact surfaces a layer of soft metals by electric-spark deposition (ESD). Soft coating (Ag, Cu, B83 or combined coating) deformation under action of high specific loads makes it possible to provide parts automatic adjustment and compensation of manufacturing errors [189].

Graphene has been used to improve tribological property due to its extraordinary properties [190-192]. Graphene oxide (GO) is considered as a promising material for

reducing friction and wear, owing to its structural features [193]. Therefore, adding the GO to the coatings is beneficial to improve the friction and wear properties of the surface.

The running-in coatings of the tin bronze surface that were formed by alternately electro-spark deposition applying the antifriction material of silver, copper, Babbitt B83 and graphene oxide. The analysis of morphology, composition and properties of the coatings were investigated.

3.4.1 Deposition process parameters

The ESD machine DZ-4000III has a control panel to change the electrical parameters including ESD voltage (20 V- 250 V), capacitance (30 µF – 420 µF) and frequency (1300 Hz – 6000 Hz).

Travel speed in both cases was 2 mm/s. The frequency of the first layer was 3 kHz, the frequency of the second layer was 4 kHz and the frequency of the third and the fifth layers were 5 kHz. Deposition was carried out using a hand-held gun at room temperature with the argon gas (Ar 99%) protection (10 L/min flow rate), which avoids contamination of the deposit zone by interstitial elements such as oxygen or nitrogen.

The GO solution was applied to the surface of the specimens by manual pre-coating method, and then the specimens was dried by natural air, followed by the fifth layers with B83 electrode.

The electro-spark deposition process parameters (electrodes, voltage, capacitance and efficiency) are shown in Table 3.17.

Table 3.17 – The ESD parameters of the running-in coatings

Specimens	Coatings	Voltage (V)	Capacitance (μF)	Efficiency (min/cm^2)
1#	Ag+Cu+B83+	60/40/30	90/90/30	2/1/1
	GO+B83	--/20	--/30	--/2
2#	Ag+Cu+B83+	60/40/30	150/90/30	2/1/1
	GO +B83	-/25	--/90	--/2
3#	Ag+Cu+B83+	60/40/30	150/150/90	2/1/1
	GO +B83	-/30	--/150	--/2

3.4.2 The mass transfer, roughness and thickness characteristics of the running-in coatings

In this study, the analysis of deposition on mass transfer, roughness, and thickness of the running-in coatings were investigated, as shown in Table 3.18.

The electro-spark deposition running-in coatings are the result of gradual accumulation through multiple discharge and a large number of deposition points. The mass transfer is usually regarded as an important index to evaluate ESD. At the beginning of deposition, the coating mass increases most obviously. With the increase of deposition time, the mass transfer of electrode to substrate gradually decreases. Finally, with the increase of deposition time, the mass of substrate stops increasing. This is because with the increase of deposition time, the content of oxide or nitride on the surface of the coating increases, the residual stress on the surface increases, the binding force decreases, and the material is more likely to splash during discharge, which impedes the mass transfer in the process of ESD.

In this study, a precision electronic balance with an accuracy of 0.1mg was used to measure the samples and calculate the mass added to the substrate after ESD, as shown in Table 3.18.

As can be observed in Table 3.18 that increasing the pulse energy in the ESD process promotes the transfer of the mass. The minimum value of mass transfer is 90.8

mg of specimen 1# and the maximum value of mass transfer is 550.1 mg of specimen 3#.

The Bruker Contour GT-K1 3D optical profilometers was used to observe the surface of the composite coatings and measure the surface roughness. The surface roughness of the running-in coatings is shown in Table 3.18. As can be seen from Table 3.18, the minimum value of the surface roughness is 15.9 μm of specimen 2#. The measured results of the coatings surface topography and profile of specimen 2# are shown in Figure 3.20.

The surface roughness of the running-in coatings is not only affected by the deposition parameters, but also affected by the operation technology, the mechanical accuracy of the welding torch and the properties of the deposited materials.

The thickness of the running-in coatings is the most important index of ESD, followed by the surface roughness of the coatings, and the mass of the coatings directly affects the thickness of the coatings. The thicknesses of the running-in coatings are shown in Table 3.18. As can be indicated from Table 3.18, the coatings thickness tends to increase with increasing pulse energy. The minimum value of the thickness is 50 μm and the maximum value of the thickness is 200 μm.

Table 3.18 – The mass transfer, roughness and thickness characteristics of the

running-in coatings

Specimens	Coatings	Mass Transfer (mg)	Roughness R_a (μm)	Thickness (μm)
1#	Ag+Cu+B83+ GO+B83	90.8	17.5	50
2#	Ag+Cu+B83+ GO+B83	244.2	15.9	160
3#	Ag+Cu+B83+ GO+B83	550.1	24.6	200
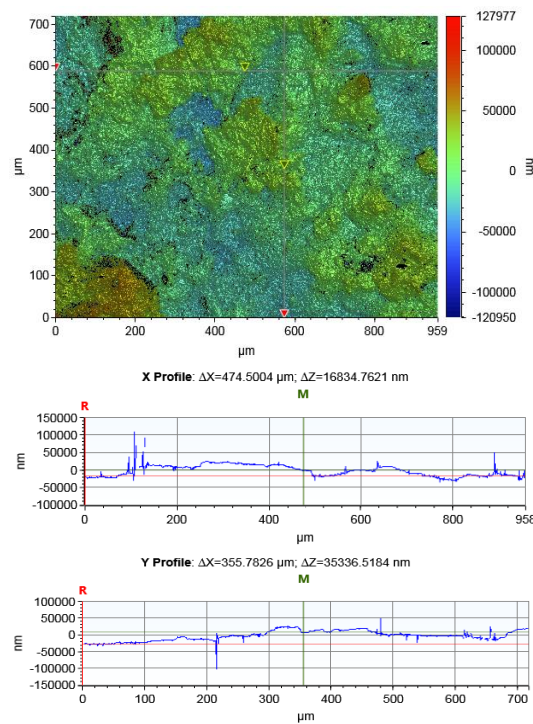
Figure 3.20 – The surface topography and profile of the running-in coatings

3.4.3 The morphology, element composition and phase composition of the running-in coatings surface

The morphology of the running-in coatings surface of specimen 2# is shown in Figure 3.21. It can be seen from the figure that the surface of the running-in coatings is sputtering stacking, which is formed by the superposition of many irregular small droplet spots melted by continuous pulse discharge. There are a few microcracks on the surface of the running-in coatings, which tend to propagate along the direction perpendicular to the surface of the coatings. This is due to the rapid heating and cooling in the process of spark discharge, the residual thermal stress in the coatings will exist, leading to the initiation of micro-cracks, and the transition layers of Ag and Cu with good plasticity can play a role in relieving the thermal stress, thus reducing the number of cracks. The multilayer structure with a low modulus ratio contributed to reduced stress concentration in harder sub-layer, thereby inhibiting crack initiation.

After deposition, only simple grinding is needed to meet the requirements of surface roughness. The microtexture on the surface of the polished running-in coatings is conducive to the storage of abrasive particles and lubricating oil during the operation of the bearing bush, reducing the wear of abrasive particles on the surface of the bearing bush, reducing the friction coefficient and improving the self-lubricating performance. The prepared coatings surface has a small amount of ferrous metal oxides due to oxidation, which is caused by the oxidation of tin in Babbitt B83.

The element composition on the surface of the running-in coatings was characterized by energy dispersion spectrum in Table 3.19. As can be seen from the table, with the increase of discharge energy, the content of copper and silver on the specimens surface gradually decreases, while the content of tin gradually increases, which also indicates that the running-in coating gradually thickens. But with the increase of discharge energy, the content of antimony on the sample surface gradually decreases, possibly because high temperatures increase antimony loss.

After alloying, surfaces were grinded with 1000 grits sandpaper, the X-ray diffraction analysis of the running-in coatings surface was carried out. Figure 3.22 shows the X-ray diffraction patterns of the substrate, Babbitt B83 and the running-in coatings surfaces.

The diffraction peaks observed for the substrate surface in Figure 3.22 (a) clearly indicate the phases corresponding to Cu and (Cu, Sn). The Cu phase shows strong diffraction intensity, suggest the content of Cu is relatively high of the substrate.

As shown in Figure 3.22 (b) the diffraction peaks for Babbitt B83 surface clearly indicate the phases corresponding to α-Sn, SbSn and Cu_6Sn_5. The α-Sn phase shows

strong diffraction intensity, suggest the content of α-Sn is relatively high of Babbitt B83.

The diffraction peaks observed for running-in coatings surface in Figure 3.22 (c) clearly indicate the phases corresponding to α-Sn, SbSn, Cu_6Sn_5 and Cu. The α-Sn phase shows strong diffraction intensity, suggest the content of α-Sn is relatively high of the running-in coatings. Moreover, in the case of running-in coatings in addition a phase of Ag_3Sn was appeared which is conducive to ensuring the metal bonding of the coatings. It is noted that oxide peaks, nitride peaks and carbide peaks were not observed. Maybe the content of these constitutions is too little to be detected by XRD. The silver can play a role in grain refinement, so that the strength and the hardness of the alloy are improved. Copper provides the preferential crystallization center, refines the grain size, and improves the microstructure and mechanical properties of the alloy.
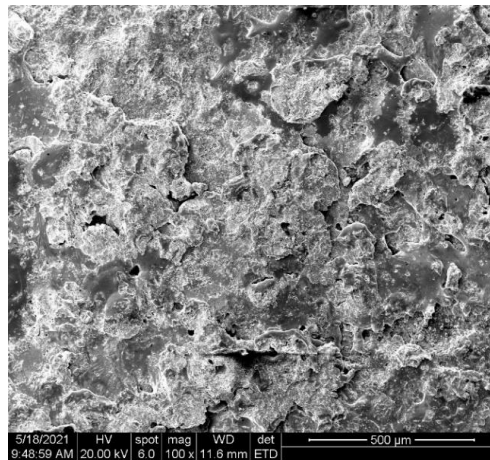
Figure 3.21 – The morphology of the running-in coatings surface

Table 3.19 – The elemental composition of the running-in coatings surface

Specimens	Cu (%)	Ag (%)	Sn (%)	Sb (%)
1#	9.48	1.54	77.21	16.78
2#	7.08	1.51	77.01	14.41
3#	7.09	0.52	83.32	9.08

(a)

(b)

(c)
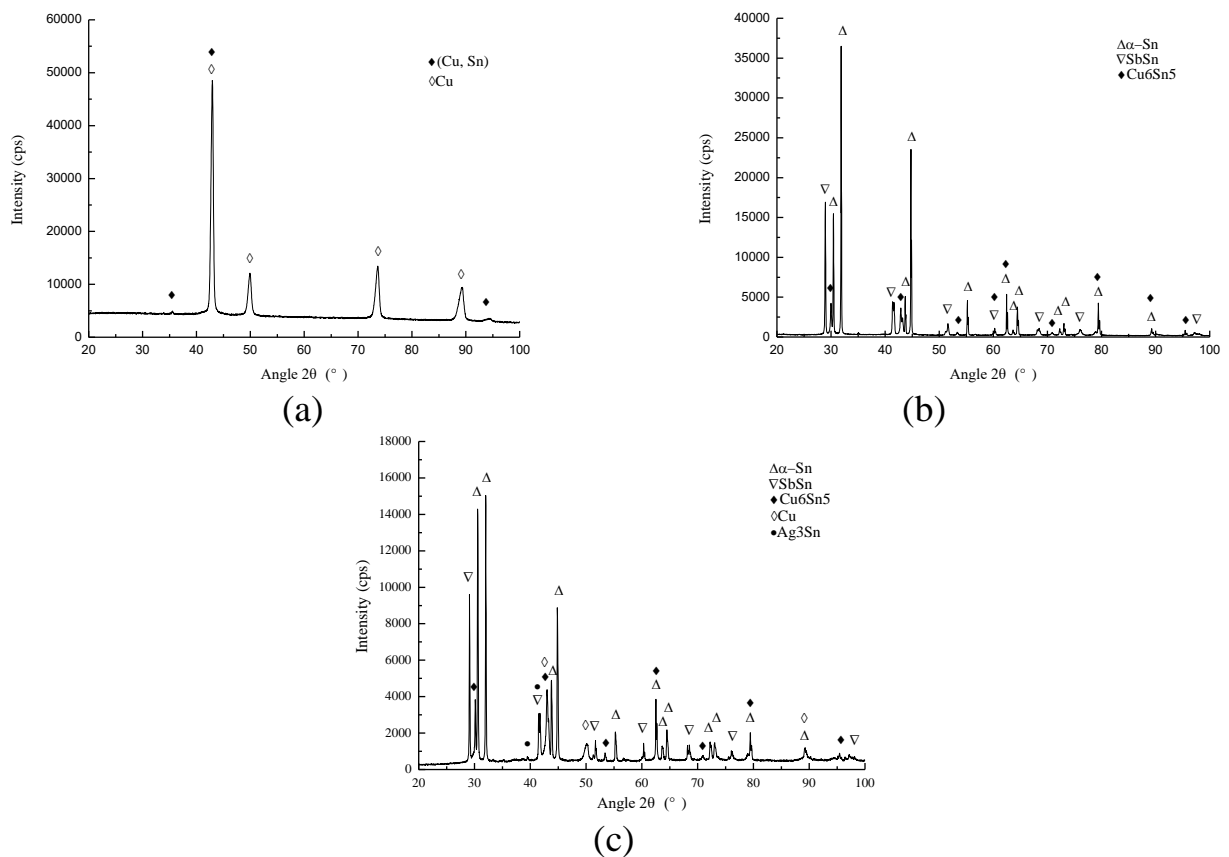
Figure 3.22 – The X-ray diffraction patterns: a - the substrate; b - Babbitt B83; c - the running-in coatings

3.4.4 The cross section morphology of the running-in coatings

The cross section morphology of the ESD treated running-in coatings and Babbitt B83 were analyzed using scanning electron microscopy and metallographic microscopy.

Figure 3.23 (a) shows the cross section morphology of the ESD running-in coatings. As can be seen in the cross-sectional image of the sample with the electro-spark running-in coatings, it has a very good cohesion with the substrate, the microstructure of the deposition layer is compact and the boundary between the coating and the substrate material is clear, but there are a few defects such as micro-cracks and holes in some places. The running-in coatings are Babbitt B83, GO, Cu and silver from the surface to the substrate. However, because the wettability of silver and copper is very good, the silver-white silver coating can rarely be observed and the coatings are

completely fused together during the electro-spark deposition, forming the alloy layer. Since the ESD is a process of continuous superposition of the antifriction materials, the thickness of the deposited layer increases with the increase of the antifriction materials deposited on the surface.

During ESD, the instantaneous high temperature generated by high frequency pulse discharge melts and vaporizes the materials in the discharge area, and melts, diffuses and alloys occur on the deposited surface. Then the substrate surface is rapidly cooled and solidified, resulting in large cyclic thermal stress and microstructure stress in the running-in coatings, resulting in micro-cracks or pores on the surface of the deposition. In the process of layer by layer covering, a small number of micro-cracks or pores on the surface of the coating cannot be completely filled by the molten material, forming holes. Moreover, the high viscosity of the molten metal may prevent it to flow into the valleys even if metal were ejected in its direction prior to its solidification. As a result, a void is left where the valleys once were.

Figure 3.23 (b) presents the metallographic diagram of the material Babbitt B83. It indicates that the square or rectangle with bright color is SnSb, the dark color is α-Sn, and the chain or elongated needle is Cu_6Sn_5. However, as can be seen from Fig. 3.23(a) that the grains in the running-in coatings are very dense, refined and uniformly distributed which is due to the rapid heating and cooling of the antifriction materials by ESD technology.

(a)   (b)
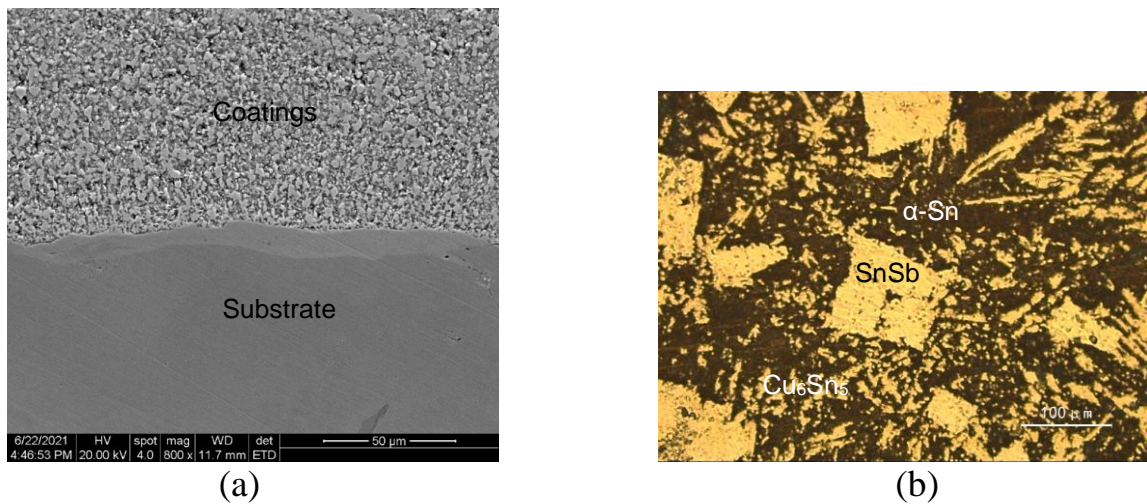
Figure 3.23 – The cross section morphology: a - the running-in coatings; b - Babbitt

B83

3.4.5 The nanoindentation properties of the running-in coatings

Electro-spark deposition technology can effectively change the modulus, the hardness and the deformation rate of the nanoindentation properties of the treated material.

Figure 3.24 shows the nanoindentation curve of the substrate, Babbitt B83 and the running-in coatings. The nanoindentation curve of the substrate is shown in Figure 3.24 (a), and the curve is the change of displacement into surface with load on sample, which can be divided into three segments in turn: load segment type, hold segment type and unload from peak segment type. At the maximum load on the substrate, the modulus is 77.1 GPa, the hardness is 1.93 GPa, and the displacement into surface is 3445.8 nm. When completely unloaded, the displacement into surface is 2980.1 nm and the deformation rate of the substrate is 86.49%. The nanoindentation curve of Babbitt B83 in Figure 3.24 (b) shows the change of displacement into surface with load on sample, which can be divided into three segments: load segment type, hold segment type and unload from peak segment type. At the maximum load on the Babbitt B83, the

modulus is 52.8 GPa, the hardness is 0.352 GPa, and the displacement into surface is 7754.9 nm. When completely unloaded, the displacement into surface is 7249.2 nm and the deformation rate of the Babbitt B83 is 93.48%. The nanoindentation curve of the running-in coatings is the change of displacement into surface with load on sample in Figure 3.24 (c), which can be divided into: load segment type, hold segment type and unload from peak segment type. At the maximum load on the running-in coatings, the modulus is 19.2 GPa, the hardness is 0.281 GPa, and the displacement into surface is 8901.0 nm. When completely unloaded, the displacement into surface is 8482.9 nm and the deformation rate of the substrate is 95.30%.

The modulus, hardness and deformation ratio of the substrate, Babbitt B83 and running-in coatings are shown in Table 3.20. The modulus of the running-in coatings is 36.4% of Babbitt B83 and 24.9% of the tin bronze substrate. The hardness of the running-in coatings is 79.8% of Babbitt B83 and 14.2% of the bronze substrate. The deformation ratio of the running-in coatings is 1.9% higher than that of Babbitt B83 and 10.2% higher than that of the substrate. The application of the electro-spark deposited running-in coatings led to a considerable decrease in modulus and hardness in relation to the substrate material.

(a)
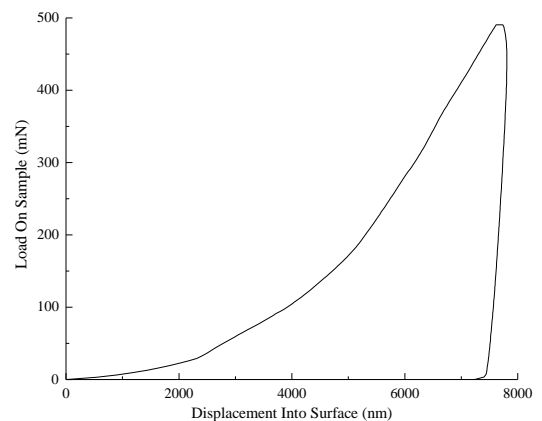
(b)
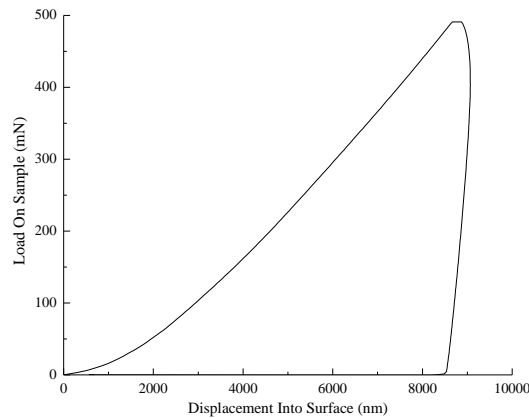
(c)

Figure 3.24 – The nanoindentation curve: a - the substrate; b - Babbitt B83; c - the

running-in coatings

Table 3.20 – The modulus, hardness and deformation ratio of the substrate, Babbitt B83

and the running-in coatings

Specimens	Modulus (GPa)	Hardness (GPa)	Deformation Ratio (%)
substrate	77.1	1.983	86.49
B83	52.8	0.352	93.48
coatings	19.2	0.281	95.30

3.4.6 Tribological properties of the running-in coatings

Table 3.21 shows the evolution of the coefficient of friction at the applied loaded of

5 N, 10 N and 15 N of the specimens sliding against a GCr15 steel ball in air. For the

initial 600 seconds at load of 5 N of the substrate, the friction coefficient with an

average value of about 0.333. The following 600 seconds at load of 10 N, the friction

coefficient is about 0.330. And then to 15 N for the final 600 seconds, the friction

coefficient is about 0.324. For the initial 600 seconds at load of 5 N of Babbitt B83, the

friction coefficient with an average value of about 0.206. The following 600 seconds at

load of 10 N, the friction coefficient is about 0.188. And then to 15 N for the final 600

seconds, the friction coefficient is about 0.192.

The investigation of the tribological properties of the coatings in dry friction show

that the lower resistance is exhibited by the running-in coatings deposited using the antifriction material. The surface friction coefficient of the specimen 1# is the minimum of the composite coatings after running-in stage, but the value of the coatings thickness of the Specimen 1# is 50 μm. Due to the small coatings thickness, the bearing bush surface may be scratched when running in under different working conditions. Therefore, specimen 2# is the best choice.

From the evolution of the coefficient of friction of the tin bronze substrate with the running-in coatings of the specimen 2# in Figure 3.25, it is clear that wear process indicated is rather complicated because of the influence of different surface topography and chemical composition during running-in phase. For ESD coatings, at the beginning of steady stage its friction coefficient shows to some extent direct response to surface roughness. And for the initial 600 seconds at load of 5 N, the friction coefficient is about 0.287 influenced by the surface roughness in Figure 3.25 (a). GCr15 with high hardness produces material loss of running-in coatings counterpart (with relative low hardness) through dominant abrasion mechanism. With the generation of tribofilm, abrasion of running-in coatings-GCr15 sliding couples is transferred to interfacial sliding. Similar to other sliding couples, the steady-state fiction coefficients become more or less independent of surface roughness. After the first running-in stage, the soft antifriction composite coatings demonstrated a relatively stable friction coefficient with an average value of about 0.227 after the following 600 seconds at load of 10 N in Figure 3.25 (b). After the second running-in stage, Figure 3.25 (c) presents the friction coefficient with an average value of about 0.210 at load of 15 N. The friction coefficient stabilizes after running-in, and becomes stable throughout the test. After running-in, the friction

coefficient of specimen 2# is 64.8% of the substrate, which is similar to that of Babbitt B83.

The surfaces of wear traces were analyzed in order to understand the friction and wear resistance mechanisms of the coatings. The wear scars of the tin bronze substrate with and without the running-in coatings after tribological testing are shown in Figure 3.26.

It was found from analysis of wear scars in Figure 3.26(a) that the wear mechanism of the tin bronze substrate is dominated by severe ploughing wear and fatigue delamination. A lamellar structure can be distinguished on the surface of the worn substrate. This can be responsible for low friction under these conditions.

However, it can be seen from Figure 3.26 (b) that the running-in coatings may effectively restrain fatigue delamination, showing plastic deformation, abrasive wear and slight polishing. Plastic deformation dominated on the relatively soft antifriction coatings. The initial surface microgeometry was changed during load application and its surface became smooth with fine shallow scratches observed after the wear test. After the smooth surface was formed, the friction and wear stabilized.

The elemental compositions of the running-in coatings surfaces after tribological testing are shown in Table 3.22. Table 3.19 and Table 3.22 show that copper content on the surface of specimen 1# increases from 9.48% to 23.14%, silver content increases from 1.54% to 2.75%, tin content decreases from 77.21% to 54.35%, and antimony content decreases from 16.78% to 5.89 after friction test. It indicates that the running-in coatings on the surface of specimen 1# has been severely worn away and part of the tin bronze substrate is exposed. In addition, oxygen elements were detected on the surface,

indicating the formation of oxides after surface wear. Table 3.19 and Table 3.22 show that the contents of copper, silver, tin and antimony on the surface of specimen 2# and specimen 3# have little change after friction test. This indicates that the running-in coatings on the surface of specimen 2# and specimen 3# is thick and stable. In addition, the oxygen content detected on the surface indicates that due to the poor stability of tin, the oxides are generated after surface wear.

The surface profile of the substrate, Babbitt B83 and running-in coatings after tribological testing is shown in Figure 3.27.

It was found from analysis of surface profile in Figure 3.27 (a) that the surface of the tin bronze substrate is severely worn, and the wear depth is up to 30 μm. It can be seen from Figure 3.27 (b) that Babbitt B83 is deformed to both sides by extrusion, and the wear depth is 25 μm. Figure 3.27 (c) shows that the running-in coatings deform in the direction of extrusion force, and the wear deformation depth reaches 40 μm.

Facilitation of running-in conditions and improvement of friction surface operating regime in the post running-in period are provided by improving the bearing bush by applying to the composite coatings by ESD. The running-in coatings deformation under action of high specific loads provides parts automatic adjustment and compensation of manufacturing errors.

Table 3.21 – The friction coefficient during the substrate, Babbitt B83 and the running-in coatings tests at loads of 5 N, 10 N, and 15 N

Specimens	5 N	10 N	15 N
substrate	0.333	0.330	0.324
B83	0.206	0.188	0.192
1#	0.265	0.175	0.208
2#	0.287	0.227	0.210
3#	0.374	0.326	0.217
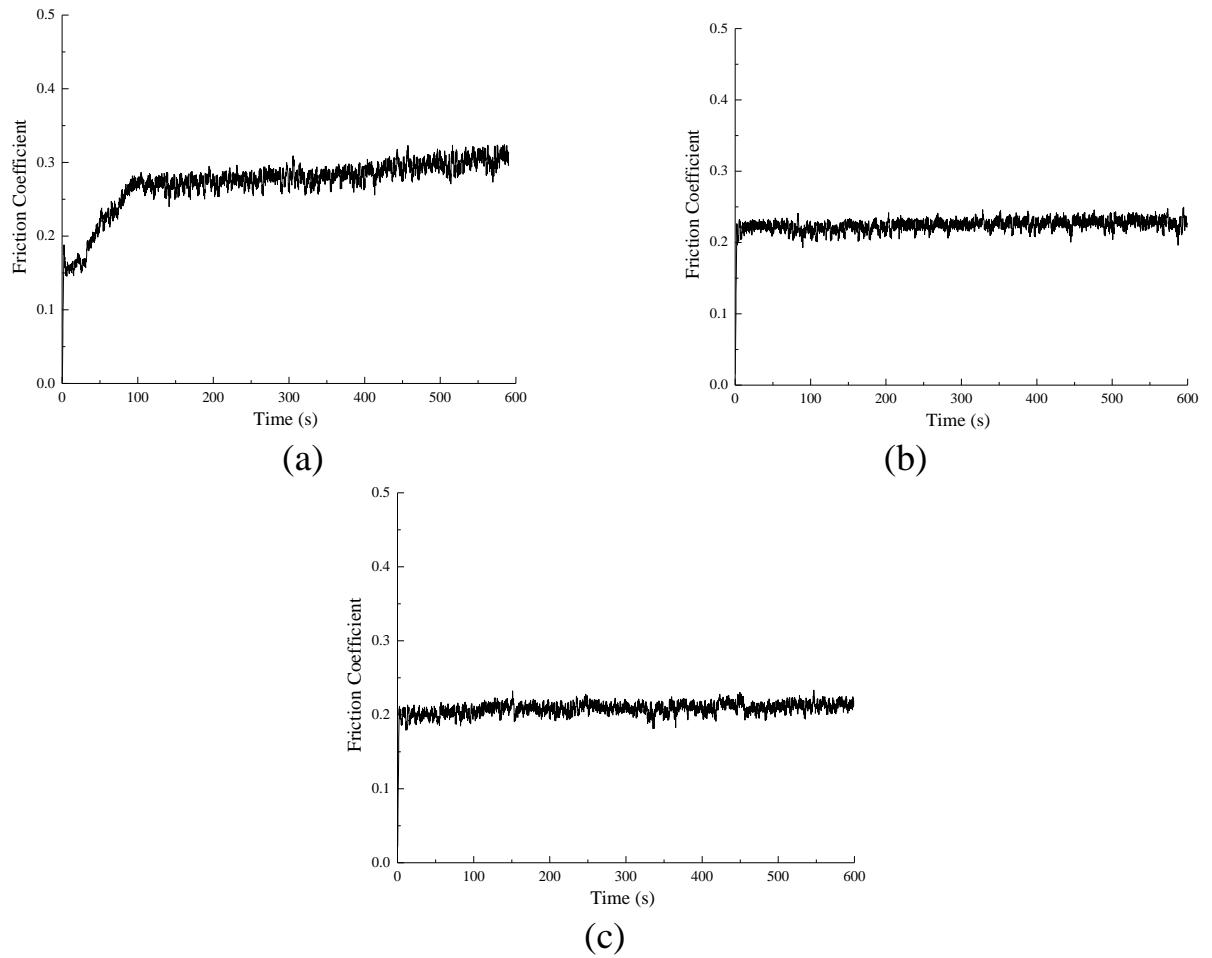
Figure 3.25 – Friction coefficient variation during the running-in coatings tests at

loads: a - 5 N; b - 10 N; c - 15 N
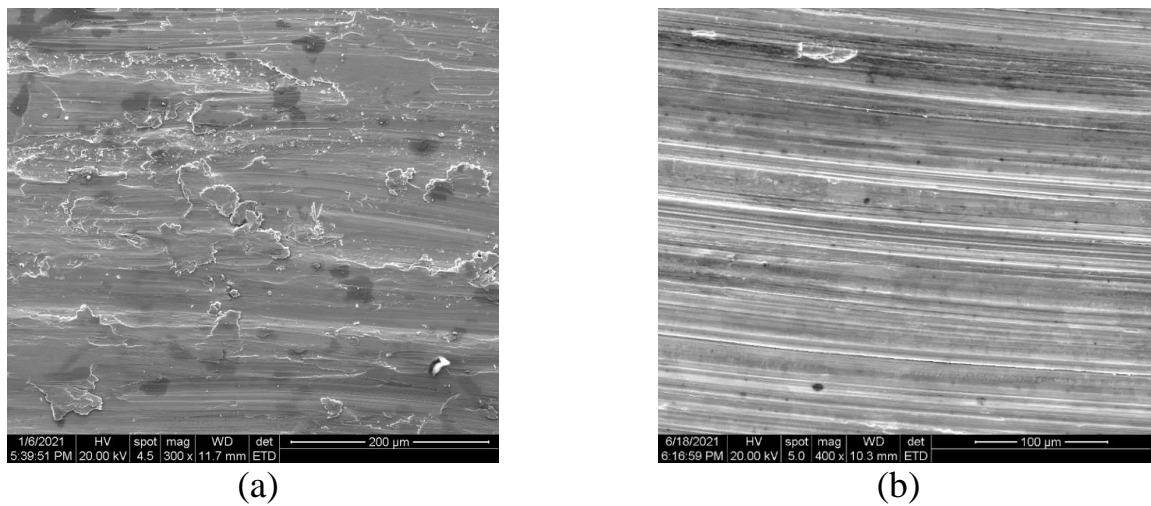
Figure 3.26 – The wear scars after tribological testing: a - the tin bronze substrate; b -

the tin bronze substrate with the running-in coatings

Table 3.22 – The elemental composition of the running-in coatings surface after

tribological testing

Specimens	O (%)	Cu (%)	Ag (%)	Sn (%)	Sb (%)
1#	13.88	23.14	2.75	54.35	5.89
2#	22.10	6.07	0	62.04	9.78
3#	12.77	4.54	0	71.21	11.49

(a)

(b)

(c)
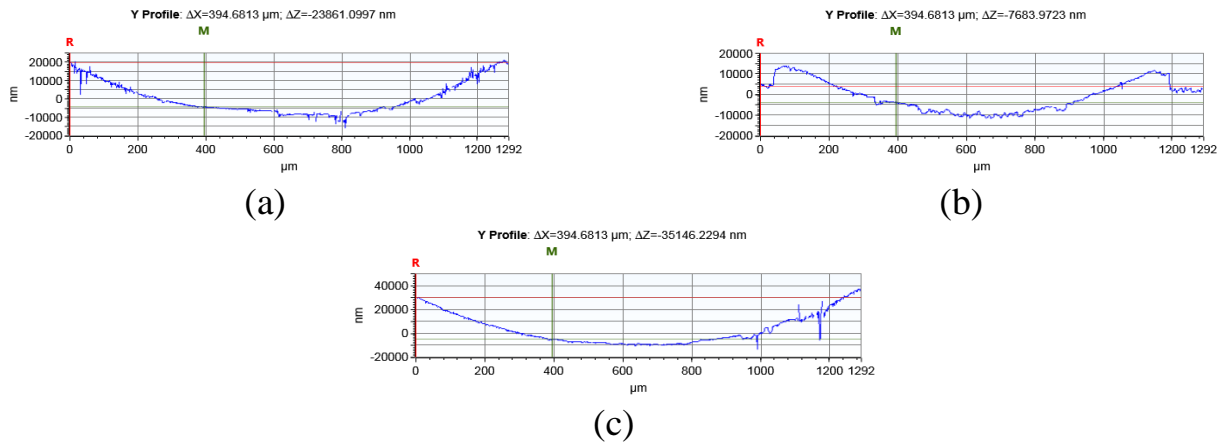
Figure 3.27 – The surface profile after tribological testing: a - the substrate; b - Babbitt

B83; c - the running-in coatings

3.5 Summary

In this chapter, the fabrication methods and process parameters of the silver coatings, Ag+B83 coatings, Ag+Cu+B83 coatings and Ag+Cu+B83+GO+B83 coatings are introduced, and the properties of different coatings are tested and analyzed.

(1) Under the optimal process parameters of the Ag coatings, the minimum friction coefficient of the Ag coatings is about 0.31. However, the performance of silver as antifriction material coatings needs to be further improved.

(2) The minimum friction coefficient of the Ag+B83 composite coatings is about 0.177 after running-in stage. The wear mechanism of the Ag+B83 composite coatings is dominated by plastic deformation and abrasive wear.

(3) Under the optimal process parameters, from the surface of the Ag+Cu+B83

composite coatings to the substrate, the hardness of the composite coatings first increases, then decreases, and finally increases. The surface microhardness of the composite coatings is 29 $HV_{0.01}$, which is 82% lower than that of the tin bronze substrate (161 $HV_{0.01}$).

The surface friction coefficient of the composite coatings (0.180) is 55.6% of the tin bronze substrate (0.324). The wear mechanism of the tin bronze substrate is dominated by severe ploughing wear and fatigue delamination. However, the soft antifriction composite coatings may effectively restrain fatigue delamination, showing plastic deformation accompanied by slight polishing.

(4) Under the optimal process parameters of the Ag+Cu+B83+GO+B83 coatings, the modulus of the running-in coatings is 36.4% of Babbitt B83 and 24.9% of the tin bronze substrate. The hardness of the running-in coatings is 79.8% of Babbitt B83 and 14.2% of the bronze substrate. The deformation ratio of the running-in coatings is 1.9% higher than that of Babbitt B83 and 10.2% higher than that of the substrate.

The friction coefficient of the running-in coatings (0.210) is 64.8% of the substrate (0.324), which is similar to that of Babbitt B83 (0.192). The wear mechanism of the running-in coatings is dominated by plastic deformation, scratching, and slight polishing.

The running-in coatings deformation under action of high specific loads provides parts automatic adjustment and compensation of manufacturing errors.

CHAPTER 4. INDUSTRY APPLICATION OF THE OBTAINED SCIENTIFIC RESULTS

4.1 The traditional technology of bearing bush machining

Bearing is made of copper alloy casting after machining, in order to improve its friction performance, often in the inner surface of the bearing pouring a layer of Babbitt alloy, pouring and then machining. Usually, the traditional pouring process of Babbitt alloy bearing Bush is divided into five processes: cleaning of Bush tire, protection of Bush tire, hanging tin, alloy melting and pouring.

(1) Cleaning of Bush tire

The Bush tire must be cleaned according to the following steps: before the tile tire is hung with tin, the oxide on the tin hanging surface must be checked, and the oxide must be eliminated. The rust can be removed by brushing with 10% hydrochloric acid, and then immersed in hot water at $75℃$ for cleaning after pickling. If oil or other dirt is found on the surface of the tile tire before hanging tin, it can be scrubbed with acetone solution, mechanical processing or electric furnace heating to ensure that the tin plating surface is clean. The surface to be hung with tin shall be evenly coated with a layer of zinc chloride solution before hanging tin to prevent oxidation.

(2) Protection of Bush tire

Attention should be paid to the protection of the bushing: use asbestos mud to plug the process hole on the bushing to prevent the invasion of tin liquid when hanging tin and alloy liquid when pouring. A uniform layer of protective agent is coated on the surface which does not need tinning.

(3) Hanging Tin

Tin is applied to the bronze bushing to ensure that the Babbitt adheres reliably to the bronze substrate. After the tile body is cleaned and protected, it shall be tin-hung immediately.

(4) Alloy melting

And preheat that crucible to about 200℃ before smelting the Babbitt alloy. Removing dirt on the surface of the alloy ingot, putting the alloy ingot into a crucible, and carrying out slag removal treatment after the alloy is completely melted. Heat to about 420℃ and refining with dehydrate ammonium chloride. The dosage of the ammonium chloride is 0.1% to 0.15% of the alloy liquid. If continuous pouring, it can be treated every 1 hour. Before pouring, that alloy liquid is evenly stirred for 5 minutes, and then the slag is removed.

(5) Pouring

There are two casting methods: static casting and centrifugal casting. Only the centrifugal casting process is described here. Before centrifugal casting, first check whether the centrifuge and its auxiliary equipment are in good condition. Place the bearing Bush between the driving and driven chucks with a preheated clamp, fasten it with bolts, and clamp it on the centrifuge. Seal the gap between the Chuck and the bearing shell with asbestos. The Bush shall be clamped and installed quickly to ensure that the temperature of the Bush body is not lower than 280℃ before pouring, otherwise it is necessary to re-tin. The pouring temperature is about 420℃. And select that speed change grade of the centrifugal casting machine accord to the inner diameter of the bearing Bush. Install the runner, start the centrifuge, and pour a certain amount of alloy solution after the specified speed is reached. The alloy solution shall be injected

smoothly, evenly and continuously. After that poured alloy is pour completely, the pouring is stopped for a while, then water is spray to the outer surface of the bearing Bush for cooling, and when the temperature is reduced to below $200℃$, the water spraying is stopped and the machine is shut down. Carefully remove the bearing Bush, lightly hoist it in a furnace at about $100℃$, and slowly cool it to room temperature.

The metallographic structure of Babbitt alloy should distribute uniform, dispersed and fine SnSb cubic crystals, and a small amount of rod-shaped, needle-shaped or punctiform crystals are allowed to exist. If the SnSb hard particles are large or unevenly distributed, the pressure borne by a single crystal in the alloy is too large, and the crystal is cracked to cause the bearing Bush to be damaged. The reason is that the interfacial area of single SnSb crystal increases and the matrix is fragmented, which reduces the strength and impact toughness. The larger the crystal is, the more uneven the distribution of the crystal is, and the larger the force applied on a single crystal, the more deformation and slip occur in the crystal, and the grain boundary is destroyed, so that the fatigue strength of the alloy is reduced and the alloy is ruptured. Only when the crystal of SnSb is fine and evenly distributed, can it have better carrying capacity. This is because the SnSb crystals on the matrix cause the distortion of the matrix lattice and increase the deformation resistance. The finer the crystal, the more the grain boundaries and the more disordered the atomic arrangement, which can increase the deformation resistance and provide the strength and impact toughness of the alloy. The distribution of Cu_6Sn_5 is also similar. Therefore, in order to improve the mechanical properties of the bearing, it is necessary to refine the crystal and make it distribute evenly.

4.2 Optimum industrial application scheme of running-in coatings

Wear and breakdown of the machine components and mechanisms as a rule commence from a surface, and therefore in order to improve the operating properties of machines and mechanisms it is necessary to improve component surface quality. One of the most effective improvements of surface quality and component operating properties is provided by application of special coatings.

The coatings of the tin bronze surface that were formed by alternately electro-spark deposition applying the antifriction material of silver, copper, Babbitt B83 and graphene oxide. The analysis of morphology, composition and properties of the coatings were investigated. The comprehensive assessment results from different researchers are always full of uncertainty [194-196]. Therefore, we have to find an effective comprehensive method for the assessment of the characterization of the coatings by electro-spark deposition, which has the characteristics of objectivity, simple operation and little interference.

Here, the entropy method and the TOPSIS model were employed to the comprehensive evaluation of the characterization of the coatings by electro-spark deposition. Shannon information entropy, which is an objective and applicable method for the determination of weight value, was introduced into the comprehensive assessment. The TOPSIS model can calculate the ordering of each object more effectively in the comprehensive assessment of the characterization of the coatings by electro-spark deposition.

4.2.1 Deposition process parameters

The ESD machine DZ-4000III has a control panel to change the electrical

parameters including ESD voltage (20 V – 250 V), capacitance (30 µF – 420 µF) and frequency (1300 Hz – 6000 Hz). The ESD machine has the ground attachment, the shielding gas outlet and the applicator attachment. The rotation speed (2600 r/min) and direction can be controlled on the applicator.

Travel speed in both cases was 2 mm/s. The frequency of the first layer was 3 kHz, the frequency of the second layer was 4 kHz and the frequency of the third and the fifth layers were 5 kHz. Deposition was carried out using a hand-held gun at room temperature with the argon gas (Ar 99%) protection (10 L/min flow rate), which avoids contamination of the deposit zone by interstitial elements such as oxygen or nitrogen.

The GO solution was applied to the surface of the specimens by manual pre-coating method, and then the specimens was dried by natural air, followed by the fifth layers with B83 electrode.

The electro-spark deposition process parameters (electrodes, voltage, capacitance and efficiency) are shown in Table 4.1.

Table 4.1 – The ESD parameters of the coatings

Coatings	Voltage (V)	Capacitance (µF)	Efficiency (min/cm^2)
Ag	60	90	1
Ag+B83	60/30	90/90	1/3
Ag+Cu+B83	60/60/30	150/150/90	3/3/4
Ag+Cu+B83+GO +B83	60/40/30/-/25	150/90/30/-/90	2/1/1/-/2

4.2.2 The experiment results and analysis of the running-in coatings

In this study, the analysis of the experiment results of the running-in coatings were investigated, as shown in Table 4.2.

The material prices of the running-in coatings are shown as C_1. With the increase of the number of layers, the kinds of coating materials increase, and the comprehensive price of coating materials increases. The lowest price of silver coating is 60 Yuan, and

the highest price of Ag+Cu+B83+GO+B83 composite coating is 165 Yuan.

The coatings deposition time is shown in Table 4.2 in C_2. The minimum deposition time is 5 minutes for silver coatings and the maximum deposition time is 50 minutes for Ag+Cu+B83 coatings.

In this study, a precision electronic balance with an accuracy of 0.1 mg was used to measure the samples and calculate the mass transfer C_3 to the substrate after ESD. As can be observed in Table 4.2 that the minimum value of mass transfer is 25.0 mg of Ag coatings and the maximum value of mass transfer is 394.2 mg of Ag+Cu+B83 coatings.

The Bruker Contour GT-K1 3D optical profilometers was used to observe the surface of the composite coatings and measure the surface roughness. The surface roughness of the running-in coatings is shown as C_4. As can be seen from Table 4.2, the minimum value of the surface roughness is 15.46 μm of Ag coatings and the maximum value of the surface roughness is 32.30 μm of Ag+Cu+B83 coatings.

The thicknesses of the running-in coatings are shown as C_5. As can be indicated from Table 4.2, the thickness of the coatings increases gradually with the increase of the number of layers. The minimum value of the thickness is 15 μm and the maximum value of the thickness is 160 μm.

The friction coefficient of the coatings is denoted by C_6 in Table 4.2. The silver coating has a maximum coefficient of friction of 0.31. There is little difference in the coefficient of friction of the other three coatings as the surface coating is B83. The minimum friction coefficient of Ag+B83 coating is 0.177.

Table 4.2 – The experiment results of the running-in coatings

Coatings	C_1	C_2	C_3	C_4	C_5	C_6
Ag	60	5	25.0	15.46	15	0.31
Ag+B83	90	20	125.2	19.43	80	0.177
Ag+Cu+B83	105	50	394.2	32.30	100	0.18
Ag+Cu+B83+GO+B83	165	30	244.2	15.90	160	0.21

4.2.3 The entropy weight of the indicators of the running-in coatings

In order to facilitate comprehensive evaluation and comparative analysis of characteristics of ESD coatings, normalized and standardized original data were processed, and entropy method was adopted to calculate the entropy value, information utility value and weighting value corresponding to the six indicators of ESD coatings, as shown in Table 4.3.

Table 4.3 – The entropy value, information utility value and weighting value of the

indicators of the running-in coatings

Indicators	e_j	d_j	w_j
C_1	0.8059	0.1941	15.67%
C_2	0.7886	0.2114	17.07%
C_3	0.7437	0.2563	20.69%
C_4	0.8193	0.1807	14.58%
C_5	0.7851	0.2149	17.35%
C_6	0.8187	0.1813	14.64%

The smaller the entropy value is, the larger the information utility value is and the larger the entropy weight is, indicating that the indicator is more important and contains more information, which should be paid more attention to.

According to the weight of indicators in Table 4.3, in order of importance, firstly of all the indicators is mass transfer (C_3), secondly is thicknesses (C_5), then is time (C_2), then is material prices (C_1), then is friction coefficient (C_6) and finally is roughness (C_4). The weight of indicator mass transfer (C_3) is as high as 20.69%, which can not be

underestimated in the performance evaluation of ESD coatings. This is mainly because the special properties of the coatings can be realized only when the effective mass transfer of the deposited material from electrode to substrate is completed.

Among all the indicators, the average weight of 6 indicators is 16.67%, and 3 indicators higher than the average weight are respectively mass transfer (C_3), thicknesses (C_5), and time (C_2). It shows that these three indicators are more important.

Although the weight values of material prices (C_1), friction coefficient (C_6) and roughness (C_4) are lower than the average weight of 16.67% of these six indicators, but the material price directly affects the economic benefit, the friction coefficient directly reflects the friction reduction performance, and the surface roughness of the coatings directly affects the post-processing process. And the effects of material prices (C_1), friction coefficient (C_6) and roughness (C_4) should still be concerned.

4.2.4 The comprehensive evaluation ranking of the running-in coatings

In order to compare the characteristics of all electro-spark deposition coatings, the Euclidean distance, relative closeness and the comprehensive evaluation ranking of ESD coatings was obtained by using experimental data, as shown in Table 4.4.

Table 4.4 – The Euclidean distance, relative closeness and ranking of the running-in coatings

Coatings	D_i^+	D_i^-	C_i	Ranking
Ag	0.150	0.119	0.442	4
Ag+B83	0.100	0.110	0.525	3
Ag+Cu+B83	0.107	0.138	0.563	2
Ag+Cu+B83+GO+B83	0.094	0.131	0.581	1

According to the calculated Euclidean distance, the relative closeness of different evaluation objects is calculated. The schemes are ranked according to the relative closeness. The larger the relative closeness is, the better the scheme is. In order of

relative closeness, they are Ag+Cu+B83+GO+B83 coatings, Ag+Cu+B83 coatings, Ag+B83 coatings and Ag coatings. It can be indicated in the Table 4.4 that with the increase of coating materials species, the comprehensive evaluation of the coating is getting better and better.

4.3 New technology of constructing running-in coatings on tin bronze bearing surface

(1) Influence of material on product quality

A. Bearing base material

Engineering and structural cast carbon steel, with high strength, plasticity and toughness, and low cost, suitable for heavy machinery used in the manufacture of parts to withstand heavy loads. The matrix material of the cast steel bearing shell is easy to be worn due to the adoption of a thin coating, and the bearing capacity is reduced due to the adoption of a thick coating, so that the cast steel bearing shell is easy to be fatigued and is suitable for light load and medium load.

In the actual work of the bearing, tin bronze bearing has good mechanical properties and thermal conductivity but slightly higher friction force. Tin bronze can effectively eliminate the heat generated by friction as a substrate material. Thus, there is need to provide for the bronze bearing pads with special coatings improving the running conditions. In the case of coating failure, the tin bronze substrate can continue to be used as a bearing with excellent performance, which is conducive to improving the stability and reliability of the system.

The Bearing base material is tin bronze QSn10-1 commonly used as Plain bearing material provided by Zhejiang Shenfa Bearing Co., LTD. The composition of the material QSn10-1 is Cu 89.10%, Sn 9.38%, P 0.72%, Others 0.80%.

B. Coating materials

Soft metal silver is used in the design of bearings bearing high loads and high speeds and has good lubrication performance, mechanical properties and corrosion resistance. Silver and copper have very good wettability, which is conducive to improving the metallurgical bonding performance between metals during ESD. The silver can play a role in grain refinement, so that the strength and the hardness of the Babbitt alloy are improved. However, the performance of silver as anti-wear metal coating needs to be further improved. Therefore, based on the above factors, silver (Ag 99.99%) is suitable as the first transition coating material.

Pure copper is soft and has better wettability with silver. The copper in the coating can form ε-phase (Cu_6Sn_5) with the tin in the Sn-based Babbitt alloy, which is conducive to ensuring the metal bonding of the coating. Copper provides the preferential crystallization center, refines the grain size, and improves the microstructure and mechanical properties of the Babbitt alloy. And the copper (Cu 99.99%) is suitable for the second layer of transition coating material.

The overall performance of tin-based alloy is better than that of lead-based alloy, because the strength, hardness and corrosion resistance of tin-based alloy are obviously superior to that of lead-based alloy. Tin-based Babbitt is characterized in that hard phase particles are uniformly distributed on a soft phase matrix, the soft phase matrix enables the Babbitt to have very good embedding property, compliance and anti-seizure property, and after running-in, the soft matrix is concave inwards and the hard phase particles are convex upwards to play a supporting role, so that a micro gap is formed between sliding surfaces, and an oil storage space and a lubricating oil channel are formed which is

particularly beneficial to the running-in at the early stage of operation, and Babbitt B83 (SnSb11Cu6, Sn 83.10%, Sb 11.02%, Cu 5.83%, Others 0.05%) is very suitable for operation as the coating material.

Graphene has been used to improve tribological property due to its extraordinary properties. Graphene oxide (GO) is considered as a promising material for reducing friction and wear, owing to its structural features. Therefore, adding the GO to the coatings is beneficial to improve the friction and wear properties of the surface. Graphene oxide was a dispersible solution of 4mg/ml with water as the solvent.

(2) Influence of process on product quality

A. Processing technology of bearing bush

Because the inner surface of the bearing Bush and the journal are in clearance fit, when the shaft rotates at high speed, a pressure oil film is generated through the clearance between the two matched surfaces, so that the machine can work normally. The fit clearance and the inner surface roughness of the bearing shell are two important factors for the formation of the pressure oil film. Therefore, the roughness of the inner surface of the bearing Bush is required to be very high (Ra 0.1 μm). It is difficult to obtain high precision inner diameter surface of the bearing.

Usually, the grinding and polishing process can be used for the machining of the inner arc surface with the surface roughness value of 0.1 μm, but the inner surface material of the bearing Bush is a soft composite coating, and the abrasive particles will be embedded in the surface layer of the coating during polishing and grinding, which will not only fail to achieve the polishing effect, but also reduce the surface quality. If high-speed turning is used, residual area will be left on the machined surface, and high

precision surface quality can not be obtained. By adopt that scraping process technology, the scraper blade scrapes the inner surface of the bear Bush alloy in one step in the width direction of the bearing Bush, theoretically, no residual area exists on the machined surface, and meanwhile, in the scraping process, the scraping cutter has an extrusion effect on the machined surface, so that the surface quality can be further improved. Therefore, for the processing of bearing running-in coating, the scraping process can be used to obtain high-quality surface roughness.

The inner and outer surfaces of the bearing Bush are roughly machined, and then the inner surface is finely machined, and then a running-in coating is deposited on the inner surface by electric spark, and the thickness of the composite coating is more than 200 μm in order to provide enough machining allowance for subsequent processes. And then carry out fine grinding process on that outer diameter of the bearing Bush to achieve the surface roughness of Ra 0.8 μm. The semi-finish machining of the Bush coating is carried out by turning to remove the uneven surface layer and leave a finishing allowance. The finish machining (scraping machining) of the bearing Bush running-in coating is carried out on a special scraping machine tool. In order to ensure the precision requirement of the scraped surface, the secondary machining of rough and finish scraping is adopted. The purpose of rough scraping is to ensure the machining allowance of fine scraping to be uniform, and the appropriate thickness of alloy layer for rough scraping is about 50 μm, so as to avoid leaving chatter marks on the scraping surface due to the large scraping thickness; And that thickness of the fine scrape is generally controlled to be 30 μm. According to the above analysis, the processing route of the bearing shell is as follows: rough machining of the bearing shell, finish

machining of the inner surface of the bearing, electric spark deposition of running-in coating, finish machining of outer diameter of bearing shell, semi-finish machining (turning) of bearing and finish machining (rough and finish scraping) of running-in coatings.

B. Coatings process

The coating process of electro-spark deposition technology has an important impact on the deposition efficiency, cost, mass transfer, coating surface roughness, coating thickness, coating surface friction coefficient and so on. There are many process parameters of electro-spark deposition, which can be summarized as follows:

Electrode material composition, density, microstructure, manufacture technique, shape, moving speed, specific deposition time, contact force, cycle numb, deposition angle and other process parameter. Because of the great difference of resistivity, melting heat, thermal conductivity, ductility, wetting angle and other characteristics of materials, and considering the instability of electro-spark deposition process, the influence of process parameters on the preparation and performance of coatings is uncertain.

Tin bronze plain bearing pad surface roughness, cleanliness, shape, temperature.

Electrical discharge voltage, pulse current, energy storage capacitor, energy, frequency, discharge time, inductance and other power supply parameters.

The composition of gas environment and liquid environment, fluid properties, gas flow and mode, temperature and other environmental atmosphere of electric spark discharge.

(3) New environmental protection technology for bearing bush running-in coatings

A. Design, manufacture and preliminary machining of bearing bush

According to the actual operating conditions of industrial machinery design bearing size. Bearing bore diameter, length and initial radius clearance are very critical parameters in bearing design, which directly affect the bearing capacity, stiffness, bearing temperature rise and other aspects of performance [197].

The tin bronze bearing Bush blank is made by casting. After that tin bronze bearing Bush is roughly machine, the inner hole is left with 0. 5 mm of machining allowance, and the inner hole is turning on a lathe within two hours before the electric spark deposition, wherein the rotating speed is about 120 r/min, the feed amount is about 0.9 mm, and the turning depth is 0.5 mm. Before turning, the used tools, measuring tools and fixtures should be washed with alkali to remove oil stains, no lubricating oil or coolant should be added during turning, and the inner surface of tin bronze after low-speed processing should not contact with other objects. The inner hole of the tin bronze sliding bearing Bush blank shall be designed according to the drawing requirements, and the excircle shall be reserved with a machining allowance of 3 mm ~ 5 mm. Figure 4.1 is the manufactured and preliminarily machined of tin bronze bush。

Figure 4.1 – Manufactured and preliminarily machined of bearing bush

B. Construction of running-in coatings on bearing bush surface

Before the coatings are deposited by electro-spark, the Tin bronze plain bearing bush is clamped by a bench, and the electrode material to be deposited is installed on the welding gun. Connect the power supply and argon to the electric spark deposition equipment, firmly connect the cathode power supply to the bench, and adjust the argon flow to prepare for the deposition of the coating.

The running-in coatings of the tin bronze bearing bush that were formed by alternately electro-spark deposition applying the antifriction material of silver, copper, Babbitt B83 and graphene oxide. Operate the control panel of the electro-spark deposition equipment, and adjust the electrical parameters such as discharge voltage, energy storage capacitor and discharge frequency according to the parameters in Table 4.5. Adjust the rotating speed on the applicator to 2600 r/min. The discharge time of each coating is in accordance with the parameters in Table 4.5.

Travel speed in both cases was about 2 mm/s, moving according to the small ring track or the broken line network track can ensure the corresponding pressure, as far as possible to ensure the stability of the discharge voltage and the arc stability of the workpiece surface, and the excellent quality of the sediment layer can be obtained. Deposition was carried out using a hand-held gun at room temperature with the argon gas (Ar 99%) protection (10 L/min flow rate), which avoids contamination of the deposit zone by interstitial elements such as oxygen or nitrogen. And that work angle between the rotary electrode and the substrate is about 45 degrees.

The GO solution was applied to the surface of the specimens by manual pre-coating method, and then the specimens was dried by natural air, followed by the fifth layers with B83 electrode. Tin bronze plain bearing bush after electro-spark

deposition of the running-in coatings is shown in Fig. 4.2.

Table 4.5 – The ESD parameters of the running-in coatings

Coatings	Voltage (V)	Capacitance (µF)	Efficiency (min/cm^2)	frequency (kHz)
Ag+Cu+B83+GO +B83	60/40/30/-/25	150/90/30/-/90	2/1/1/-/2	3/4/5/-/5

Figure 4.2 – Construction of running-in coatings on bearing bush surface

C. Post processing and treatment of bearing shell

The running-in coatings of the bearing bush is processed by scraping, namely the machined surface is finished by scraping on the whole width of the bearing bush at one time; and as the main deflection angle and the auxiliary deflection angle of a scraping cutter are both 0 deg during processing, theoretically, no residual area exists on the machined surface, and the influence of the main deflection angle and the auxiliary deflection angle of the cutter on the surface roughness is eliminated. At this time, the factors that affect the surface roughness of the bearing inner surface are the vibration in the scraping process, the straightness error of the blade and so on. If the stiffness of the scraping machine and the geometric parameters of the scraping tool are solved, the surface roughness of the Bush coatings after scraping can meet the mirror quality requirements.

Bear bush scraping process is completed by scraping once in that width direction of the bearing bush, the scrape force is large, in order to prevent vibration generated

during scraping and influence the roughness of the scraping surface, in addition to sufficient rigidity of the arbor shaft, the fit clearance between the arbor shaft and the sliding bearing in the supporting seat is also very important. Before scrape, that bearing bush is place in a semicircular arc fixture for positioning and clamping, the extending amount of the scrape blade (namely the depth of the scraper) is adjusted, the machine tool is started, the cutter bar shaft rotates, and the scraper blade finishes scraping and machining the inner surface in one step in the width direction of the bearing bush. And when that scrape is finished, the brake has brake effect on the motor, so that the blade is stopped above the fixture seat, the bearing bush is taken out, and the scraping process is finished. In order to improve the scraping surface roughness, the bush scraping process is divided into two processes of rough scraping and fine scraping, and the corresponding cutter is also divided into rough scraper and fine scraper. The rough skiving tool and the fine skiving tool are different in material, geometry angle and so on.

D. Installation and commissioning of bearing shell

Clean it up during installation, and there should be no sundries, so as not to affect the surface of bearing bush or lubrication system. The installation standard shall be strictly implemented in the installation process of the bearing bush, so that the installation measurement dimensions shall meet the specification requirements. Special attention shall be paid to the assembly clearance between the journal and the bearing bush shall meet the requirements.

After filling the lubricating oil into the machined bearing Bush, the commissioning test with light load of 10 N and rotating speed of 700 r/min is carried out for 3 hours in total, and the external temperature of the bearing Bush is detected at any time. After the

light load commissioning test, carry out the commissioning test for 8 hours with the load of 30 N and the rotating speed of 700 r/min, and check the external temperature of the bearing Bush at any time.

According to the analysis of the test data, the tin bronze bearing bush without running-in coatings runs stably, and the external temperature of the bearing bush increases by 12°C; The running-in coated tin bronze bearing bush runs stably, and the external temperature of the bearing bush only increases by 8°C. After the commissioning test, it was found that the surface of the bearing Bush without running-in coatings was burnt and blackened, and the surface was seriously worn (Figure 4.3). There is no burning phenomenon on the surface of the bearing Bush with running-in coatings, the scratch is not obvious, and the wear is slight (Figure 4.4). The bearing shells without running-in coatings showed burning on the journal part, while the bearing shells with running-in coatings showed no burning on the journal part (Fig. 4.5). From the overall situation, that temperature rise of the slide bearing Bush with the running-in coatings is small, the operation is stable and reliable, and the durability is good.

The operating characteristics of the running-in coatings are such that it can withstand short term damage under lubricating oil dynamic conditions without seizure and at relatively high temperatures, and it has very good fatigue properties under rated load conditions.

Figure 4.3 – Uncoated tin bronze bearing bush after commissioning

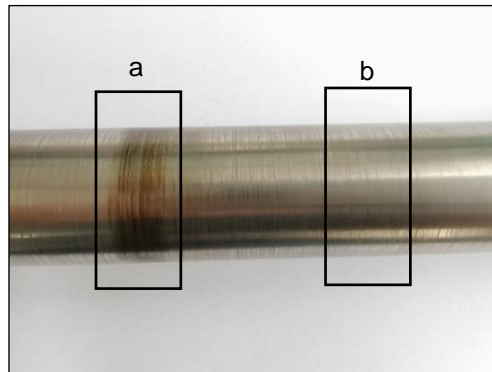Figure 4.4 – Tin bronze bearing bush with running-in coatings after commissioning

Figure 4.5 – Bearing journal after commissioning: a - The position of tin bronze bearing

bush; b - The position of tin bronze bearing bush with running-in coatings

4.4 Technical suggestion on application of running-in coatings technology for tin bronze bearings

(1) Guarantee the coatings quality of bearing bush

The coatings quality of the bearing directly affects the service life of the bearing. Before the deposition of bearing bush, clean the oil stain and oxide skin on the surface of the Bush tire, and carry out acid washing. The deposition should be careful and serious. The deposition process parameters should be well controlled to ensure that the coating is closely combined with the tile tire and the alloy grains are uniform and meticulous.

(2) Ensure the machining accuracy of bearing bush

In the aspect of machining, it is necessary to properly formulate the processing technology, use high-precision processing machine tools, select the clamping position, and control the coaxiality of the bearing bush and the dimensional accuracy of the working surface.

(3) Improving the installation quality of bearing bush

The bearing Bush needs to be scraped manually when it is installed. The quality of the bush scraping affects the installation accuracy of the shaft, and also affects the service life of the bearing Bush. The top clearance, side clearance and bush mouth clearance of the bearing bush shall meet the installation technical requirements. The side clearance and tile mouth clearance can be measured with a feeler gauge. The top clearance must be measured by the method of encapsulating and pressing lead. The accuracy of the measured data can be ensured only by tightening the screw of the tile cover. If these three parameters can not meet the requirements of installation technical conditions, the bearing bush may be glued during the test run.

(4) Ensure reliable lubrication of bearing bush

Lubrication is the key in the process of using bearing Bush, and the lubricating oil should be selected reasonably. The viscosity of lubricating oil should be matched with the clearance of bearing Bush, and it is not appropriate to change the viscosity of lubricating oil casually when the clearance of bearing bush is unchanged. The temperature and flow of lubricating oil should meet the needs of heat dissipation of bearing bush, which can take away the heat generated by bearing bush and ensure the stability of bearing bush temperature. The lubricating oil shall be clean to avoid impurity blocking the oil way or scratching the surface of the bearing bush.

4.5 Summary

In this chapter, the traditional processing and manufacturing process of plain bearing bush is briefly introduced, the test results of different running-in coatings are summarized and analyzed, the entropy method is used to determine the weight of running-in coatings index, and the TOPSIS model is used to comprehensively evaluate and sort the running-in coatings, and the best industrial application scheme is determined. The base material, coating material, processing technology and coating technology of bearing bush which affect the product quality are analyzed. A new environmental protection technology of constructing running-in coatings of tin bronze bearing bush is put forward, and the technical design, manufacture, processing, installation and trial operation are described in detail. Finally, some technical suggestions for the application of running-in coatings process of tin bronze bearing are put forward.

CHAPTER 5. SCIENTIFIC CONCLUSIONS AND RECOMMENDATIONS

5.1 Scientific conclusions

On the basis of the obtained results and their interpretation, the following conclusions can be drawn:

(1) The coatings of silver were deposited on the surface of tin bronze by electro-spark deposition. Under the optimal process parameters of the Ag coatings, the mass transfer is 25.0 mg, the surface roughness of the composite coatings is 15.46 μm and the thickness is 15 μm. The minimum friction coefficient of the Ag coatings is about 0.31. However, the performance of silver as antifriction material coatings needs to be further improved.

(2) The soft antifriction composite coatings of silver and Babbitt B83 were deposited on the surface of tin bronze by electro-spark deposition. Under the optimal process parameters, the mass transfer is 125.2 mg, the surface roughness of the composite coatings is 19.43 μm and the thickness is 80 μm. The minimum friction coefficient of the composite coatings is about 0.177. The wear mechanism of the Ag+B83 composite coatings is dominated by plastic deformation and abrasive wear.

(3) The soft antifriction composite coatings of silver, copper and babbitt B83 were deposited on the surface of tin bronze by electro-spark deposition. Under the optimal process parameters, the mass transfer is 54.4 mg/cm^2, the surface roughness of the composite coatings is 32.3 μm. The thickness of the composite coatings is about 100 μm under the optimal parameters and the maximum thickness is 160 μm.

From the surface of the composite coatings to the substrate, the hardness of the composite coatings first increases, then decreases, and finally increases. The surface

microhardness of the composite coatings is 29 $HV_{0.01}$, which is 82% lower than that of the tin bronze substrate (161 $HV_{0.01}$).

The surface friction coefficient of the composite coatings (0.180) is 55.6% of the tin bronze substrate (0.324). The wear mechanism of the tin bronze substrate is dominated by severe ploughing wear and fatigue delamination. However, the soft antifriction composite coatings may effectively restrain fatigue delamination, showing plastic deformation accompanied by slight polishing.

(4) The running-in coatings of silver, copper, Babbitt B83 and graphene oxide were deposited on the surface of tin bronze by electro-spark deposition. Under the optimal process parameters, the mass transfer is 244.2 mg, the surface roughness of the composite coatings is 15.9 μm and the thickness is 160 μm.

The modulus of the running-in coatings is 36.4% of Babbitt B83 and 24.9% of the tin bronze substrate. The hardness of the running-in coatings is 79.8% of Babbitt B83 and 14.2% of the bronze substrate. The deformation ratio of the running-in coatings is 1.9% higher than that of Babbitt B83 and 10.2% higher than that of the substrate.

The friction coefficient of the running-in coatings (0.210) is 64.8% of the substrate (0.324), which is similar to that of Babbitt B83 (0.192). The wear mechanism of the running-in coatings is dominated by plastic deformation, scratching, and slight polishing.

The running-in coatings deformation under action of high specific loads provides parts automatic adjustment and compensation of manufacturing errors.

(5) Constructed a new indicators system of the electro-spark deposition coatings. The entropy method and the TOPSIS model were employed to the comprehensive

evaluation ranking of the characterization of the running-in coatings by electro-spark deposition. Ag+Cu+B83+GO+B83 coatings have the highest comprehensive score and the best comprehensive characteristics.

The practical application of the running-in coatings of tin bronze bearing bush on industrial equipment has been completed in the enterprise. The working temperature of the running-in coatings of tin bronze bearing bushing is lower, and the stability and reliability of the bearing bush are obviously improved. Scientific results are valuable to industry.

5.2 Recommendations

In this paper, the running-in coatings were prepared on the surface of tin bronze by electro-spark deposition technology, which reduced the surface hardness and friction coefficient, and the experimental results were analyzed and discussed. The research work has achieved some results, but due to the limitation of conditions, there are still many works to be further improved and studied.

(1) In the study of running-in coatings, the effects of different coating materials, such as In, Sn, Nb, TiN, TiC, WC, WS_2, MoS_2 and so on, on the properties of the coatings need to be studied, and the quantitative relationship between the deposition process parameters and the properties of the coatings still to be established for further application. The working angle between the rotating electrode and the substrate, the rotating speed of the electrode, the argon flow rate and the discharge frequency can be further studied.

(2) Digital storage oscilloscope needs to be used to collect the voltage and current signals between the two electrodes in the process of electro-spark deposition of

running-in coatings, which is conducive to better explore the discharge mechanism.

(3) The calculation of residual stress, the measurement of electrical conductivity, the determination of the binding force between the substrate and the coatings, and the detection of the corrosion resistance of the coatings need to be carried out to explore other properties of the coatings, which is conducive to better application in enterprises.

REFERENCES

[1] R. N. Johnson and G. L. Sheldon, "Advances in the electrospark deposition coating process," *Journal of Vacuum Science & Technology A: Vacuum, Surfaces, and Films,* vol. 4, no. 6, pp. 2740-2746, 1986.

[2] A. V. Ribalko and O. Sahin, "A modern representation of the behaviour of electrospark alloying of steel by hard alloy," *Surface and Coatings Technology,* vol. 201, no. 3-4, pp. 1724-1730, 2006.

[3] J. J. Hao, Z. G. Bo, Y. F. Fan, Q. H. Bai, J. G. Zhao, and J. C. Li, "Reaction Synthesis of TiN Reinforced Fe-Based Metal Matrix Composite Coating by ESD," (in Chinese), *Rare Metal Mat Eng,* vol. 38, pp. 497-500, Apr 2009.

[4] T. Matsuyama and T. Kayaba, "A Study on the Electro-Spark Machining by the Alternating Current," *Bulletin of JSME,* vol. 2, no. 5, pp. 86-91, 1959.

[5] W. Gao, Z. W. Li, and Y. D. He, "High Temperature Oxidation Resistant Coatings Produced by Electro-Spark Deposition," *Materials Science Forum,* vol. 369-372, pp. 579-586, 2001.

[6] C. Luo, S. J. Dong, and X. Xiong, "Characteristics of TiB2 Coating on the Surface of Copper Alloy Prepared by Vibrating Electrospark Deposition," *Advanced Materials Research,* vol. 105-106, pp. 477-480, 2010.

[7] H. Pang, H. Qi, Y. He, D. Wang, and Z. Li, "High-frequency electropulse deposition of microcrystallized MGH754 ODS alloy coatings," *Science in China Series B: Chemistry,* vol. 43, no. 5, pp. 540-546, 2000/10/01 2000.

[8] K. Furutani and K. Shiraki, "608 Deposition of Lubricant Layer during Finishing Process by Electrical Discharge Machining with Molybdenum Disulfide Powder

Suspended in Working Fluid," *The Proceedings of the JSME Materials and Processing Conference (M&P),* vol. 10.2, pp. 468-473, 2002.

[9] B. D. Jin, W. S. Zhao, G. H. Cao, Z. L. Wang, and K. Xiao, "Fabrication of Micro Structure Using EDM Deposition," *Materials Science Forum,* vol. 532-533, pp. 305-308, 2006.

[10] V. S. Sychev and A. I. Bezykornov, "Residual stresses in titanium after electro-spark alloying with borides," *Soviet materials science : a transl. of Fiziko-khimicheskaya mekhanika materialov / Academy of Sciences of the Ukrainian SSR,* vol. 10, no. 5, pp. 525-527, 1976/09/01 1976.

[11] B. D. Jin, G. H. Cao, Z. L. Wang, and W. S. Zhao, "A Micro-Deposition Method by Using EDM," *Key Engineering Materials,* vol. 339, pp. 32-36, 2007.

[12] Y. Y. Li, Z. N. Guo, and G. Y. Liu, "Experimental Investigation on Metal Coating by Means of ESD," *Materials Science Forum,* vol. 626-627, pp. 357-362, 2009.

[13] P. Luo, S. J. Dong, A. Z. Yangli, S. X. Sun, and Z. Zheng, "Electrospark deposition of ZrB2-TiB2 composite coating on Cu-Cr-Zr alloy electrodes," (in English), *Int J Surf Sci Eng,* vol. 10, no. 1, pp. 41-54, 2016.

[14] X. R. Wang, Z. Q. Wang, P. He, T. S. Lin, and Y. Shi, "Microstructure and wear properties of CuNiSiTiZr high-entropy alloy coatings on TC11 titanium alloy produced by electrospark - computer numerical control deposition process," (in English), *Surf Coat Tech,* vol. 283, pp. 156-161, Dec 15 2015.

[15] M. Barlak, M. Chmielewski, Z. Werner, P. Konarski, K. Pietrzak, and A. Strojny-Nedza, "Changes of tribological properties of Inconel 600 after ion implantation process," (in English), *B Pol Acad Sci-Tech,* vol. 62, no. 4, pp.

827-833, Dec 2014.

[16] P. Luo, Z. X. Xie, S. J. Dong, A. Z. Yangli, and W. Yang, "Defects Modification of TiB2-TiC Composite Phase Coating Resistance Spot Welding Electrode via Friction Stir Processing," (in English), *Mater Trans,* vol. 55, no. 6, pp. 917-920, Jun 2014.

[17] P. Luo, S. J. Dong, Z. Q. Mei, and Z. X. Xie, "Strengthening Mechanism of TiB2-TiC Complex Phases Coated Electrode," (in English), *Materials Science and Information Technology, Pts 1-8,* vol. 433-440, pp. 251, 2012.

[18] S. K. Tang, T. C. Nguyen, and Y. Zhou, "Materials Transfer in Electro-Spark Deposition of TiCp/Ni Metal-Matrix Composite Coating on Cu Substrate," (in English), *Weld J,* vol. 89, no. 8, pp. S172-S180, Aug 2010.

[19] S. Durdu, K. Korkmaz, S. L. Aktug, and A. Cakir, "Characterization and bioactivity of hydroxyapatite-based coatings formed on steel by electro-spark deposition and micro-arc oxidation," (in English), *Surf Coat Tech,* vol. 326, pp. 111-120, Oct 15 2017.

[20] C. Y. Li, P. Q. Ge, and W. B. Bi, "Thermal simulation of the single discharge for electro-spark deposition diamond wire saw," (in English), *Int J Adv Manuf Tech,* vol. 114, no. 11-12, pp. 3597-3604, Jun 2021.

[21] W. W. Wei, D. Xiao, and W. Liu, "The analysis of optimized path selection for management mode of coastal regional circular economy based on fuzzy decision algorithm," (in English), *Expert Syst,* Mar 4 2022.

[22] N. Y. Loginov, V. A. Gulyaev, A. A. Kozlov, and D. Y. Voronov, "Testing of the mathematical model application of the wear coating electro-spark method," (in

English), *International Workshop Advanced Technologies in Material Science, Mechanical and Automation Engineering - Mip: Engineering - 2019,* vol. 537, 2019.

[23] R. Zhang, J. Li, M. Xiao, B. Luo, and P. Guo, "Research and Application of Micro Nanostructured Coating by Electro-spark," *Surface Technology,* vol. 42, no. 02, pp. 108-111+115, 2013.

[24] W. Gu, H. Ding, P. Di, and S. Zhu, "Investigation on Turbulent Arc in the Process of Electric Spark Automatic Strengthening," *China Surface Engineering,* vol. 23, no. 06, pp. 66-69, 2010.

[25] H. Han, J. Guo, and W. Jiao, "Discharge Mechanism of Electro-spark Deposition with Rotary Electrode," *Transactions of the China Welding Institution,* vol. 40, no. 05, pp. 67-72+164, 2019.

[26] W. Q. Wang, M. Du, X. E. Zhang, C. Q. Luan, and Y. T. Tian, "Preparation and Properties of Mo Coating on H13 Steel by Electro Spark Deposition Process," (in English), *Materials,* vol. 14, no. 13, p. 3700, Jul 2021.

[27] P. D. Enrique, S. Peterkin, and N. Y. Zhou, "Parametric Study of Automated Electrospark Deposition for Ni-Based Superalloys," (in English), *Weld J,* vol. 100, no. 7, pp. 239s-248s, Jul 2021.

[28] A. Zielinski and M. Bartmanski, "Electrodeposited Biocoatings, Their Properties and Fabrication Technologies: A Review," (in English), *Coatings,* vol. 10, no. 8, Aug 2020.

[29] V. Martsynkovskyy *et al.,* "New Process for Forming Multicomponent Wear-Resistant Nanostructures by Electrospark Alloying Method," (in English),

Springer Proc Phys, vol. 240, pp. 135-149, 2020.

[30] H. Aghajani, E. Hadavand, N. S. Peighambardoust, and S. Khameneh-asl, "Electro spark deposition of WC-TiC-Co-Ni cermet coatings on St52 steel," (in English), *Surf Interfaces,* vol. 18, Mar 2020.

[31] H. Zhao, C. Gao, X. Y. Wu, B. Xu, Y. J. Lu, and L. K. Zhu, "A novel method to fabricate composite coatings via ultrasonic-assisted electro-spark powder deposition," (in English), *Ceramics International,* vol. 45, no. 17, pp. 22528-22537, Dec 1 2019.

[32] G. Renna, P. Leo, and C. Casavola, "Effect of ElectroSpark Process Parameters on the WE43 Magnesium Alloy Deposition Quality," (in English), *Appl Sci-Basel,* vol. 9, no. 20, Oct 2019.

[33] S. Khimukhin, K. Eremina, and H. Ri, "The structure of the intermetallic coating after ultrasonic burnishing process," (in English), *Mater Today-Proc,* vol. 19, pp. 2413-2416, 2019.

[34] E. Katinas, V. Jankauskas, N. Kazak, and V. Michailov, "Improving Abrasive Wear Resistance for Steel Hardox 400 by Electro-Spark Deposition," (in English), *Journal of Friction and Wear,* vol. 40, no. 1, pp. 100-106, Jan 2019.

[35] F. V. Kiryukhantsev-Korneev, A. D. Sytchenko, A. E. Kudryashov, E. A. Levashov, and D. V. Shtansky, "The Effect of Eu2O3 Additive to the TiCNiCr Electrode on the Formation of Electrospark Coatings," (in English), *Tech Phys Lett+,* vol. 44, no. 8, pp. 753-755, Aug 2018.

[36] M. Salmaliyan, F. M. Ghaeni, and M. Ebrahimnia, "Effect of electro spark deposition process parameters on WC-Co coating on H13 steel," (in English),

Surf Coat Tech, vol. 321, pp. 81-89, Jul 15 2017.

[37] X. Hong, K. Feng, Y. F. Tan, X. L. Wang, and H. Tan, "Effects of process parameters on microstructure and wear resistance of TiN coatings deposited on TC11 titanium alloy by electrospark deposition," (in English), *T Nonferr Metal Soc,* vol. 27, no. 8, pp. 1767-1776, Aug 2017.

[38] P. D. Enrique, Z. Jiao, N. Y. Zhou, and E. Toyserkani, "Dendritic coarsening model for rapid solidification of Ni-superalloy via electrospark deposition," (in English), *J Mater Process Tech,* vol. 258, pp. 138-143, Aug 2018.

[39] Y. S. Wang, X. R. Wang, Z. Q. Wang, T. S. Lin, and P. He, "Preparation and microstructure of AlCoCrFeNi high-entropy alloy complex curve coatings," (in English), *Mater Sci Tech-Lond,* vol. 33, no. 5, pp. 559-566, 2017.

[40] A. Cakir, K. Korkmaz, and E. S. Kayali, "Study on the Al2O3/Fe-Al intermetallic duplex coating prepared with a combined technique of electro-spark deposition and micro-arc oxidation on steel," (in English), *Kovove Mater,* vol. 55, no. 2, pp. 81-87, 2017.

[41] G. Renna, P. Leo, G. Casalino, and E. Cerri, "Repairing 2024 Aluminum Alloy via Electrospark Deposition Process: A Feasibility Study," (in English), *Adv Mater Sci Eng,* vol. 2018, 2018.

[42] M. S. Yilmaz, A. Cakir, A. Ribalko, and K. Korkmaz, "Fabrication of Bioactive Coatings on Steel Substrates by Electro-Spark Deposition (ESD) and Micro-Arc Oxidation (MAO) Methods," (in English), *Acta Phys Pol A,* vol. 127, no. 4, pp. 1277-1281, Apr 2015.

[43] D. W. Heard and M. Brochu, "Development of a nanostructure microstructure in

the Al-Ni system using the electrospark deposition process," (in English), *J Mater Process Tech,* vol. 210, no. 6-7, pp. 892-898, Apr-May 2010.

[44] L. M. Felix, C. C. F. Kwan, and N. Y. Zhou, "The Effect of Pulse Energy on the Defects and Microstructure of Electro-Spark-Deposited Inconel 718," (in English), *Metall Mater Trans A,* vol. 50a, no. 9, pp. 4223-4231, Sep 2019.

[45] P. Leo, G. Renna, and G. Casalino, "Study of the Direct Metal Deposition of AA2024 by ElectroSpark for Coating and Reparation Scopes," (in English), *Appl Sci-Basel,* vol. 7, no. 9, Sep 2017.

[46] J. Milligan, D. W. Heard, and M. Brochu, "Formation of nanostructured weldments in the Al-Si system using electrospark welding," (in English), *Applied Surface Science,* vol. 256, no. 12, pp. 4009-4016, Apr 1 2010.

[47] P. He, Y. Qian, Z. L. Chang, and R. J. Wang, "Adhesion Behavior of WC Coating Deposited on Titanium Alloy by Electrospark Deposition," *Solid State Phenomena,* vol. 127, pp. 325-330, 2007.

[48] H. Yu *et al.*, "NiCr Alloy Coating Deposited on the Surface of 35CrMo Steel by the Electrospark Process," *Materials Science Forum,* vol. 575-578, pp. 827-832, 2008.

[49] F. Guo, X. J. Su, P. Li, G. L. Hou, and Z. X. Mei, "Microstructure and Properties of Ti-Al Based Composite Coating Prepared by Electrospark Deposition Process," *Advanced Materials Research,* vol. 79-82, pp. 1611-1614, 2009.

[50] P. Luo, S. J. Dong, Z. X. Xie, A. Z. Yangli, and W. Yang, "The effects of coating parameters on the quality of TiB2-TiC composite phase coating on the surface of Cu-Cr-Zr alloy electrode," (in English), *Surf Coat Tech,* vol. 253, pp. 132-138,

Aug 25 2014.

[51] M. W. Wang, R. Pan, W. Xin, W. Q. Chen, X. J. Zhao, and S. Li, "Effect of electro-spark deposition process parameter on WC coating thickness of H13 steel surface," (in English), *Material Design, Processing and Applications, Parts 1-4,* vol. 690-693, pp. 2112-2115, 2013.

[52] J. Qi, "Ultrasound-assisted Electrospark Deposition of 3Cr2NiMo Steel," (in English), *Advanced Materials and Process Technology, Pts 1-3,* vol. 217-219, pp. 463-466, 2012.

[53] H. Shafyei, M. Salehi, and A. Bahrami, "Fabrication, microstructural characterization and mechanical properties evaluation of Ti/TiB/TiB2 composite coatings deposited on Ti6Al4V alloy by electro-spark deposition method," (in English), *Ceramics International,* vol. 46, no. 10, pp. 15276-15284, Jul 2020.

[54] S. Durdu, S. L. Aktug, and K. Korkmaz, "Characterization and mechanical properties of the duplex coatings produced on steel by electro-spark deposition and micro-arc oxidation," (in English), *Surf Coat Tech,* vol. 236, pp. 303-308, Dec 15 2013.

[55] J. Gould, "Application of Electro-Spark Deposition as a Joining Technology," (in English), *Weld J,* vol. 90, no. 10, pp. 191s-197s, Oct 2011.

[56] P. V. Kiryukhantsev-Korneev, A. N. Sheveyko, N. V. Shvindina, E. A. Levashov, and D. V. Shtansky, "Comparative study of Ti-C-Ni-Al, Ti-C-Ni-Fe, and Ti-C-Ni-Al/Ti-C-Ni-Fe coatings produced by magnetron sputtering, electro-spark deposition, and a combined two-step process," (in English), *Ceramics International,* vol. 44, no. 7, pp. 7637-7646, May 2018.

[57]   C. J. Chen, Y. Z. Su, Q. Cao, and M. Zhang, "Study on Cavitation Erosion Properties of Stainless Steel Vane Wheel Enhanced by Electro-Spark Deposition (ESD) Technology," (in English), *Advanced Materials, Pts 1-4,* vol. 239-242, pp. 2229-2232, 2011.

[58]   N. Radek and J. Konstanty, "Cermet Esd Coatings Modified by Laser Treatment," (in English), *Arch Metall Mater,* vol. 57, no. 3, pp. 665-670, 2012.

[59]   D. Varecha, J. Broncek, R. Kohar, F. Novy, M. Vicen, and N. Radek, "Research of friction materials applicable to the multi-disc brake concept," (in English), *J Mater Res Technol,* vol. 14, pp. 647-661, Sep-Oct 2021.

[60]   K. A. Kuptsov, A. N. Sheveyko, D. A. Sidorenko, and D. V. Shtansky, "Electro-spark deposition in vacuum using graphite electrode at different electrode polarities: Peculiarities of microstructure, electrochemical and tribological properties," (in English), *Applied Surface Science,* vol. 566, Nov 15 2021.

[61]   Y. Kayali and S. Talas, "Investigation on Wear Behavior of Steels Coated with WC by ESD Technique," (in English), *Protection of Metals and Physical Chemistry of Surfaces,* vol. 57, no. 1, pp. 106-112, Jan 2021.

[62]   K. A. Kuptsov, A. N. Sheveyko, O. S. Manakova, D. A. Sidorenko, and D. V. Shtansky, "Comparative investigation of single-layer and multilayer Nb-doped TiC coatings deposited by pulsed vacuum deposition techniques," (in English), *Surf Coat Tech,* vol. 385, Mar 15 2020.

[63]   K. A. Kuptsov, A. N. Sheveyko, E. I. Zamulaeva, D. A. Sidorenko, and D. V. Shtansky, "Two-layer nanocomposite WC/a-C coatings produced by a

combination of pulsed arc evaporation and electro-spark deposition in vacuum," (in English), *Mater Design,* vol. 167, Apr 5 2019.

[64] M. W. Wang, W. Xin, X. J. Zhao, Q. Y. Ma, and S. Li, "Characterizations of electrospark deposition TA2 alloy coating on 7075 aluminum alloy surface," (in English), *Advances in Textile Engineering and Materials Iii, Pts 1 and 2,* vol. 821-822, pp. 873-876, 2013.

[65] L. Wang, G. Cao, X. Ma, and S. Yang, "Preparation of NiCrAlY Coating Electro-Spark Deposited on GH4169 Alloy," *Transactions of the China Welding Institution,* vol. 38, no. 07, pp. 104-108+133-134, 2017.

[66] A. Xu, X. Wang, S. Zhu, Q. Chang, X. Yuan, and K. Zhou, "Microstructure and Wear Resistance of TiN Coating Synthesized by ESD with Cluster Electrode," *China Surface Engineering,* vol. 32, no. 03, pp. 115-122, 2019.

[67] X. Wei, Z. Chen, J. Zhong, Q. Huang, Y. Zhang, and Y. Zhang, "Influence of Deposition Atmosphere on Structure and Properties of Mo2FeB2-Based Cermet Coatings Produced by Electro-Spark Deposition," *Rare Metal Mat Eng,* vol. 47, no. 04, pp. 1199-1204, 2018.

[68] Q. Huang, Z. Chen, X. Wei, L. Wang, Z. Hou, and W. Yang, "Effects of Pulse Energy on Microstructure and Properties of Mo2FeB2-based Ceramet Coatings Prepared by Electro-spark Deposition," *China Surface Engineering,* vol. 30, no. 03, pp. 89-96, 2017.

[69] X. Hong, K. Feng, Y. F. Tan, X. Wang, and H. Tan, "Effects of Process Parameters on Microstructure and Wear Resistance of TiN Coatings Deposited on TC11 Titanium Alloy by Electrospark Deposition," *T Nonferr Metal Soc,* vol. 27,

no. 08, pp. 1767-1776, 2017.

[70] A. Xu, X. Wang, Y. Zhao, S. Zhu, and G. Han, "Experiments on ESD-Heating Remelting, Rolling Dressing," *China Mechanical Engineering,* vol. 31, no. 14, pp. 1741-1746, 2020.

[71] H. Wei, W. Chu, T. Lin, and P. He, "Numerical Simulation of Temperature Field of WC-12Co Coating by Monopoles Electro Spark Deposition," *Transactions of the China Welding Institution,* vol. 36, no. 03, pp. 35-38+2-3, 2015.

[72] Z. L. Wang, B. D. Jin, G. H. Cao, Z. W. Wei, and W. S. Zhao, "Technique of Brass Spiral Structure Deposition Using Micro EDM in Gas," *Key Engineering Materials,* vol. 329, pp. 595-600, 2007.

[73] A. Bogdan, E. Emil, and A. Jaromír, "Study of the Effect of Type (Cu, Ti and Cu, Mo) Electrospark Coatings on Friction in Pin-on-Disk Testing," *Journal of Tribology,* vol. 130, no. 2, 2008.

[74] J. Pietraszek, N. Radek, and K. Bartkowiak, "Advanced Statistical Refinement of Surface Layer's Discretization in the Case of Electro-Spark Deposited Carbide-Ceramic Coatings Modified by a Laser Beam," *Solid State Phenomena,* vol. 197, pp. 198-202, 2013.

[75] V. Tarelnyk, V. Martsynkovskyy, and A. Dziuba, "New method of friction assemblies reliability and endurance improvement," in *Applied Mechanics and Materials*, 2014, vol. 630: Trans Tech Publ, pp. 388-396.

[76] A. Xu and Z. Liu, "Study of the TiN Coating Synthesized by EDM of Flexible Titanium Electrode," *Transactions of the China Welding Institution,* vol. 35, no. 02, pp. 23-27+32+114, 2014.

[77]   I. Pliszka and N. Radek, "Corrosion Resistance of WC-Cu Coatings Produced by Electrospark Deposition," *Procedia Engineering,* vol. 192, pp. 707-712, 2017.

[78]   J. Padgurskas *et al.*, "Tribological properties of coatings obtained by electro-spark alloying C45 steel surfaces," *Surface and Coatings Technology,* vol. 311, pp. 90-97, 2017.

[79]   A. Esmaeili, S. A. Ghaffari, M. Nikkhah, F. Malek Ghaini, F. Farzan, and S. Mohammadi, "Biocompatibility assessments of 316L stainless steel substrates coated by Fe-based bulk metallic glass through electro-spark deposition method," *Colloids Surf B Biointerfaces,* vol. 198, p. 111469, Feb 2021.

[80]   N. Radek, J. Pietraszek, A. Gadek-Moszczak, L. J. Orman, and A. Szczotok, "The Morphology and Mechanical Properties of ESD Coatings before and after Laser Beam Machining," (in English), *Materials,* vol. 13, no. 10, May 2020.

[81]   M. S. Khan *et al.*, "The influence of in-situ alloying of electro-spark deposited coatings on the multiscale morphological and mechanical properties of laser welded Al-Si coated 22MnB5," (in English), *Mat Sci Eng a-Struct,* vol. 839, Apr 6 2022.

[82]   M. Onan, O. Sahin, E. Yildirim, and S. Talas, "Effect of WC based coatings on the wear of CK45 sheet metal forming dies," (in English), *Int J Surf Sci Eng,* vol. 15, no. 4, pp. 265-280, 2021.

[83]   S. Spadlo and P. Mlynarczyk, "Selected Properties of the Micro Electrical Discharge Alloying Process Using Copper Electrode on Aluminum," (in English), *Transp Res Proc,* vol. 40, pp. 96-101, 2019.

[84]   Y. Kayali and S. Talas, "Investigation of Wear and Corrosion Behaviour of AISI

316 L Stainless Steel Coated By ESD Surface Modification," (in English), *Protection of Metals and Physical Chemistry of Surfaces,* vol. 55, no. 6, pp. 1148-1153, Nov 2019.

[85] S. N. Karlsdottir *et al.*, "Phase Evolution and Microstructure Analysis of CoCrFeNiMo High-Entropy Alloy for Electro-Spark-Deposited Coatings for Geothermal Environment," (in English), *Coatings,* vol. 9, no. 6, Jun 2019.

[86] N. Radek, M. Scendo, I. Pliszka, and O. Paraska, "Properties of Electro-Spark Deposited Coatings Modified Via Laser Beam," (in English), *Powder Metallurgy and Metal Ceramics,* vol. 57, no. 5-6, pp. 316-324, Sep 2018.

[87] N. Radek, J. Konstanty, and M. Scendo, "The Electro-Spark Deposited Wc-Cu Coatings Modified by Laser Treatment," (in English), *Arch Metall Mater,* vol. 60, no. 4, pp. 2579-2584, 2015.

[88] Y. X. Gao and G. L. Zhang, "Preparation and Cutting Performance of YT15 Cemented Carbide Tools with Ti(C, N)/Al2O3 Composite Coating," (in English), *Material Design, Processing and Applications, Parts 1-4,* vol. 690-693, pp. 2175-2178, 2013.

[89] Y. X. Gao, C. Zhao, Z. G. Fang, and J. A. Yi, "Microstructures and Wear Properties of Micro-nanostructure Coating on Cast Iron Rolls by Electro-spark Deposition," (in English), *Materials Science and Engineering Applications, Pts 1-3,* vol. 160-162, pp. 176, 2011.

[90] Y. Zhang *et al.*, "Experimental study on aluminum bronze coating fabricated by electro-spark deposition with subsequent ultrasonic surface rolling," (in English), *Surf Coat Tech,* vol. 426, Nov 25 2021.

[91]   J. S. Wang, H. M. Meng, H. Y. Yu, Z. S. Fan, and D. B. Sun, "Wear characteristics of spheroidal graphite roll WC-8Co coating produced by electro-spark deposition," (in English), *Rare Metals,* vol. 29, no. 2, pp. 174-179, Apr 2010.

[92]   J. S. Wang, H. M. Meng, H. Y. Yu, Z. S. Fan, and D. B. Sun, "Characterization and wear behavior of WC-0.8Co coating on cast steel rolls by electro-spark deposition," (in English), *Int J Min Met Mater,* vol. 16, no. 6, pp. 707-713, Dec 2009.

[93]   Y. X. Gao and C. Zhao, "Microstructure and Properties of Electrospark Deposition Coating on Die Steel," (in English), *Materials Processing Technology, Pts 1-4,* vol. 291-294, pp. 188, 2011.

[94]   Y. X. Gao, Z. G. Fang, and J. S. Wang, "Structure and Properties of Superfine Coating on Cast Steel by Electro-Spark Deposition," (in English), *Manufacturing Process Technology, Pts 1-5,* vol. 189-193, pp. 1018, 2011.

[95]   N. Radek and K. Bartkowiak, "Laser treatment of electro-spark coatings deposited in the carbon steel substrate with using nanostructured WC-Cu electrodes," (in English), *Physcs Proc,* vol. 39, pp. 295-301, 2012.

[96]   Y. K. Mashkov, D. N. Korotaev, M. Y. Baibaratskaya, and B. S. Alimbaeva, "Nanostructured coatings synthesized by electro-spark machining," (in English), *Tech Phys+,* vol. 60, no. 10, pp. 1489-1493, Oct 2015.

[97]   Y. Zhang *et al.*, "Research status and prospect of electro-spark deposition technology," *Surface Technology,* vol. 50, no. 1, pp. 150-161, 2021.

[98]   V. B. Tarelnyk, O. P. Gaponova, O. M. Myslyvchenko, and B. O. Sarzhanov, "Electrospark Deposition of Multilayer Coatings," (in English), *Powder*

Metallurgy and Metal Ceramics, vol. 59, no. 1-2, pp. 76-88, May 2020.

[99]   A. A. Burkov and S. A. Pyachin, "Tungsten carbide decarburization by electrical discharges," (in English), *Solid State Phenomen,* vol. 213, pp. 131-136, 2014.

[100] N. I. Jamnapara *et al.*, "Microstructural studies of electrospark deposited aluminide coatings on 9Cr steels," (in English), *Surf Eng,* vol. 28, no. 9, pp. 700-704, Oct 2012.

[101] D. Wang *et al.*, "Effect of TaC particles on the microstructure and oxidation behavior of NiCoCrAlYTa coating prepared by electrospark deposition on single crystal superalloy," (in English), *Surf Coat Tech,* vol. 408, Feb 25 2021.

[102] K. A. Kuptsov, M. N. Antonyuk, A. V. Bondarev, A. N. Sheveyko, and D. V. Shtansky, "Electrospark deposition of wear and corrosion resistant Ta(Zr)C-(Fe,Mo,Ni) coatings to protect stainless steel from tribocorrosion in seawater," (in English), *Wear,* vol. 486, Dec 15 2021.

[103] X. R. Wang, Z. Q. Wang, T. S. Lin, P. He, R. J. Wang, and M. Y. Bao, "Preparation of complex surface coatings based on electrospark computer integrated deposition system," (in English), *Assembly Autom,* vol. 40, no. 2, pp. 165-173, Jan 10 2020.

[104] D. Wang *et al.*, "Effect of operating voltage on microstructure and microhardness of NiCoCrAlYTa-Y2O3 composite coatings on single crystal superalloy produced by electrospark deposition," (in English), *Surf Coat Tech,* vol. 358, pp. 628-636, Jan 25 2019.

[105] X. Wei, Z. G. Chen, J. Zhong, and Y. Xiang, "Feasibility of preparing Mo2FeB2-based cermet coating by electrospark deposition on high speed steel,"

(in English), *Surf Coat Tech,* vol. 296, pp. 58-64, Jun 25 2016.

[106] X. Hong, Y. F. Tan, X. L. Wang, T. Xu, and L. Gao, "Microstructure and wear resistant performance of TiN/Zr-base amorphous-nanocrystalline composite coatings on titanium alloy by electrospark deposition," (in English), *Surf Coat Tech,* vol. 305, pp. 67-75, Nov 15 2016.

[107] A. Radeanu, D. Uliuliuc, and R. Purcariu, "Modifications in the Superficial Layer at the Electro-Spark Processing," (in English), *Pr Int Conf Modtech,* pp. 543-546, 2009.

[108] F. Guo, X. J. Su, P. Li, G. L. Hou, and Z. X. Mei, "Microstructure and Properties of Ti-Al Based Composite Coating Prepared by Electrospark Deposition Process," (in English), *Multi-Functional Materials and Structures Ii, Pts 1 and 2,* vol. 79-82, pp. 1611-1614, 2009.

[109] D. W. Heard, J. Boselli, R. Gauvin, and M. Brochu, "Rapid Solidification of a New Generation Aluminum-Lithium Alloy Via Electrospark Deposition," (in English), *Proceedings of the 13th International Conference on Aluminum Alloys (Icaa13),* pp. 1469-1474, 2012.

[110] C. J. Chen, M. C. Wang, D. S. Wang, H. S. Liang, and P. Feng, "Characterisations of electrospark deposition Stellite 6 alloy coating on 316L sealed valve used in nuclear power plant," (in English), *Mater Sci Tech-Lond,* vol. 26, no. 3, pp. 276-280, Mar 2010.

[111] K. Korkmaz, "Investigation and characterization of electrospark deposited chromium carbide-based coating on the steel," (in English), *Surf Coat Tech,* vol. 272, pp. 1-7, Jun 25 2015.

[112] X. Hong, Y. F. Tan, C. H. Zhou, T. Xu, and Z. W. Zhang, "Microstructure and tribological properties of Zr-based amorphous-nanocrystalline coatings deposited on the surface of titanium alloys by Electrospark Deposition," (in English), *Applied Surface Science,* vol. 356, pp. 1244-1251, Nov 30 2015.

[113] M. F. Hasanabadi, F. M. Ghaini, M. Ebrahimnia, and H. R. Shahverdi, "Production of amorphous and nanocrystalline iron based coatings by electro-spark deposition process," (in English), *Surf Coat Tech,* vol. 270, pp. 95-101, May 25 2015.

[114] X. R. Wang, Z. Q. Wang, T. S. Lin, and P. He, "Mass transfer trends of A1CoCrFeNi high-entropy alloy coatings on TC11 substrate via electrospark - computer numerical control deposition," (in English), *J Mater Process Tech,* vol. 241, pp. 93-102, Mar 2017.

[115] A. A. Burkov and S. A. Pyachin, "Formation of WC-Co coating by a novel technique of electrospark granules deposition," (in English), *Mater Design,* vol. 80, pp. 109-115, Sep 5 2015.

[116] K. Korkmaz and A. V. Ribalko, "Effect of pulse shape and energy on the surface roughness and mass transfer in the electrospark coating process," (in English), *Kovove Mater,* vol. 49, no. 4, pp. 265-270, 2011.

[117] I. R. Jang *et al.*, "Direct and controlled device integration of graphene oxide on Quartz Crystal Microbalance via electrospray deposition for stable humidity sensing," (in English), *Ceramics International,* vol. 48, no. 6, pp. 8004-8011, Mar 15 2022.

[118] K. Toth, S. Bae, C. O. Osuji, K. G. Yager, and G. S. Doerk, "Film Thickness and

Composition Effects in Symmetric Ternary Block Copolymer/Homopolymer Blend Films: Domain Spacing and Orientation," (in English), *Macromolecules,* vol. 54, no. 17, pp. 7970-7986, Sep 14 2021.

[119] M. C. Kim *et al.*, "Electro-spray deposition of a mesoporous TiO2 charge collection layer: toward large scale and continuous production of high efficiency perovskite solar cells," (in English), *Nanoscale,* vol. 7, no. 48, pp. 20725-20733, 2015.

[120] M. S. Yilmaz, E. Atar, O. Sahin, and E. S. Kayali, "Improving the Surface Properties of Cp-Ti by Pulsed Electro-Spark Deposition," (in English), *Acta Phys Pol A,* vol. 125, no. 2, pp. 593-596, Feb 2014.

[121] S. Frangini and A. Masci, "A study on the effect of a dynamic contact force control for improving electrospark coating properties," (in English), *Surf Coat Tech,* vol. 204, no. 16-17, pp. 2613-2623, May 15 2010.

[122] A. V. Ribalko, O. Sahin, and K. Korkmaz, "A modified electrospark alloying method for low surface roughness," (in English), *Surf Coat Tech,* vol. 203, no. 23, pp. 3509-3515, Aug 25 2009.

[123] M. Asnavandi, M. Ghorbani, and M. Kahram, "Production of Cu-Sn-graphite-SiC composite coatings by electrodeposition," (in English), *Surf Coat Tech,* vol. 216, pp. 207-214, Feb 15 2013.

[124] J. Zhang, C. Guo, and G. M. Shang, "Properties of electrospark deposited YG8 coatings on AISI H13 steel," (in English), *Advanced Manufacturing Technology, Pts 1-4,* vol. 472-475, pp. 1392, 2012.

[125] K. Korkmaz and H. I. Bakan, "Process and properties of TiC0.7N0.3-based

cermet coating deposition on steel by electrospark deposition technique," (in English), *Kovove Mater,* vol. 48, no. 2, pp. 153-158, 2010.

[126] J. P. Luo, G. H. Sun, C. Shang, L. S. Chen, B. Li, and J. He, "Health Status Evaluation of Intelligent Power Distribution Room based on AHP- Entropy method," (in English), *C Ind Elect Appl,* pp. 176-181, 2020.

[127] C. W. Ma and Y. G. Ma, "Shannon information entropy in heavy-ion collisions," (in English), *Prog Part Nucl Phys,* vol. 99, pp. 120-158, Mar 2018.

[128] A. H. Wei, D. Li, F. G. Dai, X. J. Lang, B. H. Ma, and Y. Q. Wang, "An optimization method coupled the index-overlay method with entropy weighting model to assess seawater intrusion vulnerability," (in English), *Environ Sci Pollut R,* vol. 28, no. 27, pp. 36142-36156, Jul 2021.

[129] X. L. Cui, J. Wu, Z. H. Li, L. Peng, Z. Shen, and J. Bi, "An Integrated Assessment and Factor Analysis of Water Related Environmental Risk to Cities in the Yangtze River Economic Belt," (in English), *Water-Sui,* vol. 13, no. 16, Aug 2021.

[130] Z. W. Gao, D. H. Ma, X. D. Guo, W. Wang, and Z. T. Wang, "The Comprehensive Assessment Method of Concrete Damage after Disastrous Fire Based on Game Theory-Normal Cloud Model," (in English), *Math Probl Eng,* vol. 2019, 2019.

[131] A. H. Li, J. Zhao, Z. C. Gong, and F. H. Lin, "Optimal selection of cutting tool materials based on multi-criteria decision-making methods in machining Al-Si piston alloy," (in English), *Int J Adv Manuf Tech,* vol. 86, no. 1-4, pp. 1055-1062, Sep 2016.

[132] Y. C. Li, J. P. Chen, Y. W. Zhang, S. Y. Song, X. D. Han, and M. Ammar, "Debris

Flow Susceptibility Assessment and Runout Prediction: A Case Study in Shiyang Gully, Beijing, China," (in English), *Int J Environ Res,* vol. 14, no. 3, pp. 365-383, Jun 2020.

[133] X. B. Liang, W. Liang, L. B. Zhang, and X. Y. Guo, "Risk assessment for long-distance gas pipelines in coal mine gobs based on structure entropy weight method and multi-step backward cloud transformation algorithm based on sampling with replacement," (in English), *J Clean Prod,* vol. 227, pp. 218-228, Aug 1 2019.

[134] G. Tian, W. Yu, T. T. H. Vu, and G. Y. Ma, "Green Assessment of Imports and Exports of Wooden Forest Products Based on Forest Processing Industry: A Case Study of China," (in English), *Forests,* vol. 12, no. 2, Feb 2021.

[135] J. H. Yuan and X. G. Luo, "Regional energy security performance evaluation in China using MTGS and SPA-TOPSIS," (in English), *Sci Total Environ,* vol. 696, Dec 15 2019.

[136] L. Ma, H. L. Long, K. Q. Chen, S. S. Tu, Y. N. Zhang, and L. W. Liao, "Green growth efficiency of Chinese cities and its spatio-temporal pattern," (in English), *Resour Conserv Recy,* vol. 146, pp. 441-451, Jul 2019.

[137] J. Zhou, Q. D. Wang, and Y. Deng, "Rank Analysis of Off-campus Learning Centers Based on Students' Achievements and TOPSIS Method and Grey Correlation," (in Chinese), *Destech Trans Soc,* pp. 271-276, 2017.

[138] D. Y. Zhao, Y. Y. Ma, and H. L. Lin, "Using the Entropy and TOPSIS Models to Evaluate Sustainable Development of Islands: A Case in China," (in English), *Sustainability-Basel,* vol. 14, no. 6, Mar 2022.

[139] M. W. Wu, J. Q. Wu, and C. F. Zang, "A comprehensive evaluation of the eco-carrying capacity and green economy in the Guangdong-Hong Kong-Macao Greater Bay Area, China," (in English), *J Clean Prod,* vol. 281, Jan 25 2021.

[140] Y. Sun, L. L. Zhou, S. Zhu, J. T. Su, and J. Zhang, "Evaluation of Development Index of China's VC Industry Based on Weight Optimization Algorithm and TOPSIS," (in English), *Complexity,* vol. 2021, Jun 12 2021.

[141] X. Y. Ren *et al.*, "Effects of B on the Structure and Properties of Lead-Tin Bronze Alloy and the Mechanism of Strengthening and Toughening," (in English), *Materials,* vol. 14, no. 24, Dec 2021.

[142] T. V. Aravind and S. Arul, "Effect of deep cryogenic treatment on C93700 bearing bush material used in submersible pumps," (in English), *Mater Today-Proc,* vol. 46, pp. 4685-4690, 2021.

[143] A. Bharatish, V. Harish, R. N. Bathe, J. Senthilselvan, and S. Soundarapandian, "Effect of scanning speed and tin content on the tribological behavior of femtosecond laser textured tin-bronze alloy," (in English), *Opt Laser Technol,* vol. 108, pp. 17-25, Dec 2018.

[144] D. Dinesh and A. Megalingam, "Dry Sliding Friction and Wear Behaviour of Leaded Tin Bronze for Bearing and Bushing Application," (in English), *Arch Metall Mater,* vol. 66, no. 4, pp. 1095-1104, 2021.

[145] V. Ruusila *et al.*, "The effect of microstructure and lead content on the tribological properties of bearing alloys," (in English), *P I Mech Eng J-J Eng,* vol. 227, no. 8, pp. 878-887, Aug 2013.

[146] B. K. Prasad, S. Rathod, O. P. Modi, and M. S. Yadav, "Influence of talc

concentration in oil lubricant on the wear response of a bronze journal bearing," (in English), *Wear,* vol. 269, no. 5-6, pp. 498-505, Jul 19 2010.

[147] M. Ibrahim, M. A. Samad, K. Al-Athel, A. F. Arif, and N. Olalekan, "Evaluation of Tribological Properties of Thermally Sprayed Copper and Copper Alloy Coatings," (in English), *Arab J Sci Eng,* vol. 43, no. 9, pp. 4899-4910, Sep 2018.

[148] P. Pereteatcu, A. Ojegov, E. Ungureanu, and V. Mikhailov, "The Effect of Influence of the Magnetic Field on the Electrospark Alloying Process," (in English), *Int Conf Modtech Pr,* pp. 841-844, 2011.

[149] L. Wang, P. W. Gong, W. Li, T. Luo, and B. Q. Cao, "Mono-dispersed Ag/Graphene nanocomposite as lubricant additive to reduce friction and wear," (in English), *Tribology International,* vol. 146, Jun 2020.

[150] N. Radek, J. Pietraszek, and A. Szczotok, "Microstructure and Tribological Properties of ESD Coatings after Laser Processing," (in English), *Mater Res Proc,* vol. 5, pp. 206-209, 2018.

[151] N. Radek and K. Bartkowiak, "Performance properties of electro-spark deposited carbide-ceramic coatings modified by laser beam," (in English), *Laser Assisted Net Shape Engineering 6, Proceedings of the Lane 2010, Part 1,* vol. 5, pp. 417-423, 2010.

[152] V. B. Tarel'nik *et al.*, "Electrospark Graphite Alloying of Steel Surfaces: Technology, Properties, and Application," *Surface Engineering and Applied Electrochemistry,* vol. 54, no. 2, pp. 147-156, 2018.

[153] I. Konoplianchenko *et al.*, "Mathematical modeling a process of strengthening steel part working surfaces at carburizing thereof by electroerosive alloying

method," 2018.

[154] G. V. Kirik, O. P. Gaponova, V. B. Tarelnyk, O. M. Myslyvchenko, and B. Antoszewski, "Quality Analysis of Aluminized Surface Layers Produced by Electrospark Deposition," *Powder Metallurgy and Metal Ceramics,* vol. 56, no. 11-12, pp. 688-696, 2018.

[155] V. Tarelnyk *et al.*, "New sulphiding method for steel and cast iron parts," *IOP Conference Series: Materials Science and Engineering,* vol. 233, 2017.

[156] V. B. Tarel'nik, V. S. Martsinkovskii, and A. N. Zhukov, "Increase in the Reliability and Durability of Metal Impulse End Seals. Part 1," *Chemical and Petroleum Engineering,* vol. 53, no. 1-2, pp. 114-120, 2017.

[157] V. B. Tarel'nik, E. V. Konoplyanchenko, P. V. Kosenko, and V. S. Martsinkovskii, "Problems and Solutions in Renovation of the Rotors of Screw Compressors by Combined Technologies," *Chemical and Petroleum Engineering,* vol. 53, no. 7-8, pp. 540-546, 2017.

[158] V. Tarelnyk, V. Martsynkovskyy, A. Sarzhanov, A. Pavlov, V. Gerasimenko, and B. Sarzhanov, "Improvement of integrated technology for restoring surfaces of steel and iron parts," *IOP Conference Series: Materials Science and Engineering,* vol. 233, 2017.

[159] V. B. Tarel'nik, A. V. Paustovskii, Y. G. Tkachenko, V. S. Martsinkovskii, E. V. Konoplyanchenko, and K. Antoshevskii, "Electric-spark coatings on a steel base and contact surface for optimizing the working characteristics of babbitt friction bearings," *Surface Engineering and Applied Electrochemistry,* vol. 53, no. 3, pp. 285-294, 2017.

[160] V. B. Tarel'nik, V. S. Martsinkovskii, and A. N. Zhukov, "Increase in the Reliability and Durability of Metal Impulse Seals. Part 2*," *Chemical and Petroleum Engineering,* vol. 53, no. 3-4, pp. 266-272, 2017.

[161] V. Tarelnyk *et al.*, "New method for strengthening surfaces of heat treated steel parts," *IOP Conference Series: Materials Science and Engineering,* vol. 233, 2017.

[162] V. Tarelnik, A. Belous, B. Antoszewski, and A. Zukov, "Problems and criteria of quality improvement in end face mechanical seal rings through technological methods," *IOP Conference Series: Materials Science and Engineering,* vol. 233, 2017.

[163] V. B. Tarel'nik, V. S. Martsinkovskii, and A. N. Zhukov, "Increase in the Reliability and Durability of Metal Impulse Seals. Part 3*," *Chemical and Petroleum Engineering,* vol. 53, no. 5-6, pp. 385-389, 2017.

[164] L. Zhang, C. Yuan, C. Dong, Y. Wu, and X. Bai, "Friction-induced vibration and noise behaviors of a composite material modified by graphene nano-sheets," *Wear,* vol. 476, 2021.

[165] X. Zhang, Z. Yin, Q. Dong, and J. Cao, "Experimental comparison of the seizure loads of gray iron journal bearing and aluminum alloy journal bearing under aligned and misaligned conditions," *Mechanics & Industry,* vol. 21, no. 4, 2020.

[166] J. Zha, J. L. Wang, K. J. Liu, and Y. L. Chen, "Design, Development and Testing of Water-Lubricated Ceramic Journal Bearing," (in English), *Proceedings of the Asme International Mechanical Engineering Congress and Exposition, 2017, Vol 11,* 2018.

[167] K. Krishnakumar and A. Selvakumar, "Metallurgical investigation of failure analysis in industrial machine components," (in English), *Mater Today-Proc,* vol. 27, pp. 2076-2080, 2020.

[168] Q. Dong, Z. W. Yin, H. L. Li, G. Y. Gao, N. Zhong, and Y. H. Chen, "Simulation and experimental verification of fatigue strength evaluation of journal bearing bush," (in English), *Engineering Failure Analysis,* vol. 109, Jan 2020.

[169] J. M. Wang, F. N. Meng, X. T. Zhang, Y. A. Liang, and Z. X. Li, "Mathematical model and algorithm of interface singular stress field of oil-film bearing," (in English), *Tribology International,* vol. 116, pp. 351-361, Dec 2017.

[170] R. P. Kumar and S. Arul, "Improving the wear and corrosion resistance of nickel aluminium bronze by deep cryogenic treatment," (in English), *Mater Today-Proc,* vol. 46, pp. 4915-4918, 2021.

[171] E. O. Lagunova and M. A. Mukutadze, "Calculation of a Radial Slider Bearing with a Fusible Coating," (in English), *Journal of Friction and Wear,* vol. 40, no. 1, pp. 88-94, Jan 2019.

[172] Y. Q. Ni, G. N. Dong, Z. Tong, X. Li, and W. Wang, "Effect of laser remelting on tribological properties of Babbitt alloy," (in English), *Mater Res Express,* vol. 6, no. 9, Sep 2019.

[173] A. Amanov, B. Ahn, M. G. Lee, Y. Jeon, and Y. S. Pyun, "Friction and Wear Reduction of Eccentric Journal Bearing Made of Sn-Based Babbitt for Ore Cone Crusher," (in English), *Materials,* vol. 9, no. 11, Nov 2016.

[174] B. Leszczynska-Madej and M. Madej, "The Properties of Babbitt Bushes in Steam Turbine Sliding Bearings," (in English), *Arch Metall Mater,* vol. 56, no. 3,

pp. 805-812, 2011.

[175] Y. Q. Ni, X. Li, G. N. Dong, Z. Tong, and T. J. Mei, "The combined effect of La and heat treatment on the tribological performances of tin-Babbitt alloy," (in English), *P I Mech Eng J-J Eng,* vol. 233, no. 7, pp. 1117-1126, Jul 2019.

[176] A. D. Verhoturov, V. D. Vlasenko, and L. A. Konevtsov, "Investigation of the Adhesive Strength of Antifriction Coatings Depending on the Energy Parameters of Electro-Spark Alloying," *Journal of Friction and Wear,* vol. 39, no. 3, pp. 232-240, 2018.

[177] A. V. Kozyr, L. A. Konevtsov, S. V. Konovalov, S. V. Kovalenko, and V. I. Ivashenko, "Research of heat resistance of the multilayer coating after electro-spark alloying of C45 steel Cr-Ni alloys," *Letters on Materials,* vol. 8, no. 2, pp. 140-145, 2018.

[178] A. A. Burkov, A. V. Zaytsev, and V. O. Krutikova, "Effect of Co, Ni, Mo and W on the corrosion properties of amorphous electrospark coatings," *Letters on Materials,* vol. 8, no. 2, pp. 190-195, 2018.

[179] S. V. Nikolenko and N. A. Syui, "Investigation of coatings produced by the electrospark machining method of steel 45 with electrodes based on carbides of tungsten and titanium," *Protection of Metals and Physical Chemistry of Surfaces,* vol. 53, no. 5, pp. 889-894, 2017.

[180] A. A. Burkov, "Electrospark WC–Co coatings with different iron concentration," *Welding International,* vol. 32, no. 1, pp. 72-75, 2017.

[181] T. Chang-bin, L. Dao-xin, W. Zhan, and G. Yang, "Electro-spark alloying using graphite electrode on titanium alloy surface for biomedical applications," *Applied*

Surface Science, vol. 257, no. 15, pp. 6364-6371, 2011.

[182] S. S. Gajmal and D. N. Raut, "An Investigation on Wear Behaviour of ASTM B23 tin-Based Babbitt Alloy Developed Through Microwave-Assisted Casting," (in English), *Int J Metalcast,* Jan 8 2022.

[183] J. M. Wang, Y. W. Xue, Y. J. Zhang, and S. W. Wang, "Creep Mechanical Properties of Babbitt SnSb11Cu6," (in Chinese), *Rare Metal Mat Eng,* vol. 44, no. 6, pp. 1432-1438, Jun 2015.

[184] Z. Zhengchuan, V. Tarelnyk, I. Konoplianchenko, L. Guanjun, D. Xin, and Y. Hua, "Research on the Characterization of Ag+Cu+B83 Composite Coatings on the Surface of Tin Bronze by Electro-spark Deposition," in *2021 IEEE 11th International Conference Nanomaterials: Applications & Properties (NAP)*, 2021, pp. 1-8.

[185] Q. process parametersDong, Z. W. Yin, H. L. Li, X. Y. Zhang, D. Jiang, and N. Zhong, "Effects of Ag micro-addition on structure and mechanical properties of Sn-11Sb-6Cu Babbitt," (in English), *Mat Sci Eng a-Struct,* vol. 722, pp. 225-230, Apr 11 2018.

[186] Y. F. Zhang, H. Yuan, W. Q. Yan, S. N. Chen, M. L. Qiu, and B. L, "Atomic-Oxygen-Durable and Antistatic alpha-AlxTiyO/gamma-NiCr Coating on Kapton for Aerospace Applications," (in English), *Acs Appl Mater Inter,* vol. 13, no. 48, pp. 58179-58192, Dec 8 2021.

[187] N. Radek, J. Konstanty, J. Pietraszek, L. J. Orman, M. Szczepaniak, and D. Przestacki, "The Effect of Laser Beam Processing on the Properties of WC-Co Coatings Deposited on Steel," (in English), *Materials,* vol. 14, no. 3, Feb 2021.

[188] Z. Y. Jia, C. Y. Ma, and H. B. Zhang, "PLGA Coatings and PLGA Drug-Loading Coatings for Cardiac Stent Samples: Degradation Characteristics and Blood Compatibility," (in English), *Coatings,* vol. 11, no. 11, Nov 2021.

[189] Z. Zhang, I. Konoplianchenko, V. Tarelnyk, G. Liu, X. Du, and H. Yu, "The Characterization of Running-In Coatings on the Surface of Tin Bronze by Electro-Spark Deposition," *Coatings,* vol. 12, no. 7, p. 930, 2022.

[190] F. Bahrami *et al.*, "Single layer graphene controlled surface and bulk indentation plasticity in copper," (in English), *Int J Plasticity,* vol. 138, Mar 2021.

[191] M. Verma, P. Verma, S. K. Dhawan, and V. Choudhary, "Tailored graphene based polyurethane composites for efficient electrostatic dissipation and electromagnetic interference shielding applications," (in English), *Rsc Adv,* vol. 5, no. 118, pp. 97349-97358, 2015.

[192] Z. Zhang, X. Lu, J. Xu, and H. Luo, "Characterization and Tribological Properties of Graphene/Copper Composites Fabricated by Electroless Plating and Powder Metallurgy," *Acta Metallurgica Sinica (English Letters),* vol. 33, no. 7, pp. 903-912, 2020.

[193] F. Wu, W. J. Zhao, H. Chen, Z. X. Zeng, X. D. Wu, and Q. J. Xue, "Interfacial structure and tribological behaviours of epoxy resin coating reinforced with graphene and graphene oxide," (in English), *Surf Interface Anal,* vol. 49, no. 2, pp. 85-92, Feb 2017.

[194] G. Q. Liang, D. X. Niu, and Y. Liang, "Sustainability Evaluation of Renewable Energy Incubators Using Interval Type-II Fuzzy AHP-TOPSIS with MEA-MLSSVM," (in English), *Sustainability-Basel,* vol. 13, no. 4, Feb 2021.

[195] Y. C. Li, L. Zhao, and J. J. Suo, "Comprehensive Assessment on Sustainable Development of Highway Transportation Capacity Based on Entropy Weight and TOPSIS," (in English), *Sustainability-Basel,* vol. 6, no. 7, pp. 4685-4693, Jul 2014.

[196] H. L. Wang, "The Comprehensive Evaluation of the Graduate School's Teaching Quality Based on Entropy-Weight and TOPSIS Methods," (in English), *High Performance Networking, Computing, and Communication Systems,* vol. 163, pp. 401-406, 2011.

[197] Z. Zhengchuan *et al.*, "Industry Application of the Coatings on the Bearing Bush by Electro Spark Alloying Technology," *Scientific Bulletin of Ivano-Frankivsk National Technical University of Oil and Gas,* no. 1(52), pp. 15-23, 06/30 2022.

APPENDICES

APPENDIX A. List of publications on the topic of the dissertation and information on

the approbation of the results of the dissertation

List of publications in which the main scientific results of the dissertation are published:

1. **Zhang Zhengchuan**, Liu Guanjun, Viacheslav Tarelnyk, Ievgen Konoplianchenko. Application of Electro-Spark Deposition Technology to Functional Coatings Create. Compressor and Power Engineering. 2019, 4(58), 14-16.

2. **Zhang Zhengchuan**, Liu Guanjun, Ie. Konoplianchenko, V. Tarelnyk, Ge Zhiqin, Du Xin. A review of the electro-spark deposition technology. Bulletin of Sumy National Agrarian University, The Series: Mechanization and Automation of Production Processes. 2021, 2(44), 45-53.

https://doi.org/10.32845/msnau.2021.2.10

3. **Zhang Zhengchuan**. The characterization of silver coating on the surface of tin bronze by electro-spark deposition. Bulletin of Sumy National Agrarian University, The Series: Mechanization and Automation of Production Processes. 2021, 4(46), 60-66.

https://doi.org/10.32845/msnau.2021.4.9

4. **Zhang Zhengchuan**, Ievgen Konoplianchenko, Viacheslav Tarelnyk, Liu Guanjun, Du Xin, Ju Yao, Song Zhaoyang. Industry Application of the Coatings on the Bearing Bush by Electro Spark Alloying Technology. Scientific Bulletin of Ivano-Frankivsk National Technical University of Oil and Gas. 2022, 1(52), 15-23.

https://doi.org/10.31471/1993-9965-2022-1(52)-15-23

5. **Zhang Zhengchuan**, Ievgen Konoplianchenko, Viacheslav Tarelnyk, Liu Guanjun, Du Xin, Yu Hua. The Characterization of Running-In Coatings on the Surface of Tin Bronze by Electro-spark Deposition. Coatings. 2022, 12(7), 930-945.

https://doi.org/10.3390/coatings12070930   **(Web of Science)**

6. **Zhang Zhengchuan**, Ievgen Konoplianchenko, Viacheslav Tarelnyk, Liu Guanjun, Du Xin, Yu Hua. The Characterization of Soft Antifriction Coating on the Tin Bronze by Electro-spark Alloying. Materials Science (Medžiagotyra). 2023, 29(1), 40-47.

http://dx.doi.org/10.5755/j02.ms.30610   **(Web of Science)**

7. **Zhang Zhengchuan**, Viacheslav Tarelnyk, Ievgen Konoplianchenko, Liu Guanjun, Du Xin，Ju Yao. Characterization of Tin Bronze Substrates Coated by Ag+B83 through Electro-spark Deposition Method. Surface Engineering and Applied Electrochemistry. 2023, 59(2), 220-230.

https://doi.org/10.3103/S1068375523020187   **(Web of Science)**

8. **Zhang Zhengchuan**, Viacheslav Tarelnyk, Ievgen Konoplianchenko, Liu Guanjun , Wang Hongyue, Du Xin，Ju Yao, Li Zongxi. New Evaluation Method for the Characterization of Coatings by Electroerosive Alloying. Materials Research Express. 2023, 10(3), 036401.

https://doi.org/10.1088/2053-1591/acc15b   **(Web of Science)**

9. **Zhang Zhengchuan**, Viacheslav Tarelnyk, Ievgen Konoplianchenko. The use of electro-spark technologies in the formation of running-in coatings. Youth and Agricultural Machinery in the XXI Century. April 4-5th, 2019.

10. Ie. Konoplianchenko, **Zhang Zhengchuan**. Improving the running-in conditions quality of sliding bearing by the formation of running-in coatings. Технології XXI сторіччя: Збірник тез за матеріалами 25-ої міжнародної науково-практичної конференції (15-20 вересня 2019 р.). Ч.3. – Суми: СНАУ, 2019 – С. 53-54.

11. **Zhang Zhengchuan**, Viacheslav Tarelnyk, Ievgen Konoplianchenko. Application of electro-spark deposition technology to functional coatings create. Sumy National Agrarian University. April 18th, 2019.

12. Konoplianchenko, I., Tarelnyk, V., Martsynkovskyy, V., Gaponova, O., Lazarenko, A., Sarzhanov, A., Mikulina, M., **Zhengchuan, Z.**, Pirogov, V. New technology for restoring Babbitt coatings (2021) Journal of Physics: Conference Series, 1741 (1), art. no. 012040.

https://doi.org/10.1088/1742-6596/1741/1/012040   **(SCOPUS)**

13. Konoplianchenko, I., Tarelnyk, V., Gaponova, O., Bondarev, S., Vasilenko, O., Belous, A., Smolyarov, G., Semirnenko, Y., **Zhang, Z.**, Mikulina, M., Kutakh, A., Semirnenko, S., Gerasimenko, V. Increasing the Efficiency of Running-In the Titanium Nitride Nanostructures Formed on R6M5 and 12KH18N10T Steels by Sulphidizing with Electric Spark Alloying Method (2020) Proceedings of the 2020 IEEE 10th International Conference on "Nanomaterials: Applications and Properties", NAP 2020, art. no. 9309700.

https://doi.org/10.1109/nap51477.2020.9309700   **(Web of Science, SCOPUS)**

14. **Zhang Zhengchuan**, Viacheslav Tarelnyk, Ievgen Konoplianchenko, Liu Guanjun, Du Xin, Yu Hua. Research on the Characterization of Ag+Cu+B83 Composite

Coatings on the Surface of Tin Bronze by Electro-spark Deposition (2021) Proceedings of the 2021 IEEE 11th International Conference on "Nanomaterials: Applications and Properties", NAP 2021, pp. 1-8.

https://doi.org/10.1109/NAP51885.2021.9568514   **(SCOPUS)**

15. **Zhang Zh.**, Konoplianchenko Ie.V., Tarelnyk V.B., Du X. The future research direction of the ESD deposition technology. Машинобудування очима молодих: прогресивні ідеї – наука – виробництво: матеріали XX Міжнародної науково-технічної конференції (м. Суми, 29 вересня – 1 жовтня 2021 року) / редкол.: В. О. Залога, В. О. Іванов. – Суми: Сумський державний університет, 2021. – С. 21-23.

16. Ju Yao, Ie. Konoplianchenko, **Zhang Zhengchuan**. AlCoNiFeCrSi high-entropy alloy coating on the surface of H13 steel by laser cladding. ТехнологіїXXI сторіччя: Збірниктеззаматеріалами 27-ої міжнародної науково-практичної конференції (24-26 листопада 2021 р.). Ч.1. – Суми: СНАУ, 2021 – С. 214-215.

17. Ju Y., Konoplianchenko Ie., **Zhang Zh.** Practical application of high-entropy alloy obtained on the H13 steel by laser cladding technology. Машинобудування очима молодих: прогресивні ідеї – наука – виробництво: матеріали XX Міжнародної науково-технічної конференції (м. Суми, 29 вересня – 1 жовтня 2021 року) / редкол.: В. О. Залога, В. О. Іванов. – Суми: Сумський державний університет, 2021. – С. 12-14.

APPENDIX B. Documents on the protection of rights to inventions and utility models

on the topic of the dissertation

国 家 知 识 产 权 局

453000

河南省新乡市凤泉区区府路宏铭时代华府 6 号楼 1 单元 603 室
新乡市平原智汇知识产权代理事务所(普通合伙) 杨杰(0373-3052076)

发文日：

2022 年 12 月 03 日

申请号或专利号：202211543478.X   发文序号：2022120301468630

专 利 申 请 受 理 通 知 书

根据专利法第 28 条及其实施细则第 38 条、第 39 条的规定，申请人提出的专利申请已由国家知识产权局受理。现将确定的申请号、申请日、申请人和发明创造名称通知如下：

申请号：202211543478.X
申请日：2022 年 12 月 03 日
申请人：河南起重机器有限公司
发明创造名称：一种起重机轴瓦表面电火花沉积复合涂层工艺

经核实，国家知识产权局确认收到文件如下：
实质审查请求书 每份页数:1 页 文件份数:1 份
发明专利请求书 每份页数:5 页 文件份数:1 份
权利要求书 每份页数:1 页 文件份数:1 份 权利要求项数： 8 项
专利代理委托书 每份页数:2 页 文件份数:1 份
说明书摘要 每份页数:1 页 文件份数:1 份
说明书 每份页数:5 页 文件份数:1 份

提示：
    1. 申请人收到专利申请受理通知书之后，认为其记载的内容与申请人所提交的相应内容不一致时，可以向国家知识产权局请求更正。
    2. 申请人收到专利申请受理通知书之后，再向国家知识产权局办理各种手续时，均应当准确、清晰地写明申请号。
    3. 国家知识产权局收到向外国申请专利保密审查请求书后，依据专利法实施细则第 9 条予以审查。

审 查 员：自动受理   审 查 部 门：专利局初审及流程管理部

200101   纸件申请，回函请寄：100088 北京市海淀区蓟门桥西土城路 6 号 国家知识产权局受理处收
2019.11   电子申请，应当通过电子专利申请系统以电子文件形式提交相关文件。除另有规定外，以纸件等其他形式提交的
            文件视为未提交。

国 家 知 识 产 权 局

453000

河南省新乡市凤泉区区府路宏铭时代华府 6 号楼 1 单元 603 室
新乡市平原智汇知识产权代理事务所(普通合伙) 杨杰(0373-3052076)

发文日:

2022 年 11 月 01 日

申请号或专利号: **202211348829.1**   发文序号: **2022110100063830**

专 利 申 请 受 理 通 知 书

根据专利法第 28 条及其实施细则第 38 条、第 39 条的规定,申请人提出的专利申请已由国家知识产权局受理。现将确定的申请号、申请日、申请人和发明创造名称通知如下:

申请号: 202211348829.1
申请日: 2022 年 10 月 31 日
申请人: 河南起重机器有限公司
发明创造名称: 一种锡青铜轴瓦表面电火花合金化软减摩涂层工艺

经核实,国家知识产权局确认收到文件如下:
权利要求书 每份页数:2 页 文件份数:1 份 权利要求项数: 9 项
发明专利请求书 每份页数:5 页 文件份数:1 份
说明书 每份页数:7 页 文件份数:1 份
专利代理委托书 每份页数:2 页 文件份数:1 份
实质审查请求书 每份页数:1 页 文件份数:1 份
说明书摘要 每份页数:1 页 文件份数:1 份

提示:
1. 申请人收到专利申请受理通知书之后,认为其记载的内容与申请人所提交的相应内容不一致时,可以向国家知识产权局请求更正。
2. 申请人收到专利申请受理通知书之后,再向国家知识产权局办理各种手续时,均应当准确、清晰地写明申请号。
3. 国家知识产权局收到向外国申请专利保密审查请求书后,依据专利法实施细则第 9 条予以审查。

审 查 员: 自动受理   审查部门: 专利局初审及流程管理部

200101   纸件申请,回函请寄: 100088 北京市海淀区蓟门桥西土城路 6 号 国家知识产权局受理处收
2019.11   电子申请,应当通过电子专利申请系统以电子文件形式提交相关文件。除另有规定外,以纸件等其他形式提交的文件视为未提交。

APPENDIX C. Documents on the implementation of the results of the dissertation

Certification

Zhang Zhengchuan completed the industry practical application of the running-in coatings of tin bronze bearing Bush in the industrial equipment. The new environmental protection technology of running-in coatings of tin bronze bearing Bush was implemented, and the process design, manufacture, processing, installation and commissioning were carried out. The running-in coatings of tin bronze bearing Bush has low operation temperature, and the stability and reliability of the bearing Bush are obviously improved. The scientific results are valuable for industry.

Hereby certify.

Xinxiang Senrui Machinery Co., LTD

July 4, 2022